School of

OCEANOGRAPHY

An Oceanic Microstructure Measuring System

by

D. R. Caldwell
and
T. M. Dillon

Reference 81-10
September 1981

OREGON STATE UNIVERSITY

An Oceanic Microstructure Measuring System

D. R. Caldwell

T. M. Dillon

School of Oceanography.

Oregon State University.

Corvallis, Oregon 97331

ACKNOWLEDGEMENTS

Over the years many people have taken part in the development of this instrument and these procedures, among them Steve Wilcox, Mark Matsler, George Marmorino, John Brubaker, Priscilla Newberger, Mike Brown and Jim Cantey. Financial support has been provided by the National Science Foundation, the Office of Naval Research, and the National Aeronautics and Space Administration.

TABLE OF CONTENTS

TABLE OF CONTENTS (cont.)

I. INTRODUCTION

The system now in use at Oregon State University to obtain profiles of "microstructure" in the upper 200 m of the ocean has been under development since 1973. Scientific results depending on this system have now been published in a number of papers (Caldwell, 1976; Marmorino and Caldwell, 1978a; Caldwell, Brubaker and Neal, 1978; Marmorino and Caldwell, 1978b; Caldwell, 1978; Dillon and Caldwell, 1978; Dillon and Caldwell, 1980a; Dillon and Caldwell, 1980b; Caldwell, Dillon, Brubaker, Newberger and Paulson, 1980; Newberger and Caldwell, 1981a; Caldwell, Chriss, Newberger and Dillon, 1981; Newberger and Caldwell, 1981b; Dillon, Richman, Hansen and Pearson, 1981). The only description in print discusses the system in an early stage of its evolution (Caldwell, Wilcox and Matsler, 1975). Since that description was written significant changes have been made, and we have found out quite a bit more about its operation, particularly with respect to the frequency-response of the thermistors used to measure microscale temperature gradients. To make better evaluation of the scientific works possible, a description of the system and its functioning is presented here. The system is described in the form it has taken in the summer of 1981. Continuing evolution is expected, and no final form of the beast is anticipated.

Our primary purpose in developing this instrument is to measure vertical temperature fluctuations in the ocean to the smallest scales at which they exist. This goal dictates the basic concept of the instrument, as C. S. Cox saw in the 1960's. Vertical temperature changes are seen as changes with time of the temperature sensed by a thermistor mounted on a freely-falling instrument. Because the response time of available thermistors presents a limitation, rate of descent must be slow. In

order that the time series can be interpreted as a spatial record, the descent must be smooth, as it cannot be if the instrument hangs from a ship. On the other hand, in order for the fluctuations to appear "frozen" as the sensor passes through them, as we would like, the descent rate must be kept substantially faster than the small-scale motions in the water. It turns out that descent rates of 5-15 cm/sec can be profitably used. Another approach is to use a much faster-responding sensor which can resolve the temperature fluctuations while falling much faster (Elliott and Oakey, 1975). This approach has its own set of problems which will not be discussed here.

Although the measurement of temperature fluctuations is the main business of this instrument, some supporting measurements are necessary and others are desireable. The depth-history of the instrument must be recorded with the fluctuations. The mean temperature profile is required as well as the salinity profile. Shear measurements would be highly desirable, along with small-scale vertical-velocity measurements, but these are difficult, especially because they require an exceedingly smooth descent. We have found measurements of optical transmissivity to be interesting as well, particularly in the bottom layer.

Several versions of the freely-falling microstructure instrument as constructed by others preserve much of Cox's original design. Data are recorded internally, and the inclusion of the tape recorder enforces a minimum size for the instrument. Components necessary for the recovery of a completely free instrument add to its weight and size, and the necessity of changing tapes sets a minimum time between casts. For the herein-described system, a combination data-link and recovery line is used, so that the tape recorder can remain on shipboard, and the instru-

ment is recovered by simply reeling in the line, which is kept slack on descent so that the instrument is still decoupled from ship's motion while data are being taken.

Other unique features of our system and others involve the operation of the electronics in a case filled with Freon or oil and kept at ambient pressure rather than a pressure case, direct-current data transmission to the ship through fine wires, and the use of redundant data-channels for signals derived from the same sensor. The conductivity circuitry is unique, we believe, as is the incorporation of light-transmissivity sensors. The determination of the response of the temperature-sensing thermistors, the most important of the calibration procedures, we have done in several ways which differ somewhat from the standard method. Also our method of separating signal from noise is not commonly used with this type of instrumentation.

Recently the instrument has been modified so that data are collected on ascent rather than descent. Measurements to the air-water interface are made possible by this development (Dillon, Richman, Hansen and Pearson, 1981).

The principal limitation of the system lies with the depth attainable. Because of the inevitable relative motion between the ship and the deeper sections of the water column, casts to depths greater than 300 m are not practical under ordinary conditions.

II. PHYSICAL DESCRIPTION

The instrument is basically a 2" OD tube, vertically aligned, with sensors at the bottom and drag element near the top. The data link is connected through the top, connecting with the electronics inside. In this section the instrument and data link will be described, as well as techniques of deployment and characteristics of motion. In Section III the individual measurement modules will be taken up one-by-one.

A. The Probe

Over the years various forms of the instrument have been used. The one currently in use comprises a metal tube 2" in outside diameter, with a nosepiece into which the sensors are plugged (Fig. II.A.1). Four holes in the nosepiece accept the various transducers, usually thermistors, thermocouples, or conductivity sensors. A guard of steel rod protects the sensors and permits resting the instrument on deck. The transducer assemblies (described in detail in Section III) are inserted into the nosepiece, with O-ring seals. The circuitry associated with each sensor is contained in an epoxy-cast module. The modules are plugged into a motherboard, which runs along the length of the tube (Fig. II.A.2). At the top of the motherboard is a connector for the data-link termination. The case is filled with either Freon or oil. We use Freon for descending casts because it is heavier than water, does not mix with water, and leaves the instrument clean when it is removed. A small "leak" at the top assures pressure equilibration. When the instrument is used in the ascending mode, it is upside-down, so a flexible seal must be used for pressure equilibration rather than the "leak." We have not been able to find a material that remains flexible in contact with Freon, so mineral

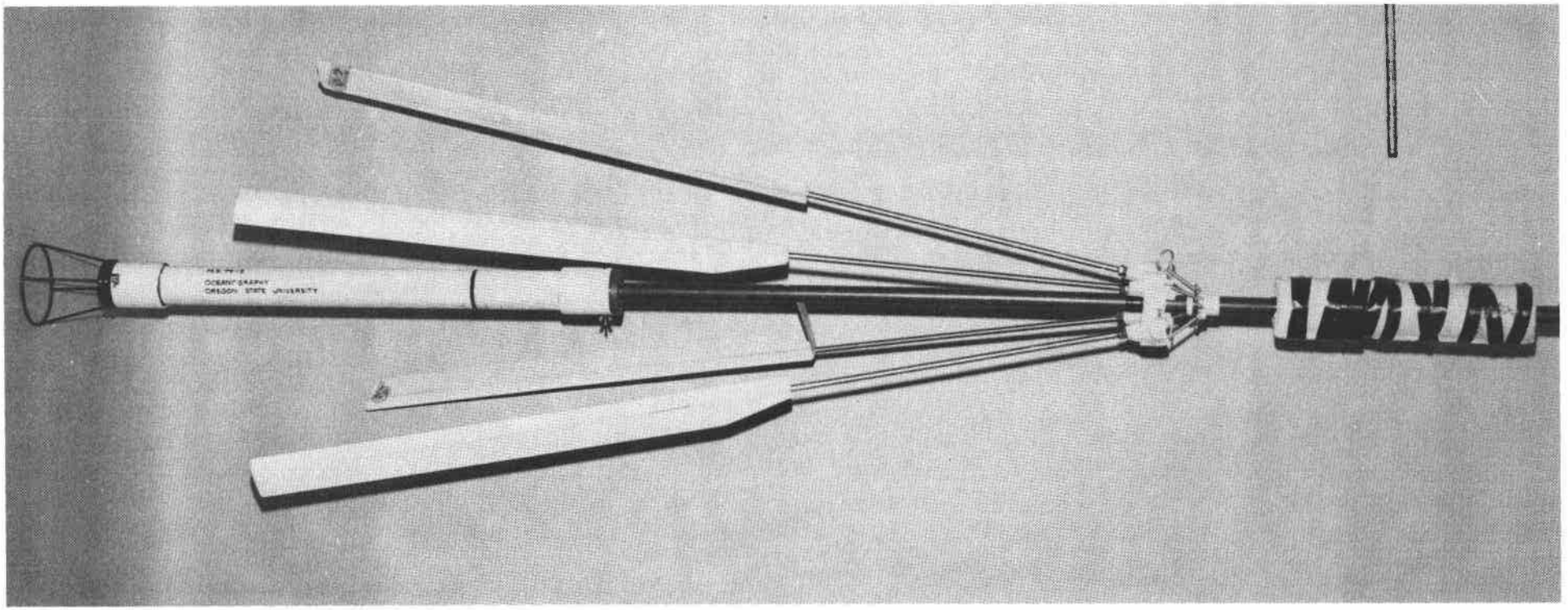

FIGURE II.A.1: The probe. At top are buoyancy elements, syntactic foam floats. The larger white tube contains the circuitry.

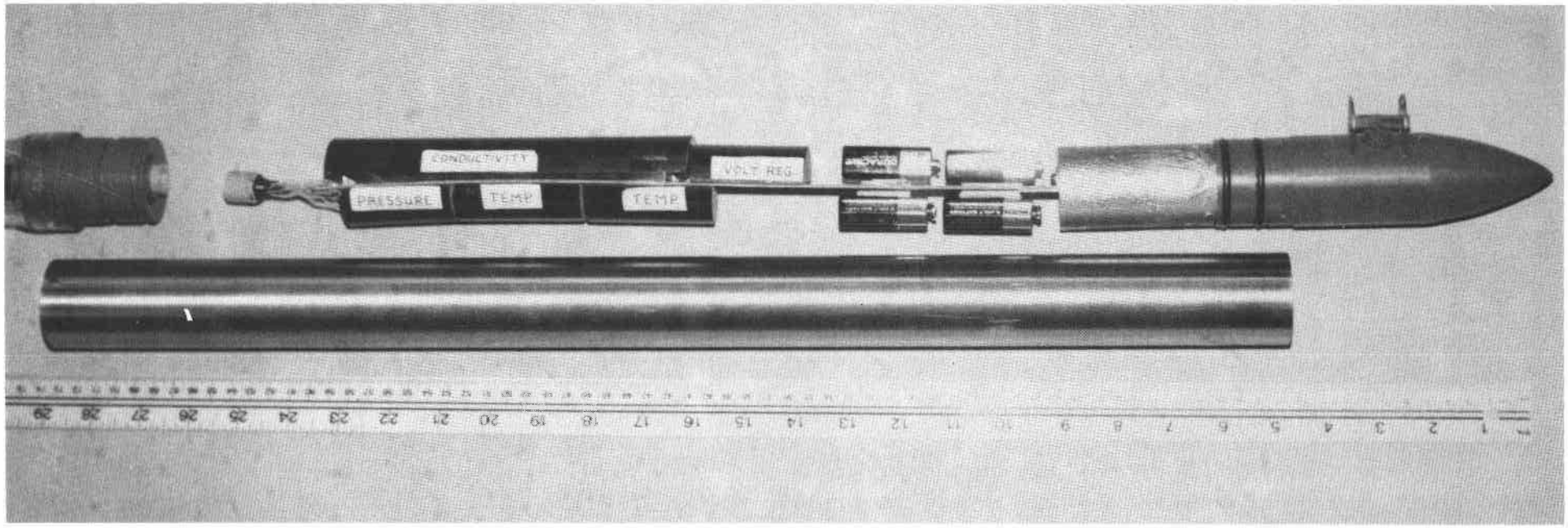

FIGURE II.A.2: The mother board with modules mounted on it. The exterior pieces shown here are those of a new, more streamlined design. A conductivity sensor is mounted on the nose, at right.

oil is used to fill the case instead. The objectives of providing a fluid-filled environment for the electronics is mainly to avoid problems with seals and to make the use of cumbersome underwater connectors unnecessary. Also no precautions against condensation are required, and the Freon in particular provides an environment free of large temperature gradients.

B. Drag Elements

Two forms of drag elements are used to slow descent to the desired rate, which is approximately 10 cm s^{-1}. The elements used when taking data on descent are wings. Four wings are attached near the top of the instrument (Fig. II.B.1) by means of a bracket which operates much like an umbrella (Fig. II.B.2). The wings fold down to lie along the instrument case during recovery, being forced to do so by their drag in the water as the instrument is dragged through the water by the recovery line. The folding of the wings facilitates recovery. When the line is released, the instrument begins to fall, and at least one wing will be forced upward by the water. The bracket linkage then forces the other wings out, so that quickly the instrument is falling with its wings extended. Each wing, a 50 cm long air foil of 5 cm chord is cast from syntactic foam over a steel tube. The tube reinforces the wing and is threaded at the inboard end for attachment to the bracket. Fall speed is governed by the angle of attack of the wings (and by the negative buoyancy of the instrument). A sample plot of descent rate vs. angle of attack shows the effect of this adjustment for one value of negative buoyancy (Fig. II.B.3). The rotation period tends to be such that a full rotation is accomplished for each meter of descent. The drag

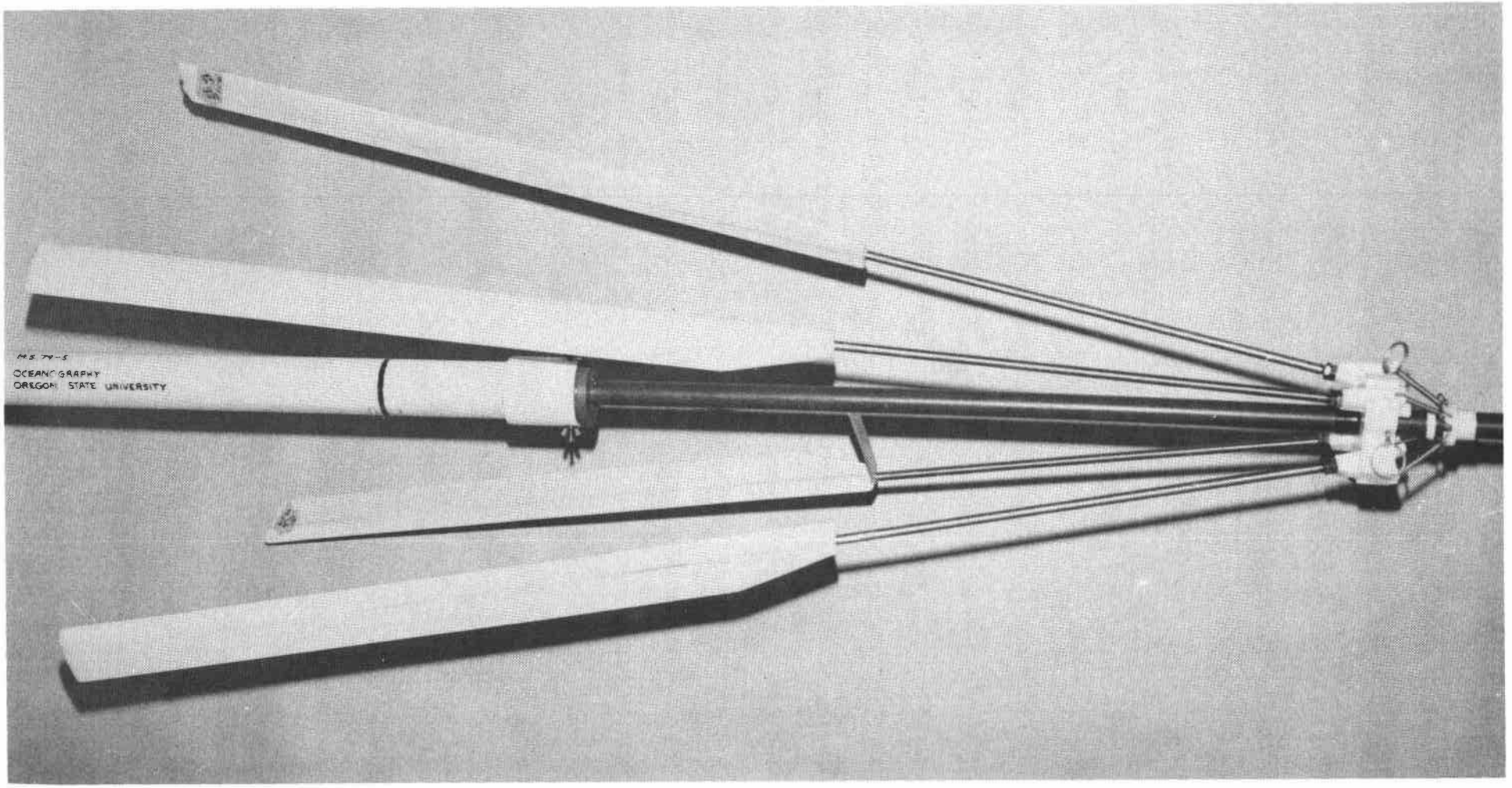

FIGURE II.B.1: Probe with wings. During data acquisition the wings pop out to a horizontal position and the instrument descends while rotating slowly. During retrieval the wings are pressed down against the body so the drag is much less.

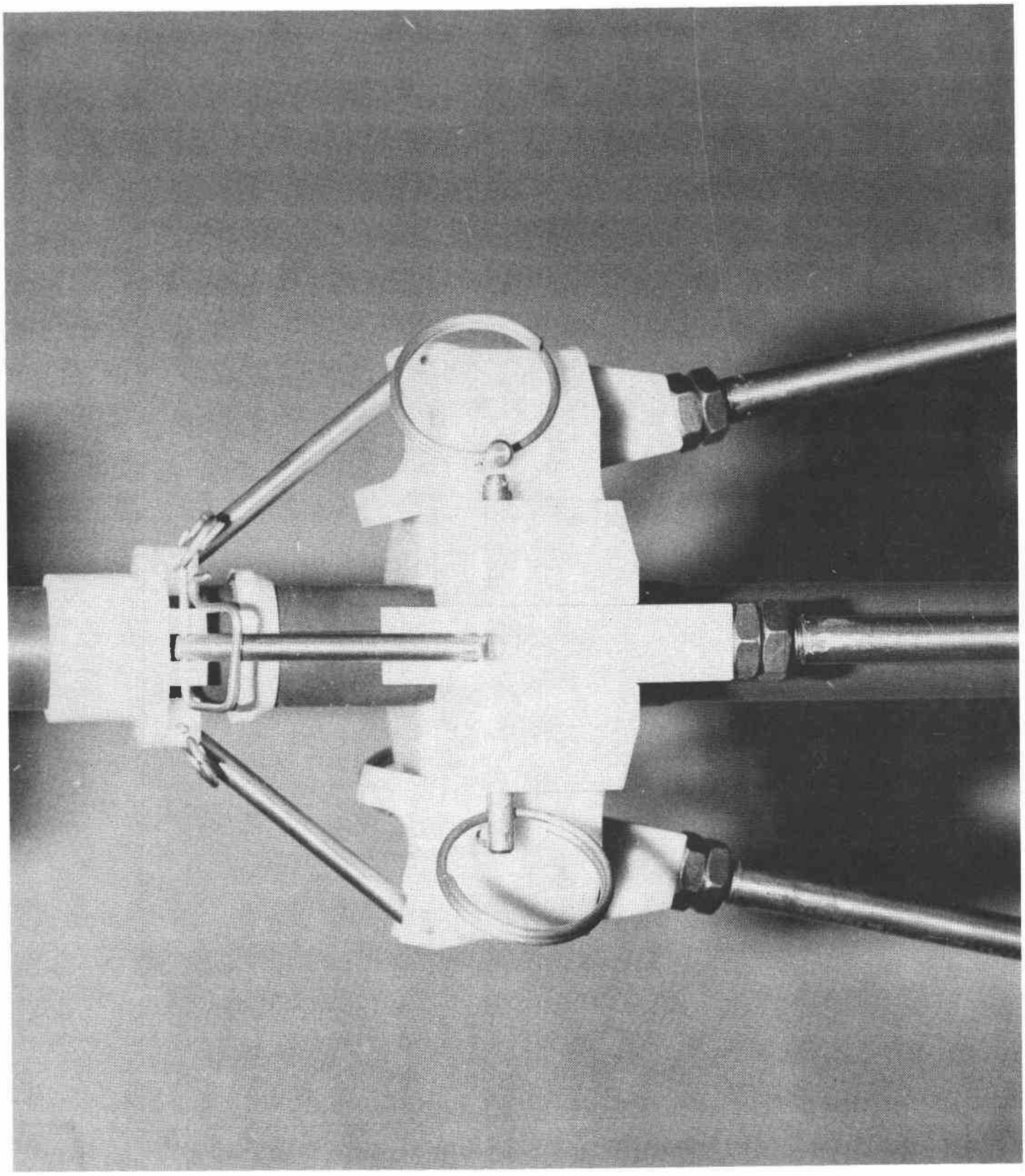

FIGURE II.B.2: Wing bracket assembly. This mechanism ensures that when the instrument is released and one wing is brought up by the force of the water, all wings are brought up.

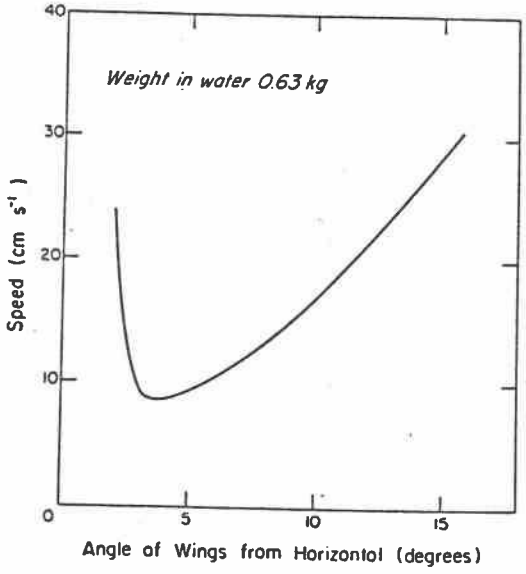

FIGURE II.B.3: Descent rate vs. angle of attack of wings for fixed negative buoyancy.

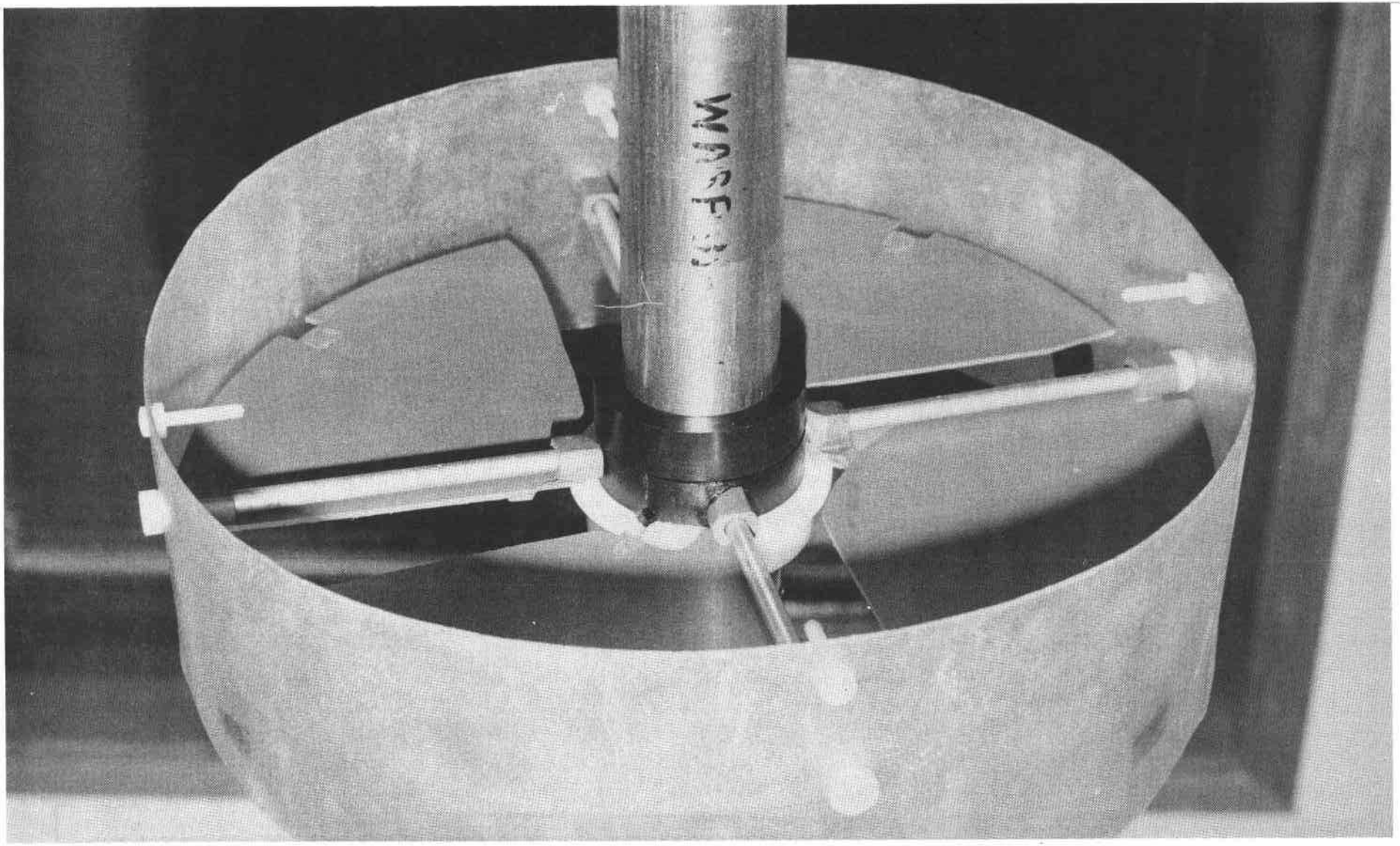

Figure II.B.4: Vented-plate drag element, used when signals are to be recorded as the instrument ascends. In this photograph the plates are nearly horizontal, as they are during ascension. The data-link/retrieval-line is connected to the end opposite the sensors, below the field of view in this picture, so that the plates are forced against the stops (white bolts) on retrieval, thereby reducing the drag.

coefficient referred to the area swept out by the wings is approximately 1.0 under near-stall conditions.

When taking data on ascent the data link connection is below the wings, and tangling of the data link in wings would be all but certain, so a different sort of drag element is used (Fig. II.B.4).

C. Data-Link/Recovery Line

To transmit the signals from the instrument to the ship and to recover the instrument quickly, a thin (0.15 cm in diameter) cable is used. It consists of four pairs of #39 guage wires, the wire-pairs used in the Sippican XBT system. The wire-pairs are purchased from Sippican and then sent to the Courtland Line Co. to be made up into the cable. A jacket of Kevlar is woven around the wires, and then a coating of syntactic foam is applied. The density of the syntactic foam is regulated to keep the line neutrally buoyant in seawater. Keeping the line neutrally-buoyant ensures that it will not fall faster than the instrument and tangle in the wings, and also will not exert a buoyant force on the instrument. For the "pop-up" form of the instrument, heavier line may be better.

The breaking strength of the line is at least 80 lbs, so that even when weakened by termination it will pull the instrument in without breaking, as long as the ship is not moving away from it. If the ship is underway, the drag is greatly increased, and at 2 knots or so it becomes too great.

Lengths of cable average 500 m. Each wire then has a resistance of 800 Ω. A single direct-current signal is fed to each wire-pair by the output of an operational amplifier, and a high-impedence differential

amplifier looks at each pair on shipboard. As long as the input-impedance of the shipboard amplifiers is much larger than the impedance of the wires, attentuation by the wires is negligible. Pressure is communicated as a frequency-modulated signal in the same wires, in the 500-1300 Hz band. Details of the shipboard electronics are given in Section IV.

When data are being recorded the line is kept slack. At first we worried that even a line slack at the ship would communicate wave motion to the ship, but it turns out that this does not happen to any significant degree (Dillon and Caldwell, 1980).

The greatest advantage of using the data-link/recovery line system is that casts can be repeated rapidly without bringing the instrument on board. For bottom-layer work on the shelf we operate the retrieval system only until the instrument has risen above the bottom layer, then release it again. A profile every 5 minutes can be obtained in this way.

Several systems are used for unreeling and retrieving the cable. We have found a large fishing reel, equipped with slip rings, quite sufficient, if somewhat laborious. A powered system has now been developed, but its use at sea has been limited.

D. Deployment

Again two modes of operation must be considered. For data-taking on descent, the ship is headed into the wind and kept under minimum steerage way. The ship must move forward with respect to the surface water so that the line, dangling from the fantail, will not be caught in the propeller. On the other hand if the ship moves too quickly it is difficult to keep the line slack and of course retrieval becomes longer

as more line is stripped on the way out. A speed of 0.25 to 0.5 knots is practicable except in heavy weather, when more speed is required to maintain steerage. We have also operated very sucessfully on the shelf with ship anchored.

When it is desired to take data on ascent, operation becomes more difficult, and as of this date we have no experience in operating in this mode from a large ship. From our houseboat in a reservoir it works quite well. The instrument's buoyancy is first redistributed so that it is at equilibrium noseupward, and has positive buoyancy. Then a weight is attached with a pressure-actuated release, so that the instrument descends to a pre-selected depth and then pops up, as data are taken. The boat is moored, and currents carry the instrument well away from it, so that it does not pop up in the wake of the boat. In operation from a ship at sea, it will be much more difficult to avoid the wake. The plan is to stop the ship and take the instrument away from it in a Zodiac, then release it.

E. Dynamic Characteristics

The ideal microstructure probe would maintain its vertical velocity constant relative to the water it moves through, and drift horizontally with horizontal water motions. Its vertical velocity relative to the mean water surface may vary, oscillating with internal or surface wave motions, for example. A real probe's vertical velocity relative to the water around it may vary because of its inertia; it may not be able to follow rapid changes in the water's vertical velocity. We also might expect some effect of the retrieval line, even though it is kept slack at the ship and is neutrally buoyant. That the winged probe described

in this report follows internal waves has been demonstrated (Dillon and Caldwell, 1980, especially Figure 2). If a probe responds perfectly to deep-water surface waves, no signal will be seen in the pressure record, because the dynamic pressure fluctuations will just balance the hydrostatic pressure fluctuations. But in shallow-water waves a signal is seen, especially as the bottom is approached. This is precisely what we find. In deep water we see no wave signal, but in shallow water we see a signal that increases toward the bottom. As the probe approaches bottom, its pressure sensor produces a signal which has an oscillatory part exactly the same as the oscillatory signal seen while the probe lies still on the bottom. So clearly the probe follows vertical fluctuations in water velocity even at surface-wave frequencies.

Horizontal fluctuations are more difficult for the probe to follow, because it has much less drag horizontally than vertically, and because the sensors are located at the opposite end of the probe from the drag element so that even if the drag-element end follows horizontal motion, the sensors may see a relative motion. In the Wave Zone Profiler (WAZP) version we are adding large fins to help the probe follow the horizontal motions of ocean swells.

III. TRANSDUCERS AND ELECTRONICS

Four d.c. signals can be transmitted through the data link. They would usually be:

1. Temperature from Thermistor #1
2. Separately-amplified temperature from Thermistor #1.
3. Temperature from Thermistor #2, or optical transmissivity
4. Conductivity

The pressure signal is transmitted in FM form, superimposed on signals 1 and 2. The circuitry associated with each transducer is cast into a separate module, each module being plugged into the motherboard. All temperature and heated thermistor modules fit the same sockets, and the conductivity and optics modules fit the same sockets, so many different combinations can be set up. Figure III.1 shows a typical set-up. Power for the circuits is drawn from a pair of 9v alkaline batteries ("transistor batteries") through a voltage regulator which provides $\pm$5 volts. The power drain changes when different combinations of modules are used, but 20 mA is a typical value. The probe will run for approximately 15 hours at 10°C before a battery change is needed.

A. Thermistor Transducers and Modules

We have been using P-85 thermistors purchased from Thermometrics because they seem to have the best combination of quickness of response and durability. They are made in such a way that the temperature-sensitive bead lies in a 0.006"-diameter glass protrusion, which sticks out perhaps 0.020" from the end of a 0.1"-diameter glass cylinder (Fig. III.A.1). These glass probes are potted into stainless-steel tubes which are glued into PVC plugs to be inserted into the nosepiece of the

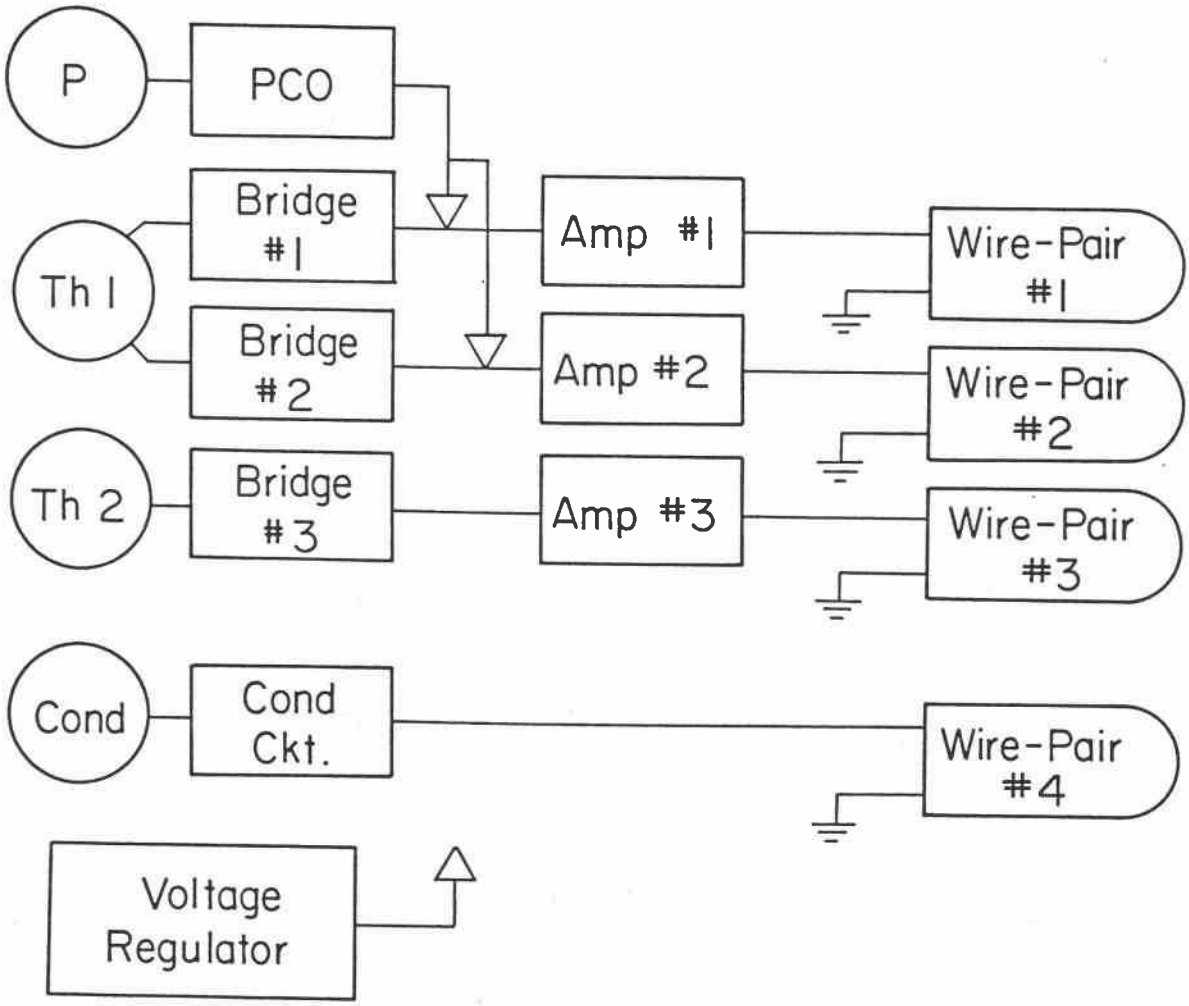

FIGURE III.1: Block diagram of probe. P represents the pressure transducer, Th1 and Th2 the thermistors, and Cond the (Neil Brown) conductivity transducer.

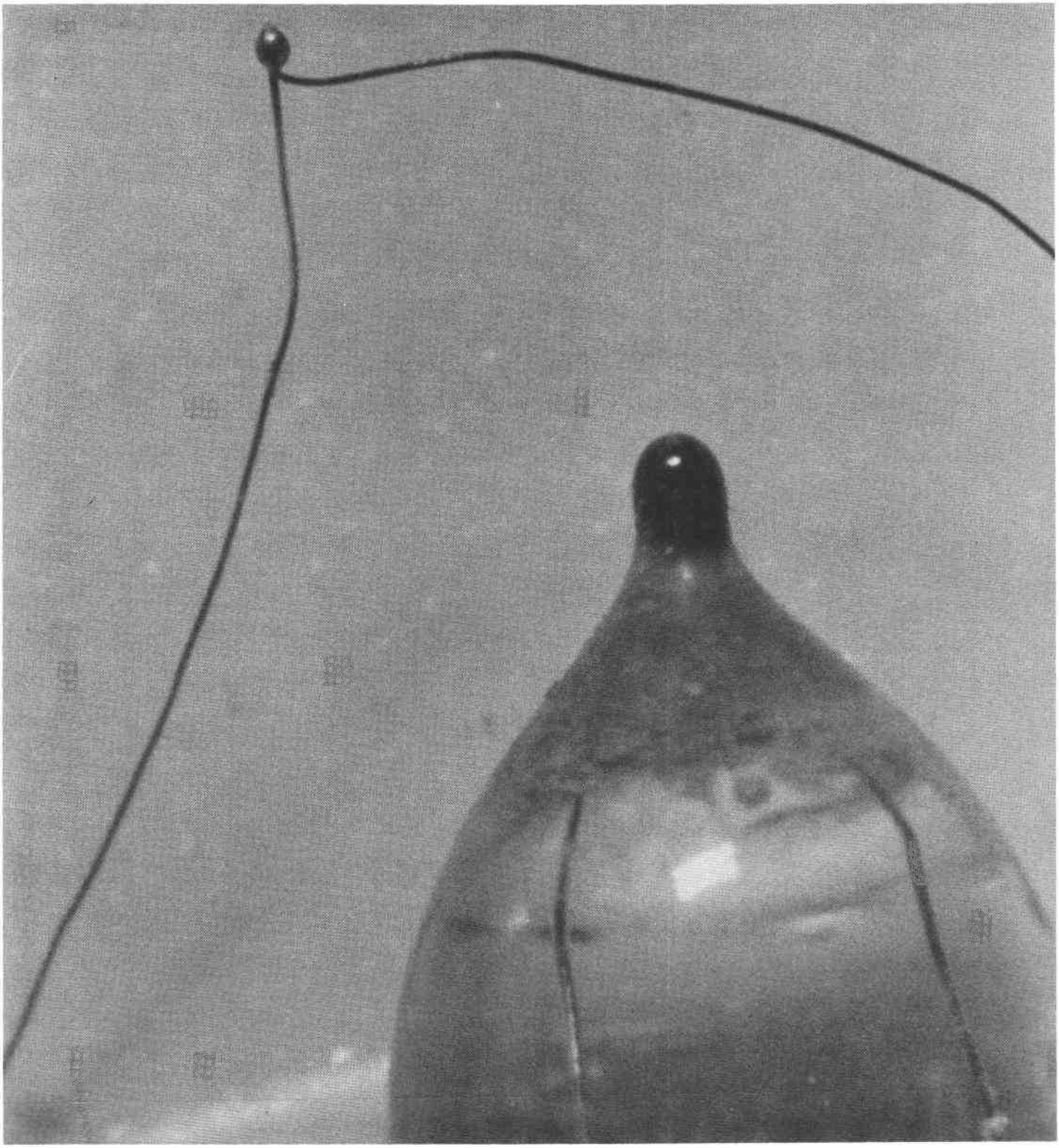

FIGURE III.A.1: The tip of a thermometrics P-85 glass thermistor probe. The temperature-sensitive material shows up as black in this picture, in the protrusion. A thermocouple junction is also shown, at top left. For scale, the thermocouple leads are 0.001 in diameter.

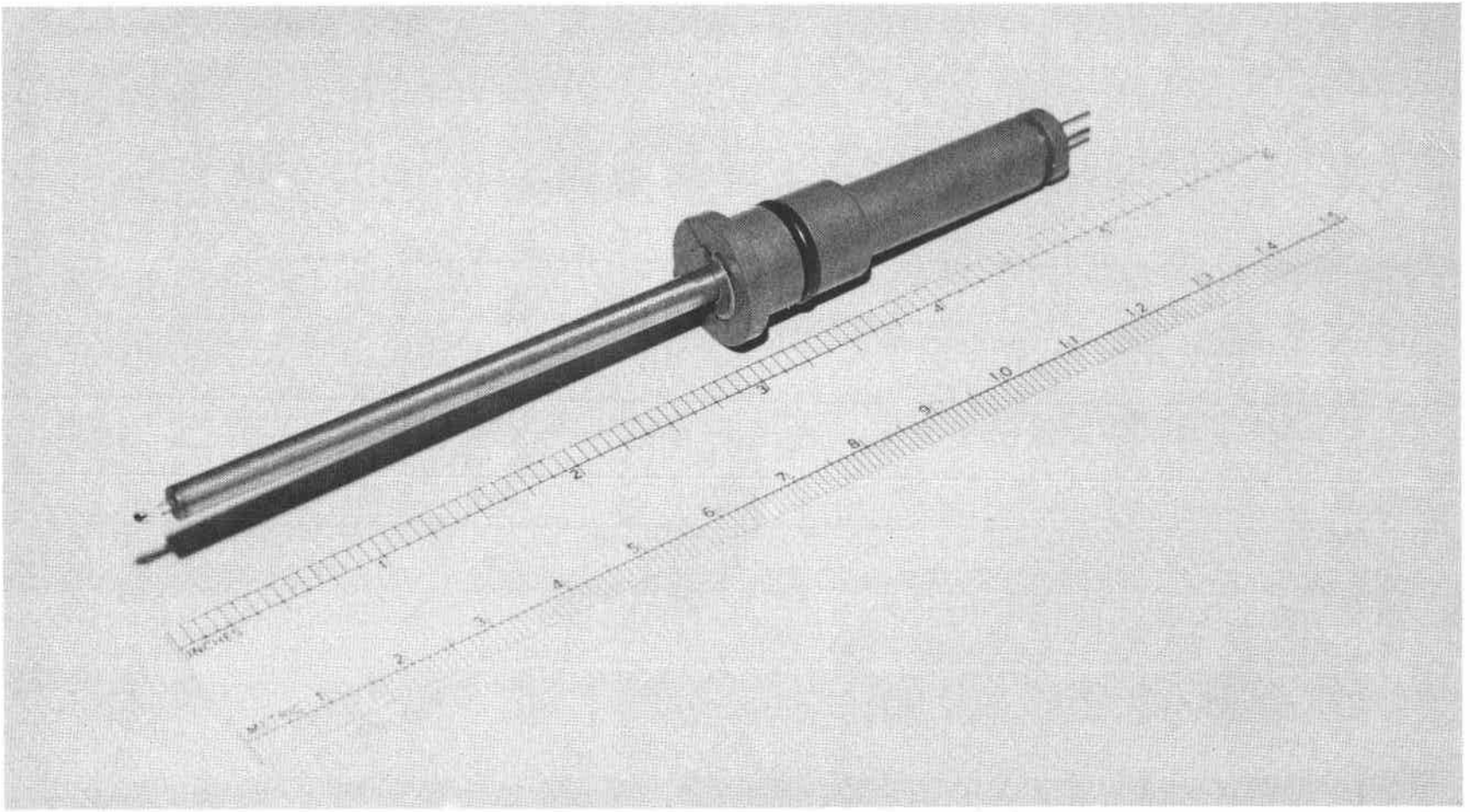

FIGURE III.A.2: Transducer assembly. At left the thermistor protrudes from the stainless-steel tube. The O-ring seal is clearly seen.

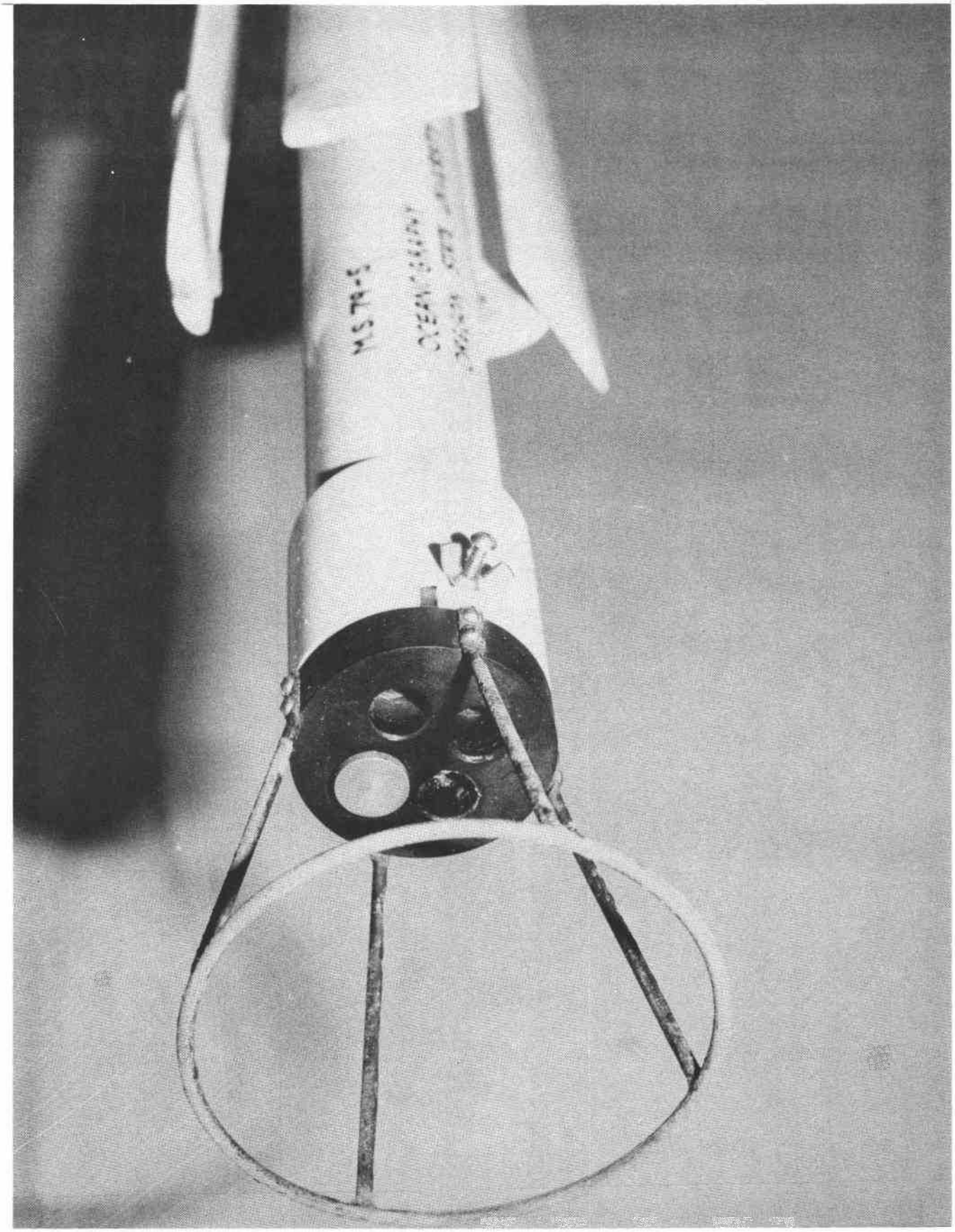

FIGURE III.A.3: One type of nose piece. Four holes in the cap accept transducer assemblies.

instrument (Figs. III.A.2, III.A.3). The joint between probe and nose-piece is O-ring sealed. Much grief has been produced by the potting process. We have been unable to find a castable material that is completely impervious to water under pressure. Absorbtion of water has caused electrical leaks to seawater. Even an extremely high-impedance leak causes noise in the transducers. The solution for this problem has been to O-ring seal the glass probes into the stainless-steel tubes before potting. Pressure-bomb tests seem to indicate success with this arrangement.

A simple d.c. bridge circuit (Fig. III.A.4) has worked best with these thermistors. The circuit is designed around the OP-7 operational amplifier from Precision Monolithics. Its crossover point between current and voltage noise lies in the neighborhood of 20 kΩ source impedance, so the circuit is designed with that source impedance. In the configuration chosen, this means that the thermistor has this resistance. We use thermistors with 10 kΩ $\pm$ 25% resistance at 25°C, so that their resistance is near 20 k for typical Oregon conditions, 10°C water.

Once the thermistor is selected, the next problem in design is to develop as much signal in the transducer as possible without introducing significant contamination of the signal by the "anemometer" effect. The anemometer effect is a term for the sensitivity of the temperature of a heated body to flow conditions. If the flow past the body increases, the body is cooled more. Flow in the environment of the thermistor is changed by unevenness in the descent. Precise measurement of this effect for small values of the power dissipated in the thermistor is difficult. We find that for 20 microwatts dissipated, the temperature rise is 19 millidegrees in still water and 14 millidegrees in well-

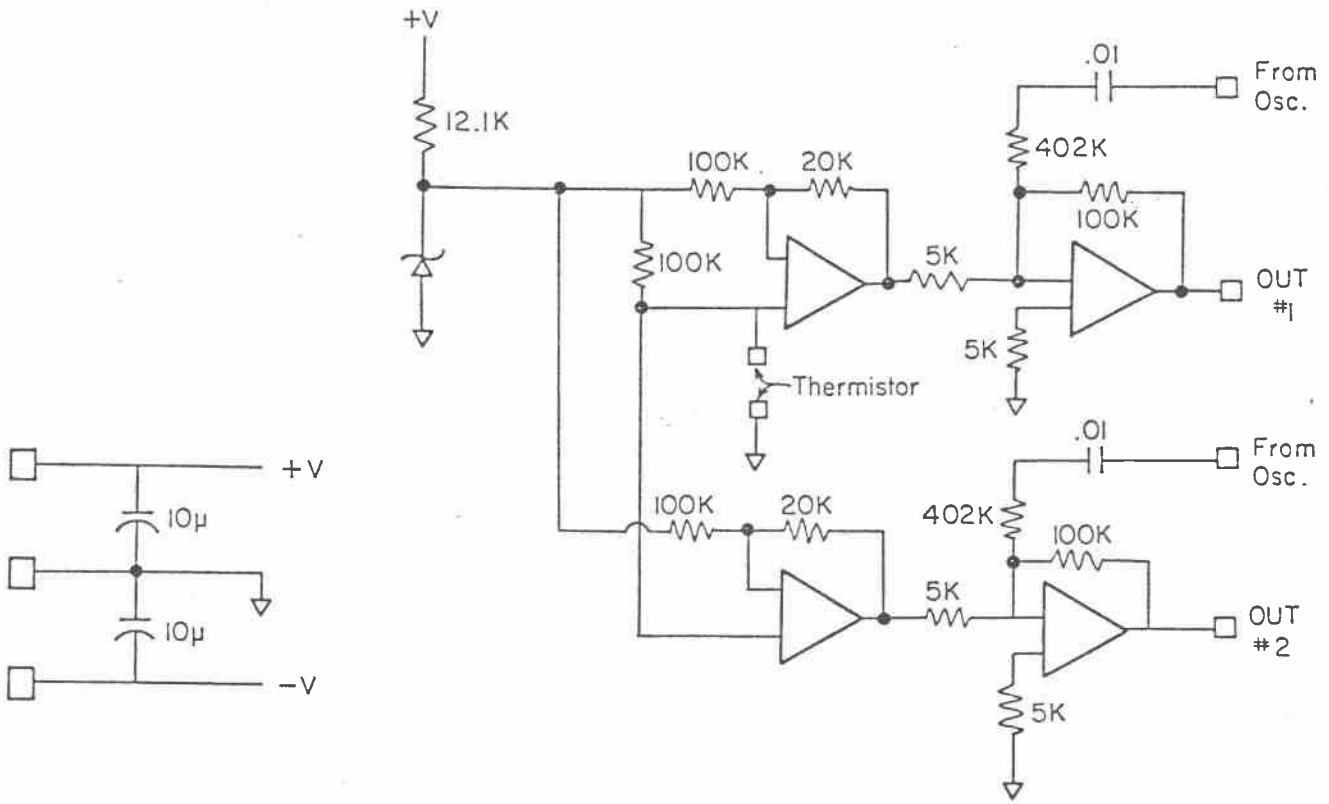

FIGURE III.A.4: Schematic of "redundant" thermistor module. The operational amplifiers are Precision Monolithics OP-07s, the Zener is ICL 8069 CCQ (1.2v).

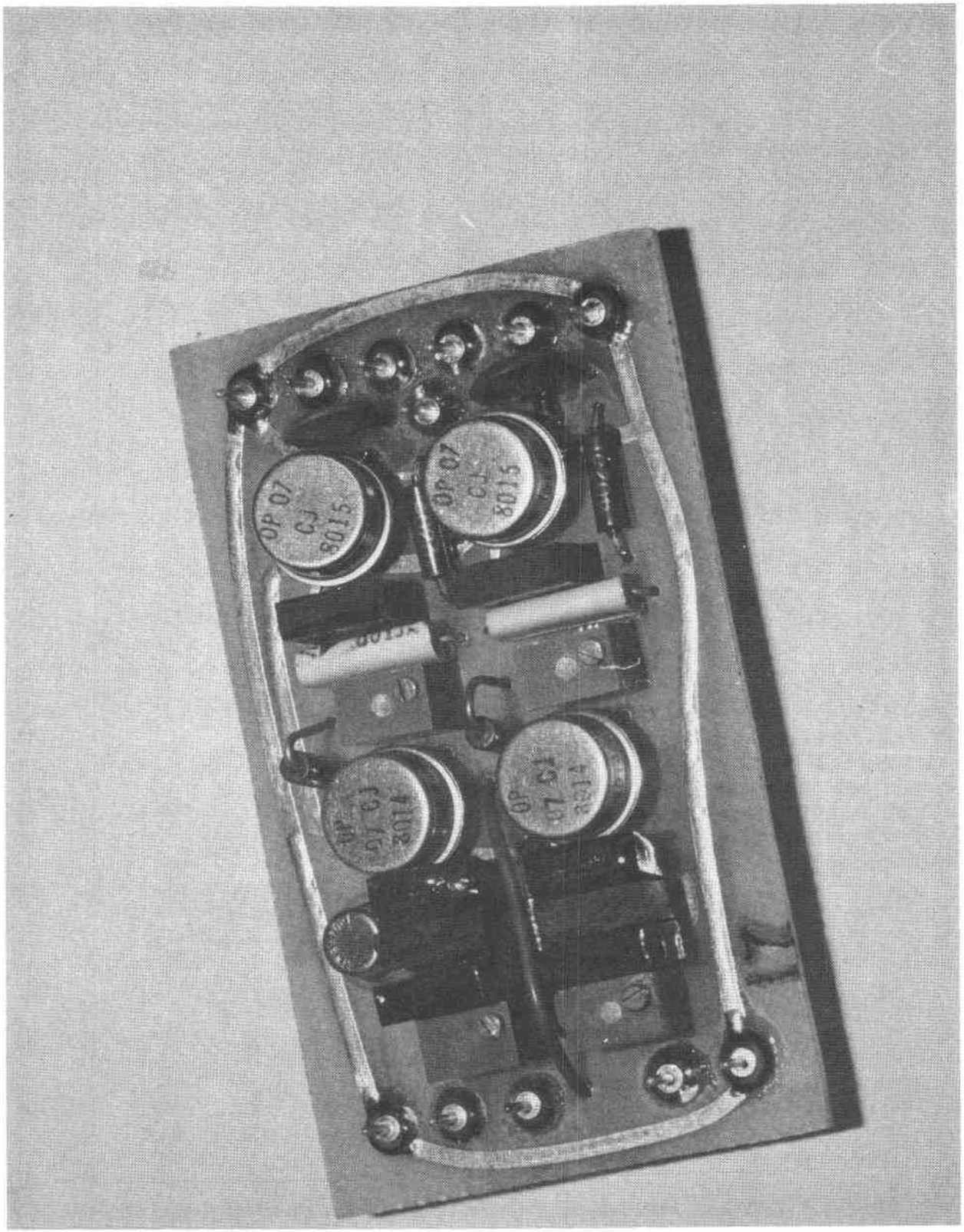

FIGURE II.A.3: Dual thermistor module, unpotted. Before use the modules are cast in epoxy resin.

stirred water. In operation approximately 2 microwatts are dissipated, so we expect that the temperature of the thermistor would rise 0.5 millidegrees if the descent were stopped. Normally the thermistor sees a mean flow of 10 cm s^{-1} with fluctuations of less than 1 cm s^{-1}, and we expect a hot-wire-like square-root variation of temperature vs. flow rate. With these assumptions a vague estimate can be made of the magnitude of the noise introduced. This estimate, 20 microdegrees, is below the noise level of the instrumentation, and so will not matter.

Once the resistance of the thermistor and the power to be dissipated in it are set, the design of a single bridge is straight-foward. We add a second, parallel amplifier (Fig. 12) so that a second data channel is established through which the same information as to the thermistor's resistance is communicated. The only information shared by the two channels is the temperature signal, the noise in the thermistor, and the noise in the reference voltage. The dominate noise source in these circuits turns out to be the first-stage operational amplifiers and, because the amplifiers are different, the noise in the two channels will be incoherent. This allows us to separate the signal from the dominate noise source when the records are processed.

The sensitivity of the bridge-amplifier is independent of frequency in the signal range (0-40 Hz). The FM pressure signal is added to the output for transmission up the data link.

B. Pressure

Because the fluid within the case transmits pressure from the water outside, the pressure transducer can be mounted directly on the circuit board. One type of sensor is used (KULITE PTQH-360) in all applications,

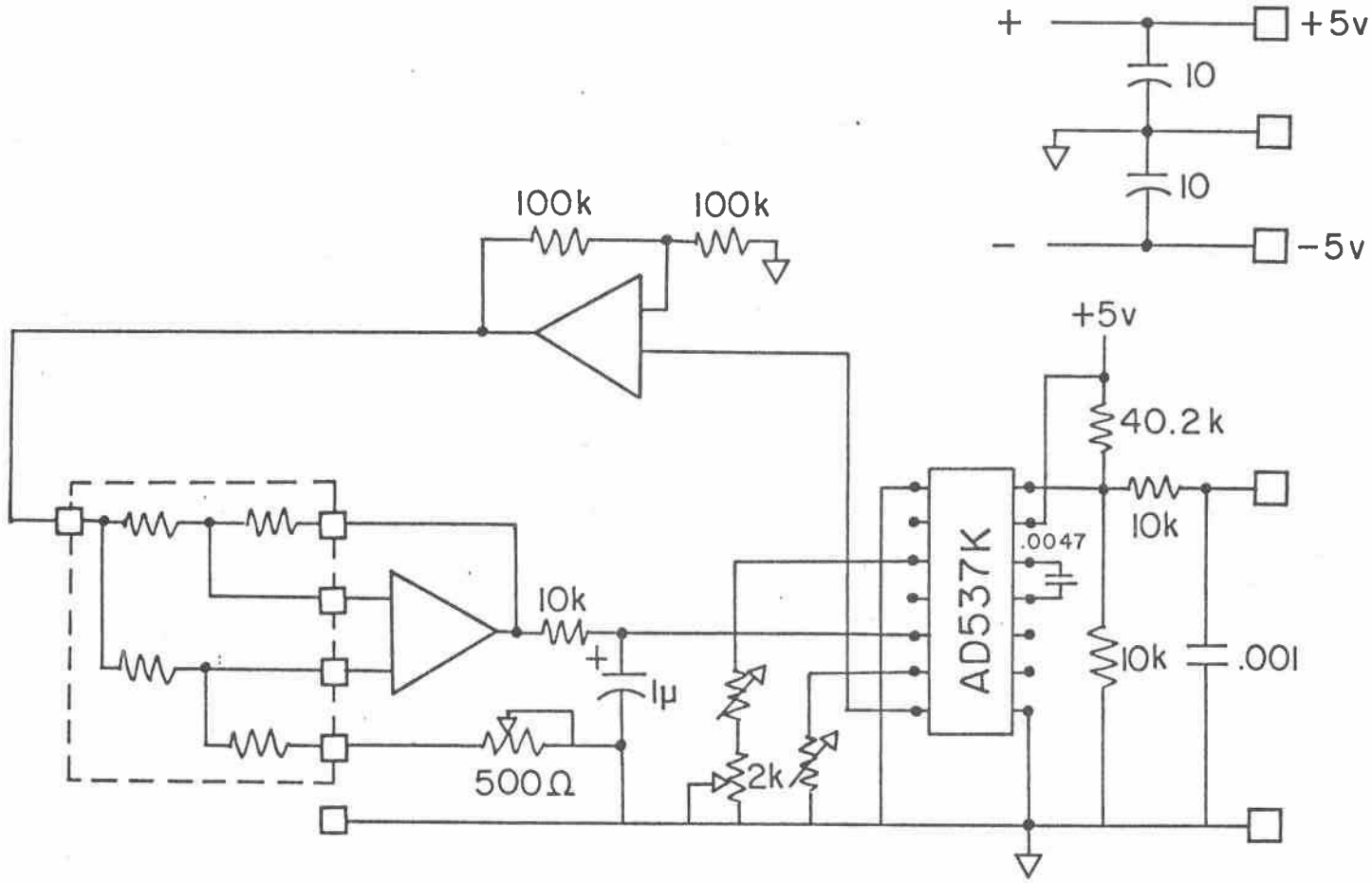

FIGURE III.B.1: Schematic of pressure-controlled oscillator module. The transducer (dotted lines) is a KULITE PTQH-360, which is available with full-scale ranges of 100, 250, or 500 PSI. The operational amplifiers are Precision Monolithics OP-07s. The resistors indicated as variable are selected to match the individual sensor.

but one of three models with different ranges is chosen for a given application. The ranges are 100 PSI (66 m depth), 250 PSI (167 m depth) and 500 PSI (335 m depth). The circuit (Fig. III.B.1) converts the signal from this transducer to an oscillating output with frequency dependent upon the pressure. The frequency varies from 500 Hz at atmospheric pressure to 1300 Hz at full range. The signal is added to the thermistor signal in the probe, then extracted from it again in the shipboard system.

C. Conductivity

The conductivity transducer is purchased from Niel Brown and attached to circuitry of our own design which is described in detail in Appendix C. The transducer is mounted on a plug which is O-ring sealed into the nosepiece. Our experience with this system is described also in Appendix C.

One point not mentioned in the Appendix is the vertical resolution of the transducer. By comparing the conductivity spectrum with the temperature spectrum in a region where conductivity variations are caused almost entirely by temperature, rather than salinity, fluctuation, we find that the averaging length for conductivity is about 8 cm.

D. Optics

E. Heated Thermistors

Our experience with heated-thermistor measurement of fluctuating velocities from the microstructure instrument is limited. Our group has accumulated considerable experience in measuring near-bottom flows from nearly-fixed installations (Caldwell and Chriss, 1979; Chriss and Caldwell, 1981a; Chriss and Caldwell, 1981b). Until recently we have felt that our relatively light and flimsy instrument would impart so much random motion of its own to whatever sensor was used that the signal would be swamped. This notion was confirmed in a trial made several years ago. We are trying again, however, for two reasons: (1) The change to a vented drag-plate, made to allow pop-up operation, seems to produce a smoother motion, and (2) The urgency of our desire for velocity-fluctuation information has increased.

The heated-thermistor transducers are precisely like the temperature probes, except that thermistors of much lower resistance (500 Ω) are substituted. The circuitry is changed so that the thermistor is over-heated by 20°C (Fig. III.E.1).

Calibrations are carried out in an annular tank which surrounds a rotating table. The transducers are mounted on an arm extending from the table, and the speed of the table is sensed optically as it rotates. The formula

$$\frac{P}{\Delta T} = A + BU^N$$

is used to fit the calibration data, and calibration are run at various temperatures. Here P is the power dissipated, ΔT is the temperature rise in the thermistor, U is the velocity, and A, B and N are determined by the calibration data.

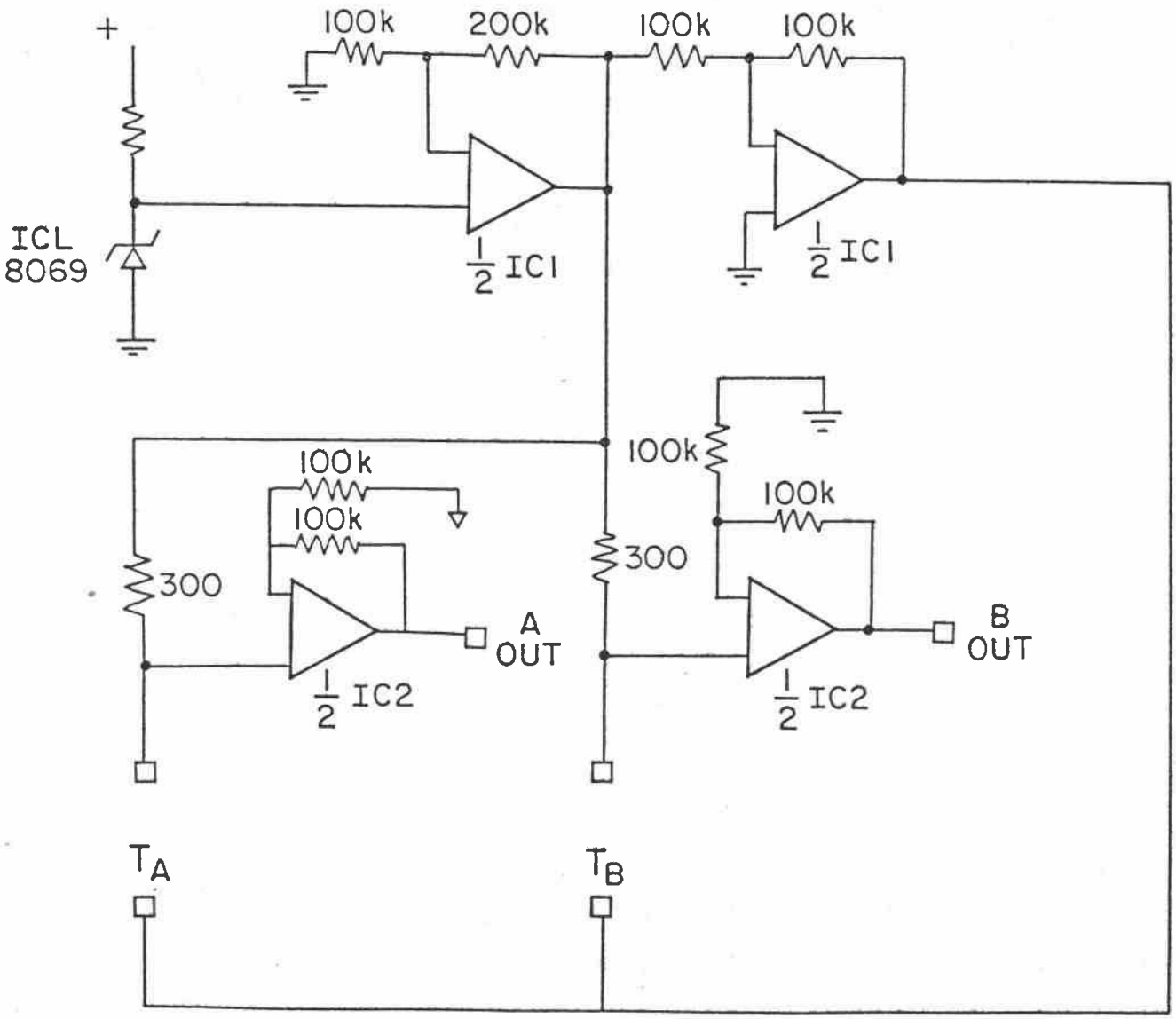

FIGURE III.E.1: Schematic of dual heated-thermistor module.

F. Voltage Regulator

To prevent the slow decline of the battery voltage from affecting the signal circuitry, the power supply for the circuitry is regulated at ±5.1 v. Magnet-actuated normally-on reed switches allow all power to be shut off when the instrument is not is use (Fig. III.F.1).

G. Batteries

We have found that ordinary 9v alkaline "transistor" batteries function quite well under pressures at least as great as 2000 PSI. Their capacity is large enough at above-zero temperatures to allow continuous operation for at least 10 hours (Fig. III.G.1). Except when the instrument is in the water or under test the power is turned off by application of a magnet to the case (see Section III.F) so the period between battery changes is much longer.

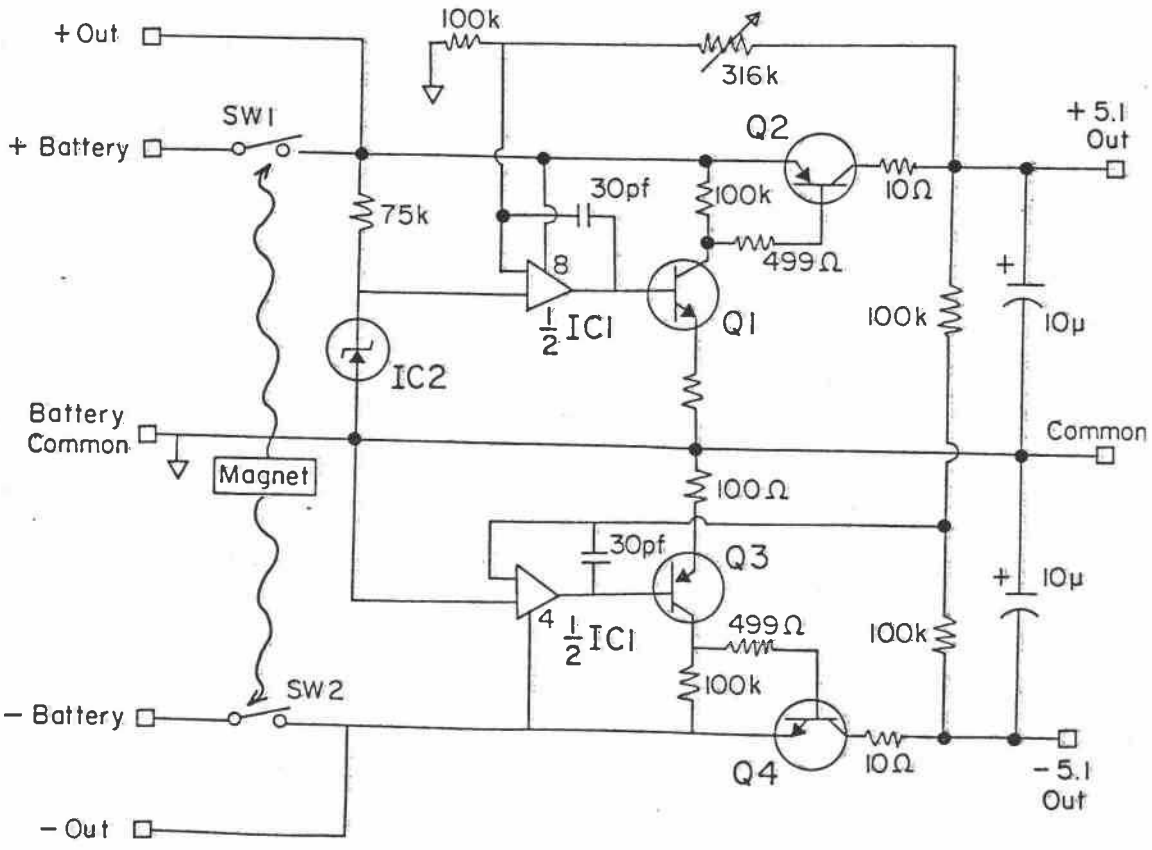

FIGURE III.F.1: Schematic of voltage regulator in probe. A magnet applied externally to the case turns off the power to conserve batteries. IC1: TIL022P; IC2: ICL 8069 CCQ; SW1,2: Hamlin MTR-2-185; Q1, Q4: 2N2222A; Q2, Q3: 2N2906A.

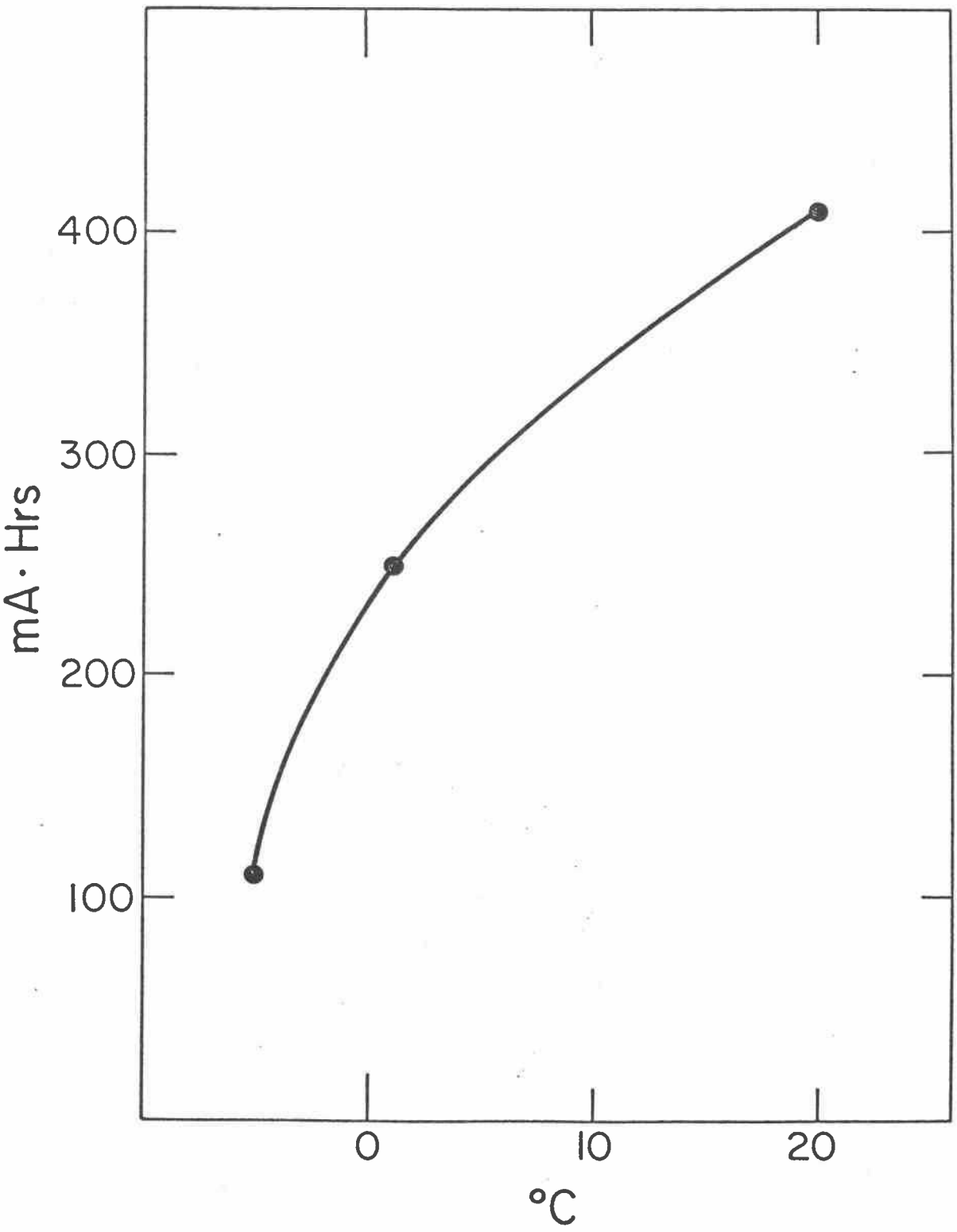

FIGURE III.G.1: Results of battery-life tests on 9v Mallory alkaline batteries. The load drew approximately 10 mA.

IV. ON-BOARD SYSTEM

The signals from the data-link pass through slip rings and are carried through a shielded cable to the on-board processing system. A high-impedance (2 mΩ) differential amplifier receives the signals (Fig. IV.1). Because of this high impedance in the amplifier, the signals are attenuated very little in the data-link. Even so, this attentuation is taken into account in numerical processing. After the input amplifer, the signal is split, a full-bandwidth signal going to the FM discriminator, and the signal to be used for temperature continuing through a 6-pole, 40 Hz low-pass filter. This filter is necessary to remove the 60 Hz noise ubiquitous aboard ships as well as the FM carrier. After the filter, the signal goes through a gain-offset amplifier and is recorded as a representation of the temperature. Because the analogue-to-digital converter in the older data-acquisition system has only 12-bit resolution, temperature can be recorded with a precision of only 4096^{-1} of the range. Therefore fluctuations are recorded as the time derivative of the signal, again filtered at 40 Hz.

The unfiltered signal is sent to the discriminator, which converts the FM signal into a voltage for recording. Also, to obtain a direct indication of descent rate this voltage is differentiated and filtered and recorded separately.

A. Input Amplifiers

We have been told that d.c. dignals cannot be successfully run through an XBT-wire pair. Our experience has been that they can, and in fact when the wire deteriorates sufficiently that the d.c. signals are affected, the FM signals are affected as well. Possibly our success is

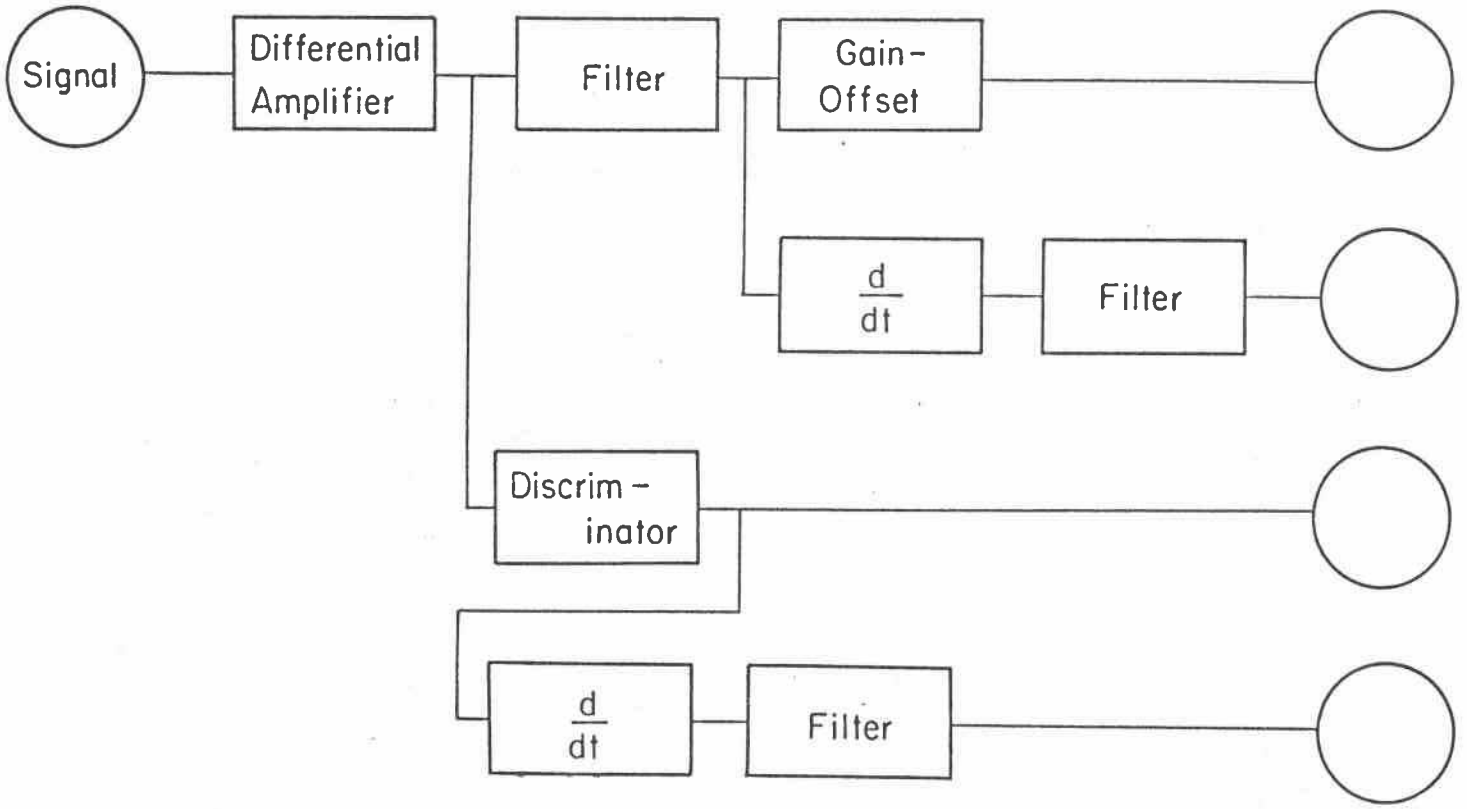

FIGURE IV.1: Block diagram of one channel of shipboard system. The circles at right represent inputs to the data-acquisition system.

due to the way the signal is driven and received. The signal is driven directly from an operational amplifier's output, which has an exceedingly low impedance. It is received by a high-impedance differential amplifier. With this system, the only serious difficulty is caused by radio interference. Radio transmission from the ship completely ruins the signal.

The amplifier is just a simple one, using operational amplifiers in a standard configuration (Fig. IV.A.1).

B. Filters

The object of the filters is to remove 60 Hz noise while admitting as wide a signal bandwidth as possible. The six-pole Butterworth filter (Fig. IV.B.1) gives a sharp cut-off at 40 Hz. With this value of the cut-off frequency, most of the recording bandwidth (45 Hz Nyquist) is filled with usable signal but 60 Hz noise is reduced by a factor of 10 (Fig. IV.B.2).

C. Gain-Offset Amplifiers

Because some of the waters we profile are cold and others quite warm at the surface, and because very small gradients must be measured in well mixed layers whereas large gradients are found below, we adjust the gain and offset to fit the circumstance, usually recording at two different gains so that one channel has the closest possible resolution for recording the mixed layer and the other has sufficient range to cover the thermocline. These amplifiers are of simple design and have no frequency-dependence in the signal band (Fig. IV.C.1). Gain is settable from 1 to 1000, input offset from -5 to +5 volts.

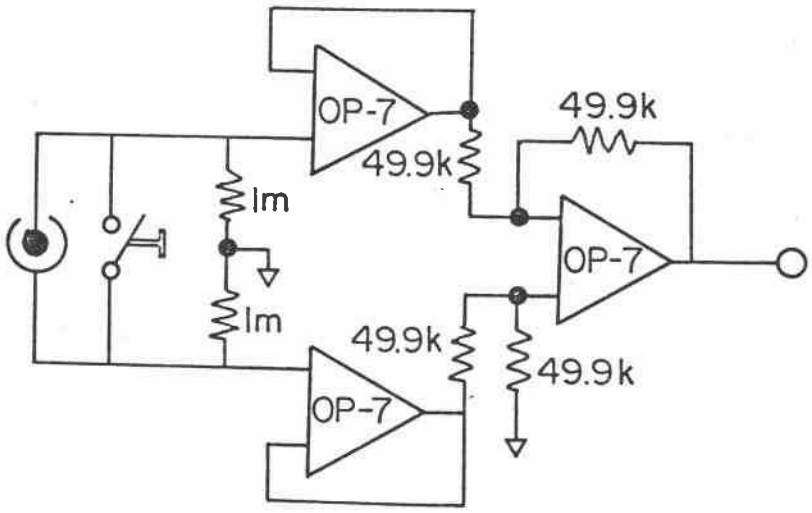

FIGURE IV.A.1: Schematic of differential amplifier. The switch is depressed to check offsets through the system.

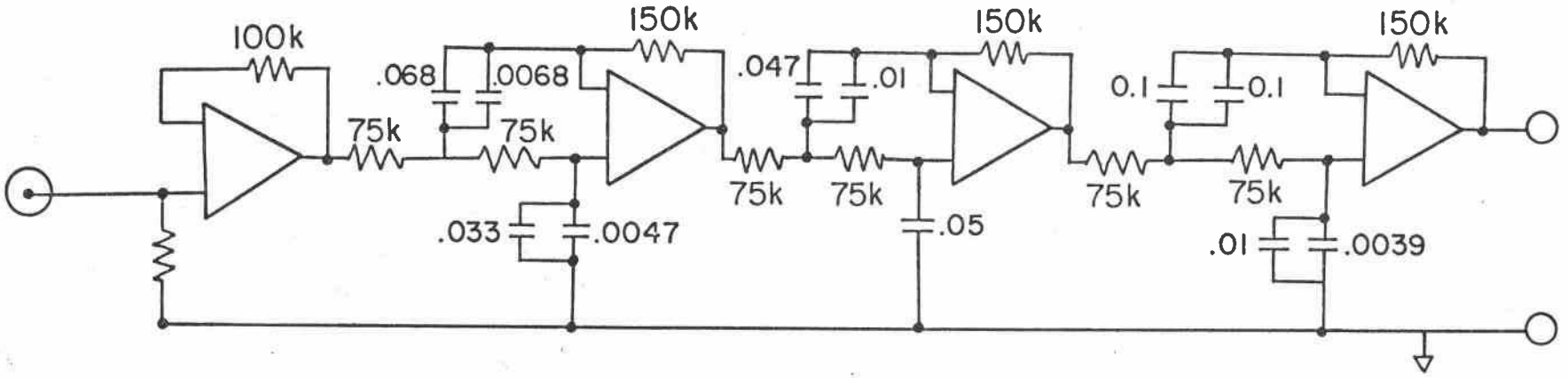

FIGURE IV.B.1: Schematic of 40 Hz filter.

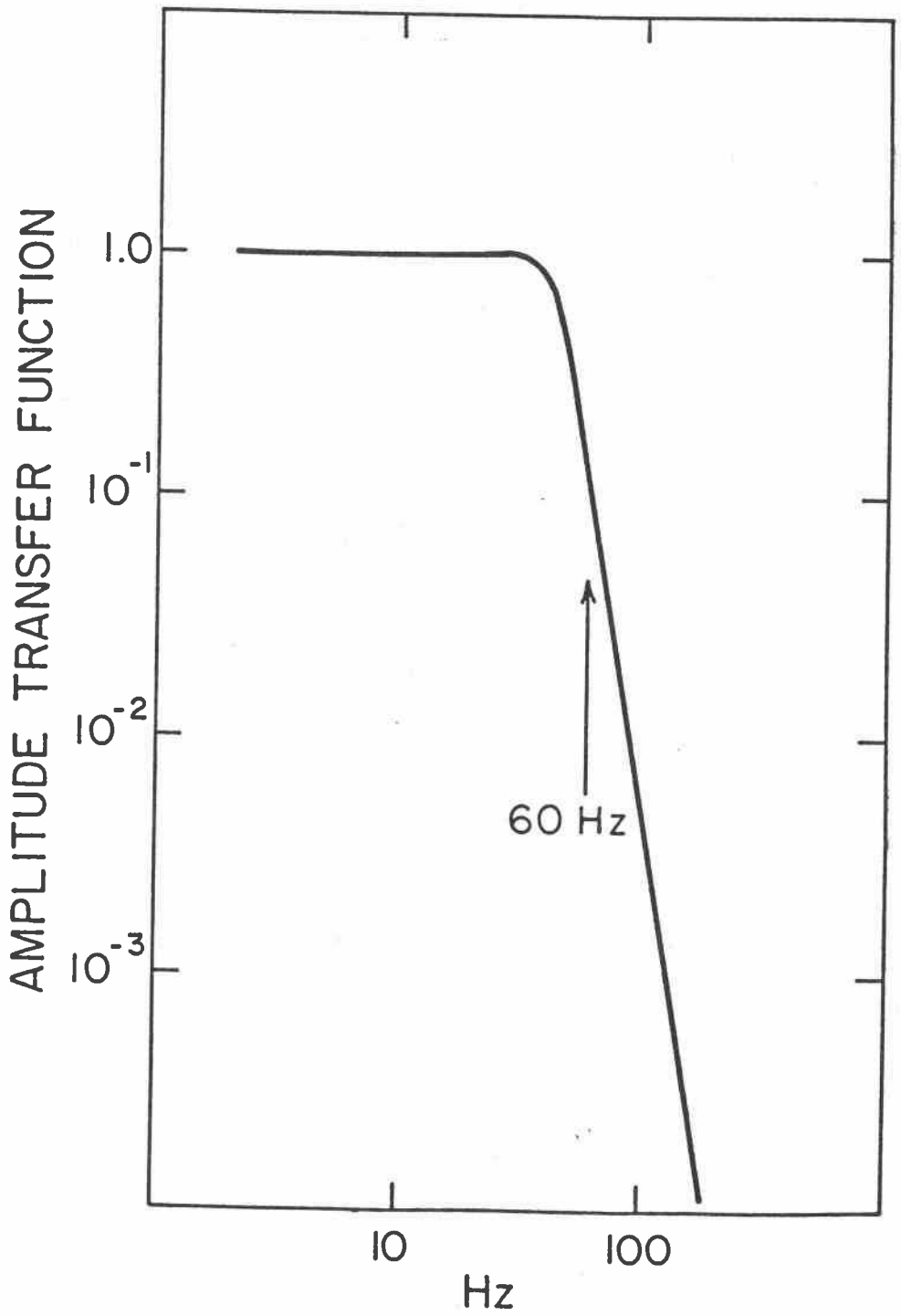

FIGURE IV.B.2: Amplitude transfer function of low-pass filters.

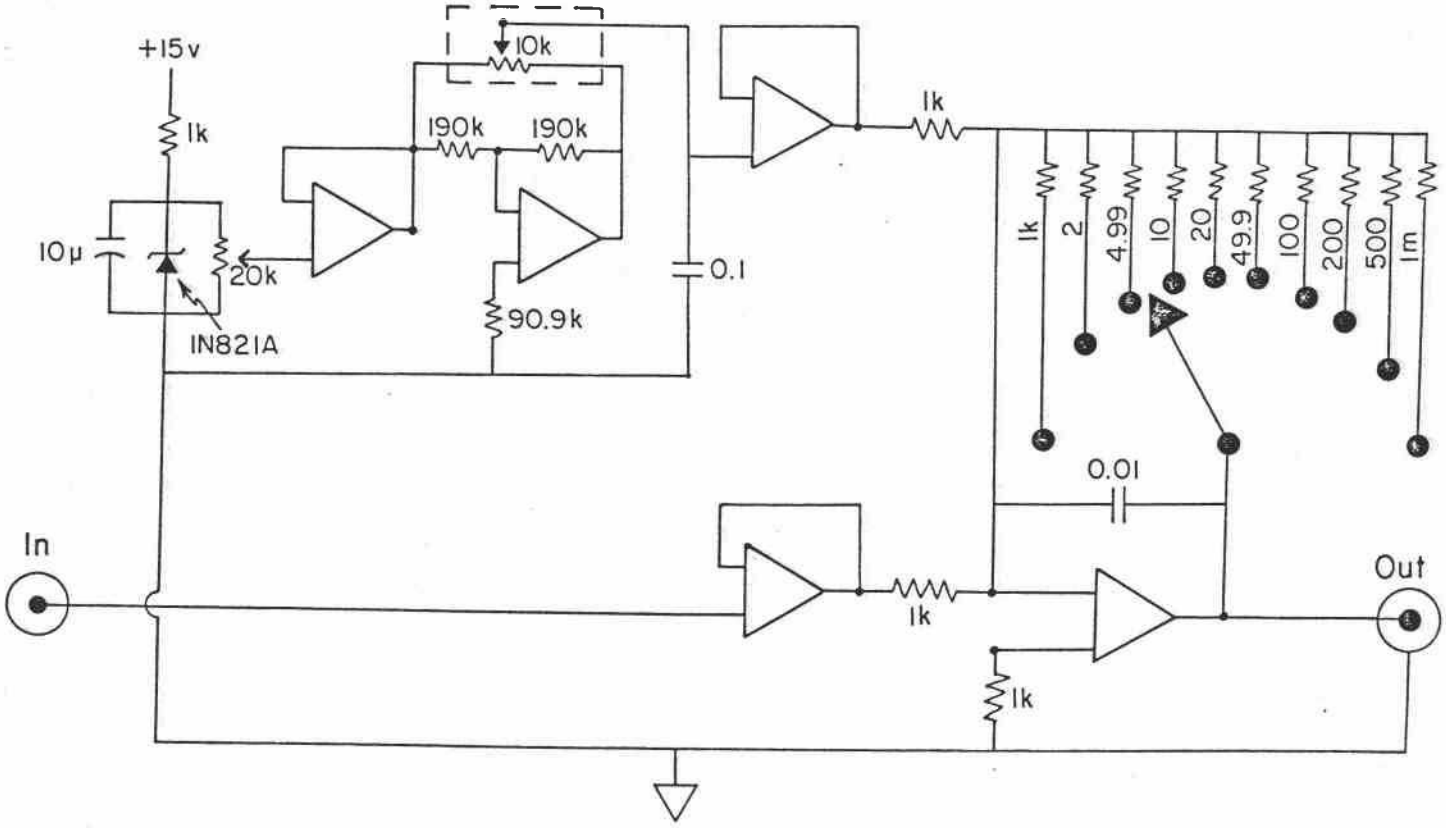

FIGURE IV.C.1: Gain-offset amplifier. The operational amplifiers should be Precision Monolithics OP-7s or the equivalent.

D. Differentiator

Ideally a differentiator would differentiate perfectly in the signal band and attenuate elsewhere. A simple circuit (Fig. IV.D.1), with variable gain, combines with the filters to approximate the ideal (Fig. IV.D.2).

E. FM Discriminator and Pressure-Differentiator

The discriminator takes the FM signal and converts it to a voltage for recording by the data-aquisition system (Fig. IV.E.1). The gain is usually set for a range of 0-200 m, so that the least count recorded is 5 cm. Descent rates over 5 m or greater scales are calculated by differencing the pressure record. To make possible speed determination on shorter scales, a differentiated version of the signal is recorded as well (Figs. IV.E.2, IV.E.3).

F. Data-Acquisition System

In this summer of 1981 we are in a state of transition between two data-acquisition systems. The older one is a hard-wired home-built system designed in 1974. It is inflexible and has but 12-bit resolution, but has served us well and will continue to be used on lakes and as a backup. The new system is based on an LSI-23 processor. It will have 16-bit resolution and a programmable data format. The older system will be described because the configuration of the new one has not been precisely established.

In the old system, a sequence of ten 12-bit words are recorded on the magnetic tape ninety times per second, so the basic Nyquist frequency is 45 Hz (Fig. IV.F.1). Six of these words (1,2,3,6,7,8) represent data

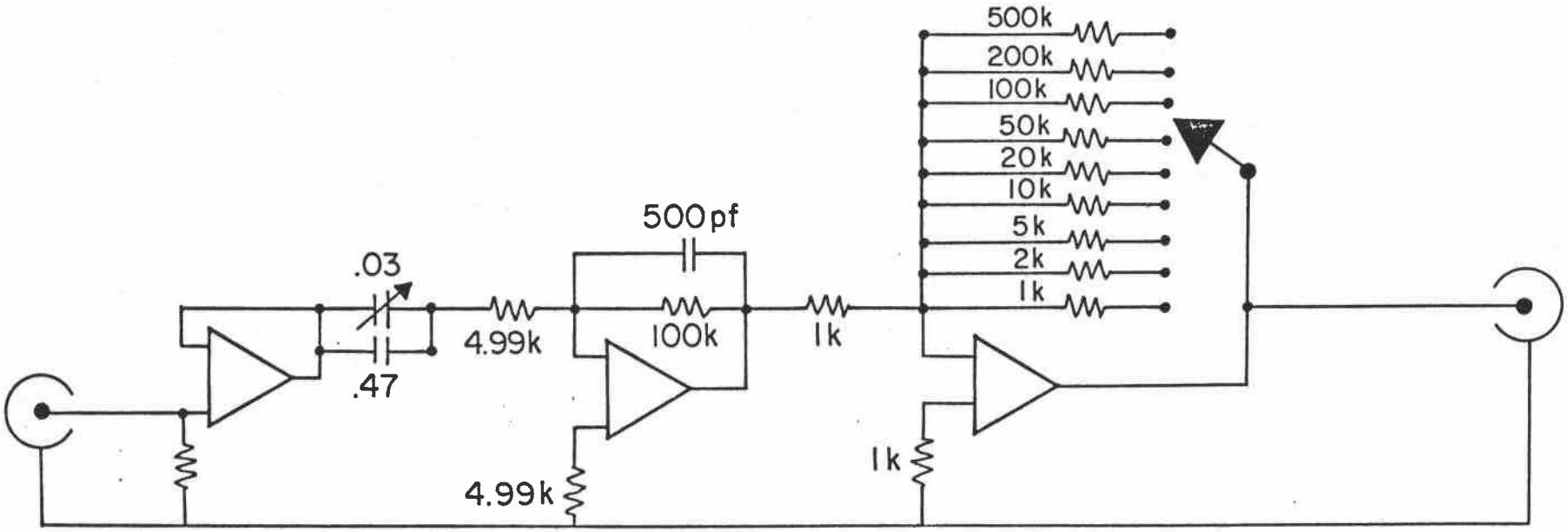

FIGURE IV.D.1: Schematic of differentiator.

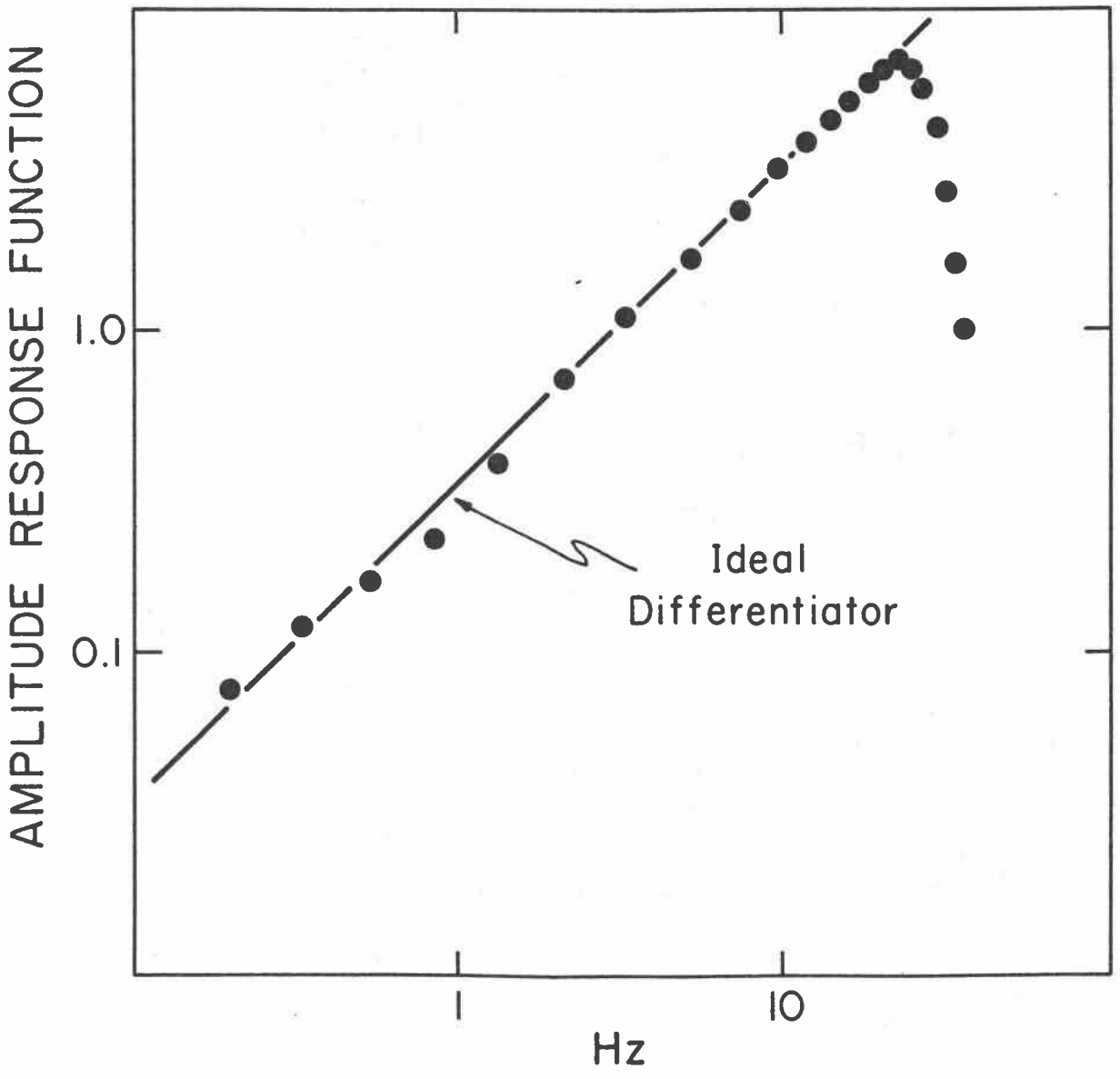

FIGURE IV.D.2: Response of differentiator circuit.

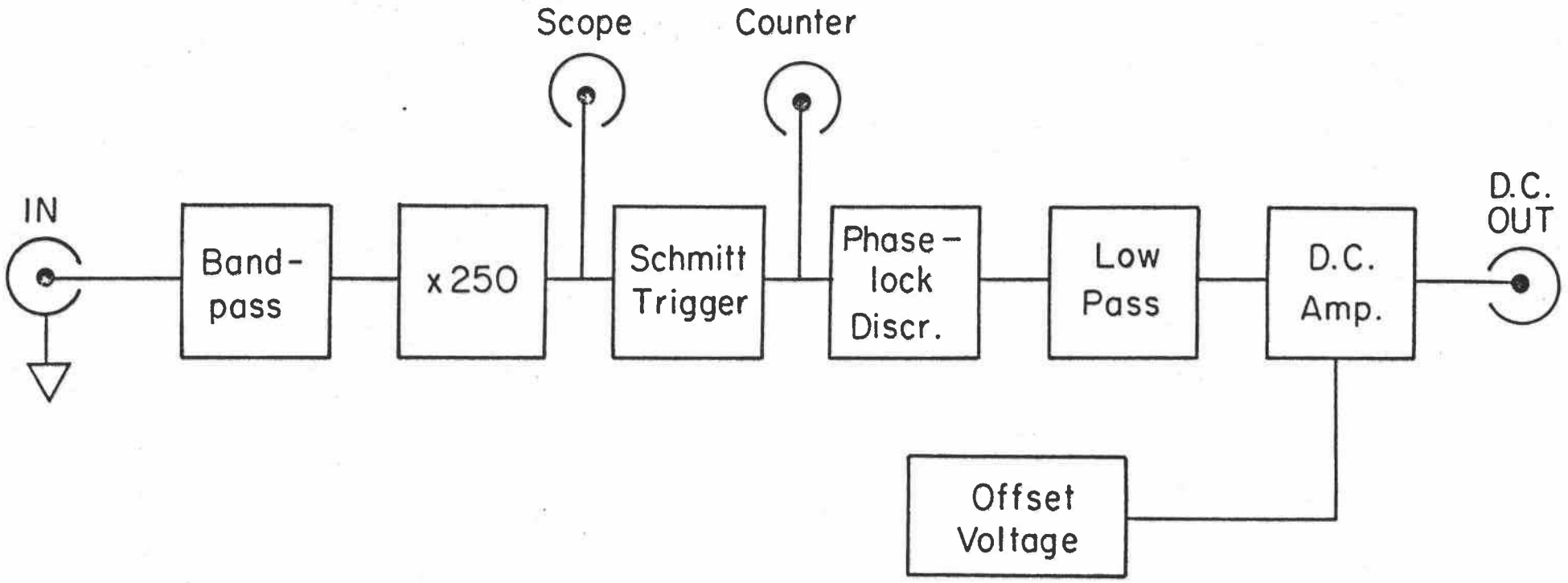

FIGURE IV.E.1: Block diagram of discriminator used to demodulate the FM pressure signal. The frequency is 500 Hz at atmospheric pressure. It rises to 1300 Hz at full scale.

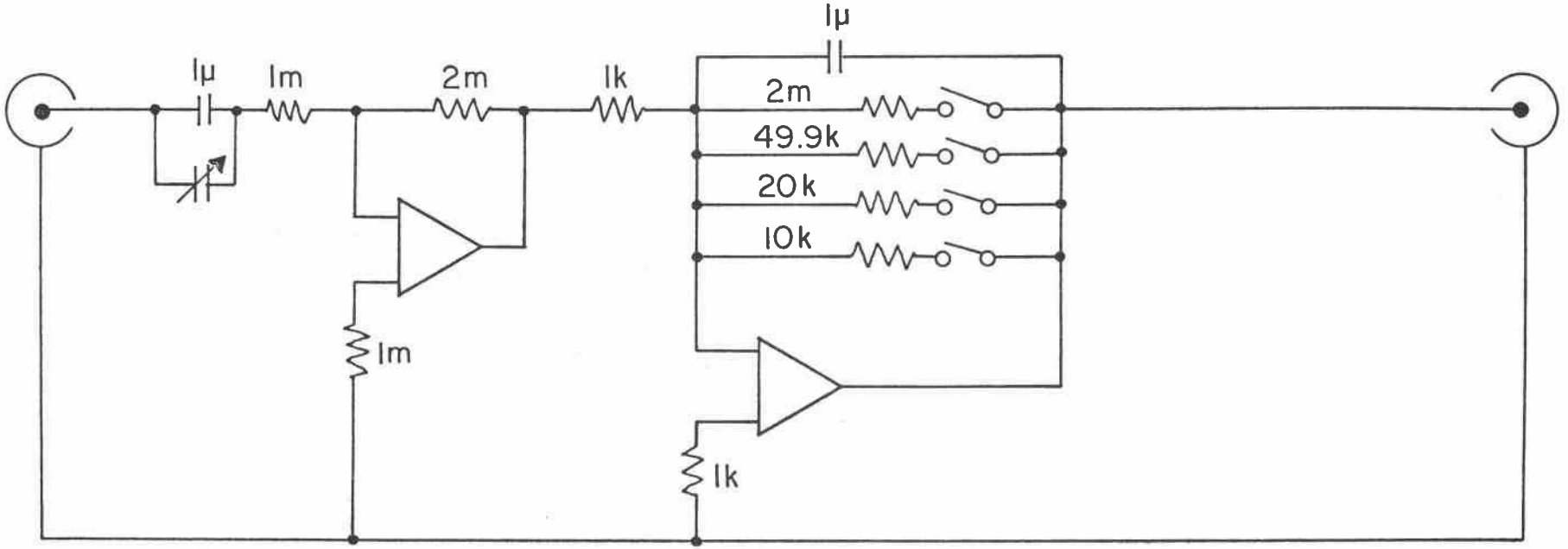

FIG. IV.E.2: Schematic of pressure-differentiator circuit. The output is proportional to the speed of the probe with respect to sea level.

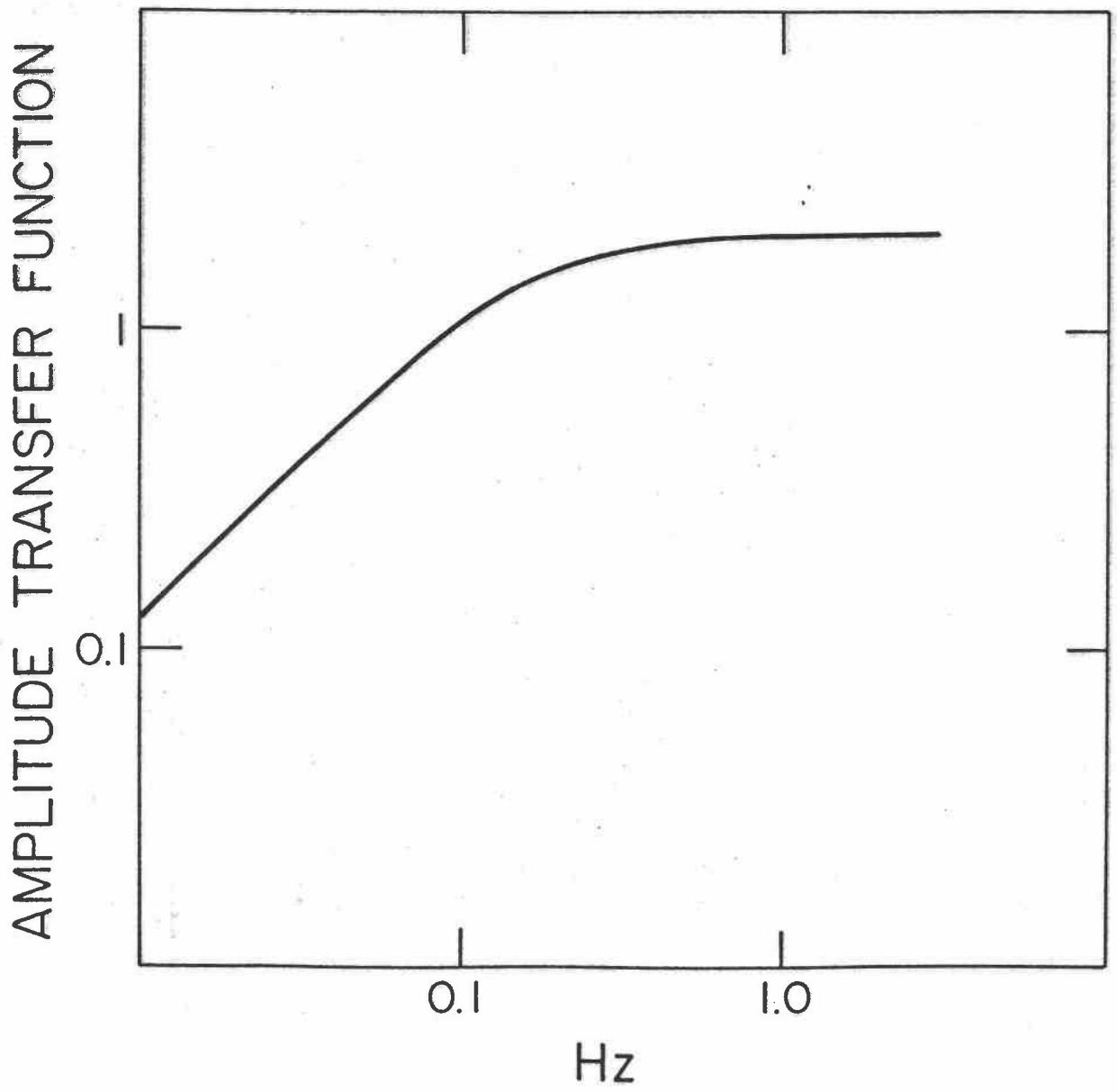

FIGURE IV.E.3: Response of pressure-differentiator circuit.

channels. One (Word 4) simply counts, incrementing once each time a sequence is recorded. Word 5 is subcommutated for recording at a rate 8 times slower. Three data channels are included in the subcommutated set. Words 9 and 10 are check words.

Thus the system accepts 9 analogue inputs. It records six of them at the 90 per second rate and three of them eight times slower. "Fast" words are usually devoted to: temperature derivative (#1,#2,#3), temperature (#4 and #5), and pressure derivative (#6). "Slow" words are used for conductivity (#7), low-gain temperature (#8) and pressure (#9). Because the words are written on the tape at even increments of time, 1/900 seconds between words, successive channels in the same scan are not synchronous, and account of this fact must be taken in computations.

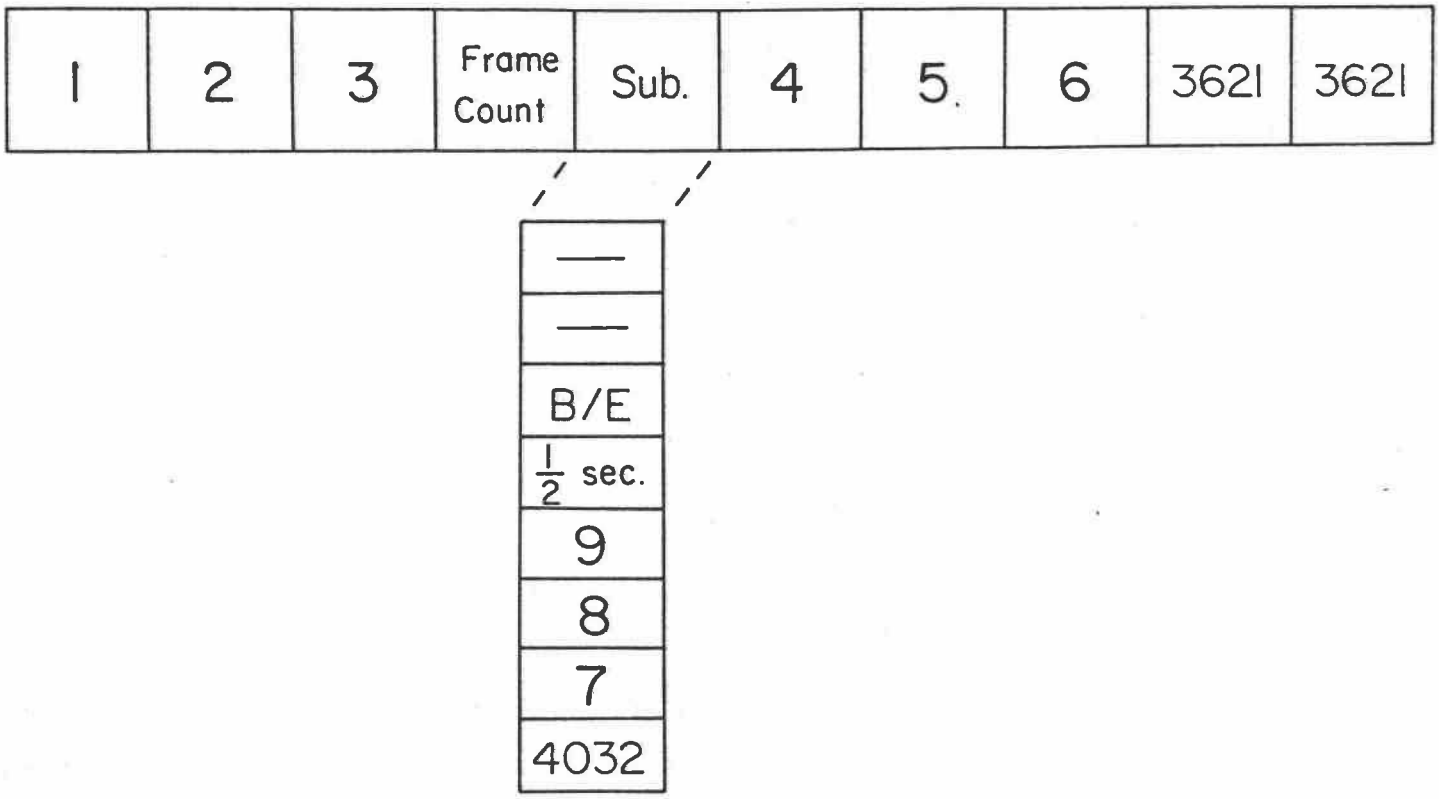

FIGURE IV.F.1: Data Format. Inputs 1-6 are recorded each scan, inputs 7-9 are subcommutated, recorded once each 8 scans. Each word is 12 bits. The B/E word records a manually-entered file ("batch") number in its first 6 bits and a manually-entered "event" number in its last 6 bits. The 3621s and 4032s are check characters.

V. TEMPERATURE-GRADIENT CALCULATIONS

The temperature profile in the water column is sensed by a thermistor which has attenuated response in the signal band. The thermistor resistance is converted to a voltage, amplified, filtered to remove noise, differentiated, filtered again, and then recorded. To calculate from the recorded time-series the original temperature-gradient requires knowledge of the transfer function of each stage. The characteristics of the circuitry have been discussed above, and will be discussed again as they affect processing of the gradient signals, but the most important transfer function, and the hardest to determine, is that between water-temperature and thermistor-resistance.

Calibration of resistance vs. temperature is straight forward when the thermistor is allowed to equilibrate with water temperature. A platinum resistance thermometer provides a standard, and even with various problems such as bath-stirring and heat leaks, an accuracy of 0.01°C is maintained. All readings and calculations are done with a precision of 0.001°C, and the system circuitry is calibrated to 0.001°C, so the estimate of 0.01°C absolute accuracy is conservative. Procedures will be described below.

Sensitivity of the thermistor to transient signals is not so easily determined. Its response is signficiantly attenuated in the signal band, so correction for the variation of response with signal frequency is essential. The length-scales of interest are so short that the determination is difficult at the higher frequencies. We have used two quite different methods. The results of these methods are compared with a determination by M. C. Gregg.

The frequency-dependent characteristics of the circuitry must also be taken into account, as described below.

A. Signal Expected

As a guide in estimating the temperature fluctuations to be encountered in natural waters, we use G. K. Batchelor's (1959) prediction of the wavenumber spectrum of a passive contaminant in turbulent flows. The question of the applicability of his concept to the ocean is discussed in Appendix B. His result is that features will rarely be found thinner than $(\nu D^2/\varepsilon)^{1/4}$. Here ν is the kinematic viscosity, approximately 0.01 $cm^2\ s^{-1}$ for water, D is the thermal diffusivity, approximately 0.001 for water, and ε is the kinetic energy dissipation per unit mass. Vastly different values of ε are encountered in natural waters and its measurement is not routine. However nearly all measurements fall between 10^{-6} and $10^{-2}\ cm^2\ s^{-3}$. Hence we expect the smallest scales to be measured to vary from 0.03 cm in the most energetic regions to 0.3 cm in the quietest (Fig. V.A.1). Corresponding spatial frequencies are 0.5 to 5.0 cycles/cm (Fig. V.A.2). If fluctuations of these scales are encountered by an instrument moving at the rate of 10 $cm\ s^{-1}$, the corresponding times of passage are 0.003 secs to 0.03 secs, 3 to 30 milliseconds. Corresponding frequencies are 5 to 50 Hz (Fig. V.A.3). So the desired bandwidth extends to 50 Hz. But the response of our thermistors cuts off with a 3-db point in the neighborhood of 7 Hz. For only the least energetic region are corrections not necessary. Indeed, working backward through this calculation it can be seen that the limitation of our maximum signal bandwidth to 40 Hz restricts full-signal resolution to regions in which ε is less than 0.004 $cm^2\ s^{-3}$. In fact because of limitations on

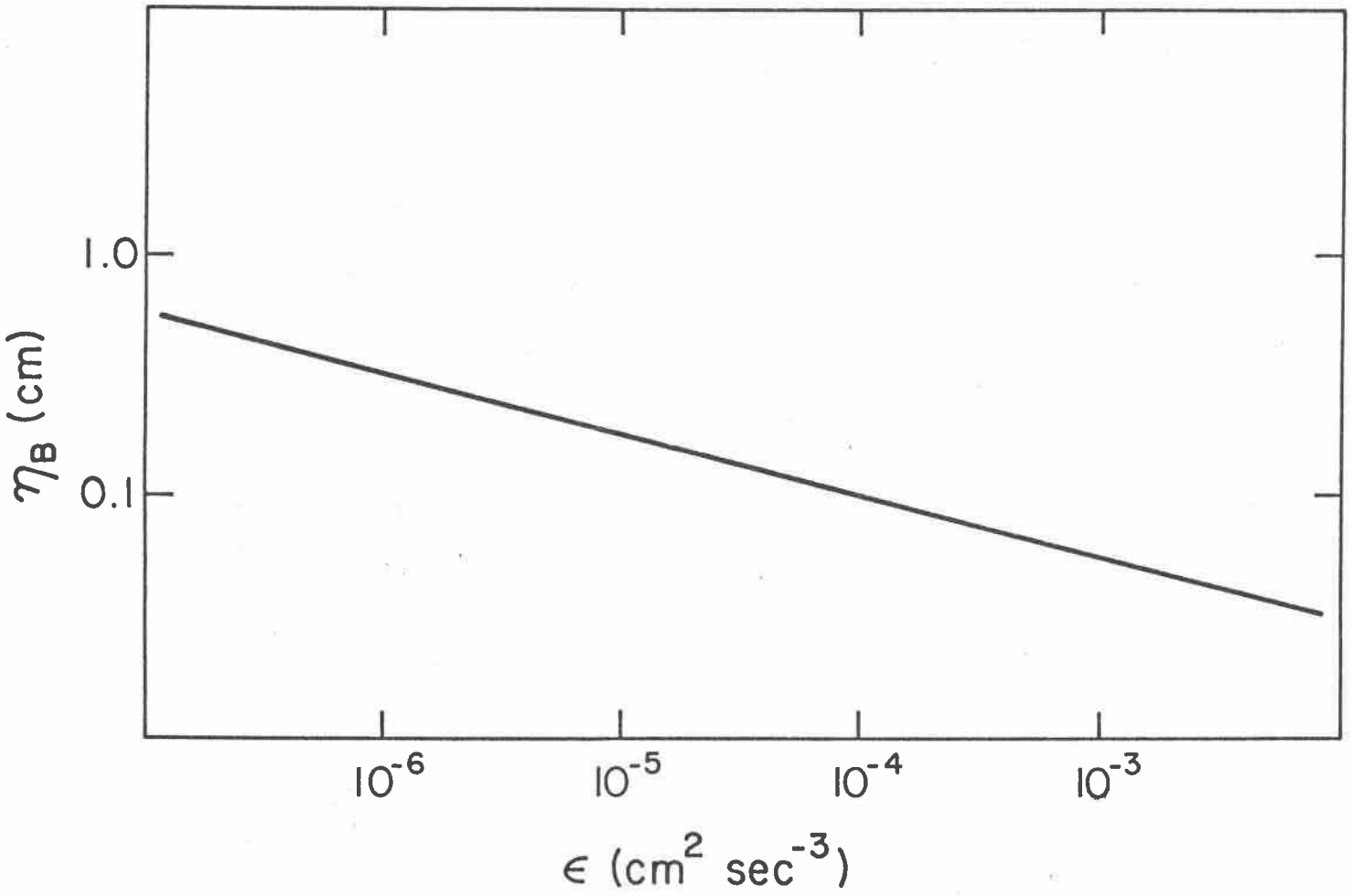

FIGURE V.A.1: Estimate of extent of thinnest temperature features vs. kinetic energy dissipation rate, ϵ, according to G.K. Batchelor's prediction.

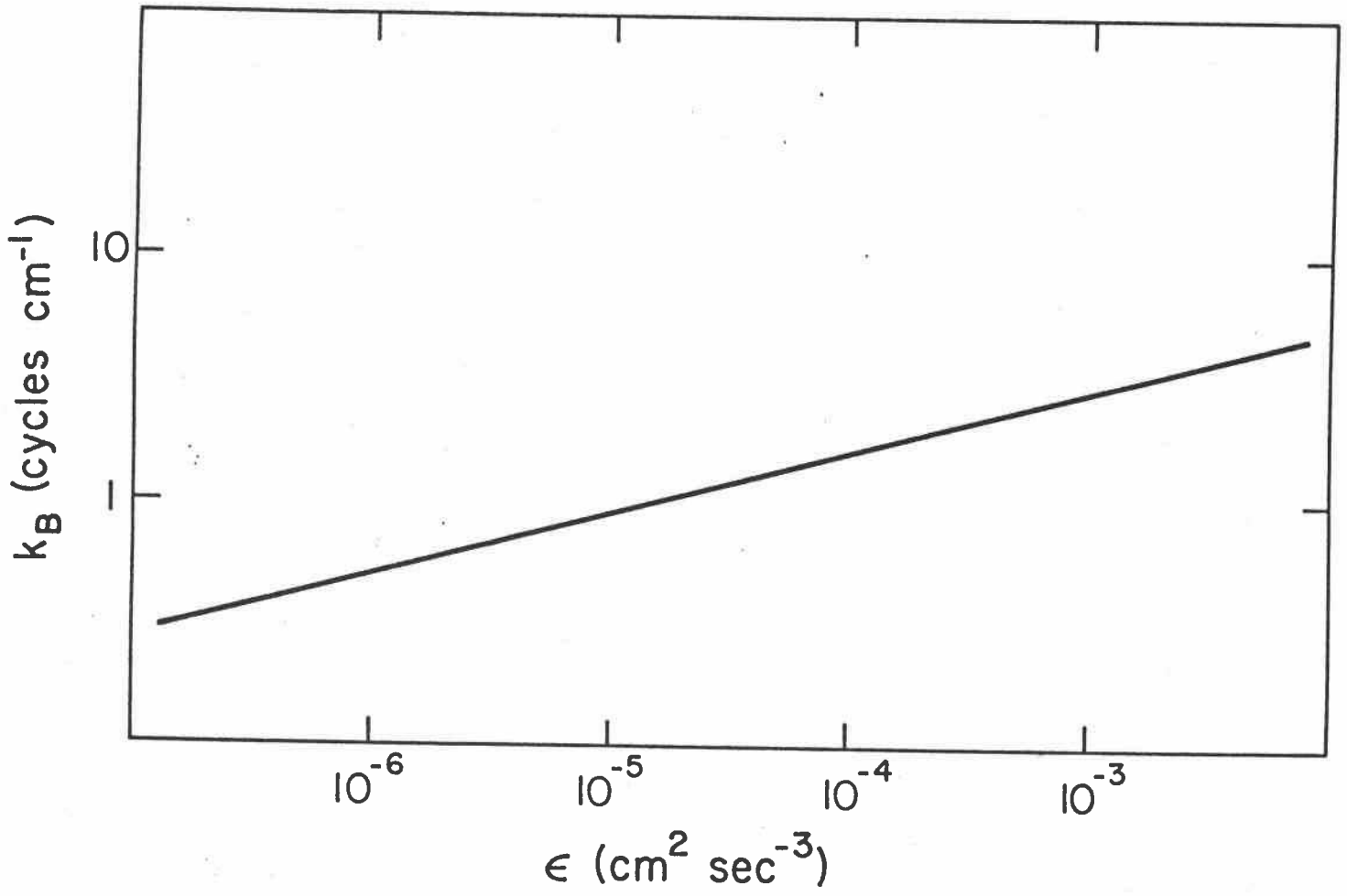

FIGURE V.A.2: Estimate of cut-off wave number, in cycles/cm, vs. kinetic energy dissipation rate, ε, according to G.K. Batchelor's prediction.

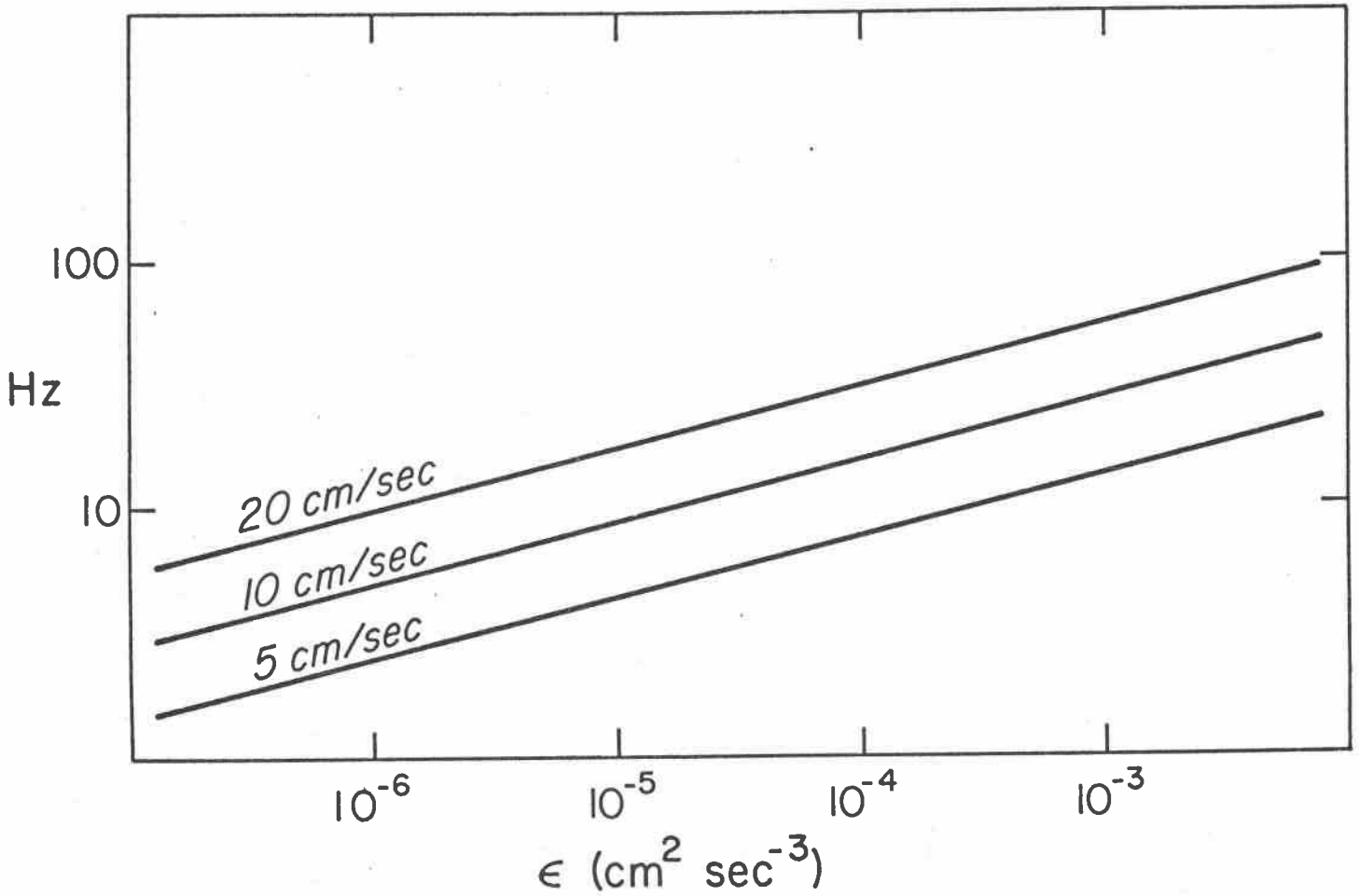

FIGURE V.A.3: Bandwidth required to fully resolve temperature-gradient spectrum vs. kinetic energy dissipation rate, ε, for three rates of descent of the observing instrument, according to the prediction of G.K. Batchelor.

the accuracy of determinations of thermistor corrections, we usually restrict the bandwidth for computations to 30 Hz, for which ε is .0013 $cm^2\ s^{-3}$. Fortunately .0013 is usually exceeded only very near the sea surface.

One might think of slowing the instrument's speed to narrow the required bandwidth in high-energy regions. Unfortunately these are just the regions where the turbulence intensity is highest. The descent rate must be kept far greater than the turbulence velocities to avoid smearing the spectra, so we cannot slow down too far.

B. Equilibrium Calibration vs. Temperature

The basic calibration vs. temperature is a two-stage process. First the resistance vs. temperature characteristic is determined for each thermistor probe. Then the output voltage vs. resistance curve is determined for each bridge module. Using this procedure any transducer can be used with any bridge module, without calibrating each combination. The resistance of each thermistor is measured for a dozen or so temperatures from 0 to 25°C in a stirred bath. The temperature is measured with a platinum resistance thermometer. These data are fit to the formula

$$R(T) = R(4°)\ \exp[\beta(\frac{1}{273 + T} - \frac{1}{277})]$$

where R(T) is the resistance at temperature T, and R(4°) and β are determined by a least-squares fit. Discrepancies between fit and data points are typically a few millidegrees.

The bridge modules are then calibrated as voltage output V(R) vs. resistance R, fitting to the formula

$$V(R) = \frac{R_o - R}{A - B(R_o - R)}$$

Here A, B and R_o are determined by a least squares fit.

Finally these formulas are combined, for specific gain and offset settings of the onboard processing system, taking into account the calibration of the A/C, into a quartic formula for calculating temperature from the numbers on the tape.

The above procedure gives also the factor for converting recorded numbers to temperature gradients, but for the gradients, time-response must be taken into account. This is done in the frequency or wavenumber domain - we have not had use for corrected time series.

C. Thermistor Response: Jet Tests

The standard method for determining the response characteristics of thermistors was originated by Fabula (1963). In this method the sensor is traversed through a plume generated by a heated wire or wires. The shape of the plume is mapped by passing the sensor very slowly through it. The sensor is assumed to see the same signal when passed rapidly through it (even though plumes characteristically fluctuate). The response function of the sensor is then calculated by comparing the frequency spectrum obtained on the fast traverse with the frequency spectrum a probe moving at the fast speed through the mapped plume would see. The response is dependent on traverse speed.

The highest wavenumber to which the response can be determined is fixed by the accuracy of mapping and the repeatibility of the plume shape.

To push this technique higher in frequency, we replace the heated wire plume with a thin, gentle laminar jet. Warm, dyed water is fed

through a slit 0.05 cm wide in the direction of traverse. The sensor passes 0.2 cm above the nozzle. This jet is much narrower than a plume, and has a near-Gaussian shape. Its bandwidth in wavenumber space is 5.3 cycles/cm (3-db point), so its spectrum is very nearly flat in the signal band. Because the jet signal covers the desired signal band without significant attenuation, the computation of probe response amounts to little more than inspection of the frequency spectrum from the thermistor (Fig. V.C.1). Several forms have been fit to 10 cm s^{-1} traverses:

$$[1 + af^2 + bf^4 + cf^6]^{-1}$$

where $a = 2.64 \times 10^{-2}$, $b = -2.19 \times 10^{-6}$, and $c = 3.26 \times 10^{-8}$ and

$$\{[1 + (\frac{f}{f_1})^2][1 + (\frac{f}{f_2})^2]\}^{-1}$$

where $f_1 = 6.6$ Hz and $f_2 = 30.5$ Hz. If the band of interest is restricted to 20 Hz, a single pole form suffices to describe the response. This form is useful for estimating errors at low frequencies - it is not used in computations:

$$[1 + (\frac{f}{f_o})^2]^{-1}$$

For this thermistor f_o is 5.83 Hz. The procedure and its difficulties are discussed in detail in Appendix C.

D. Thermistor Response: Field Test

Copper and constantan wires, each 0.001" in diameter, can be butt-welded to form a junction smaller than 0.002". The response-time of such a junction under relevant conditions is not known, but arguments can be made that it is less than 0.005 secs, so that temperature signals

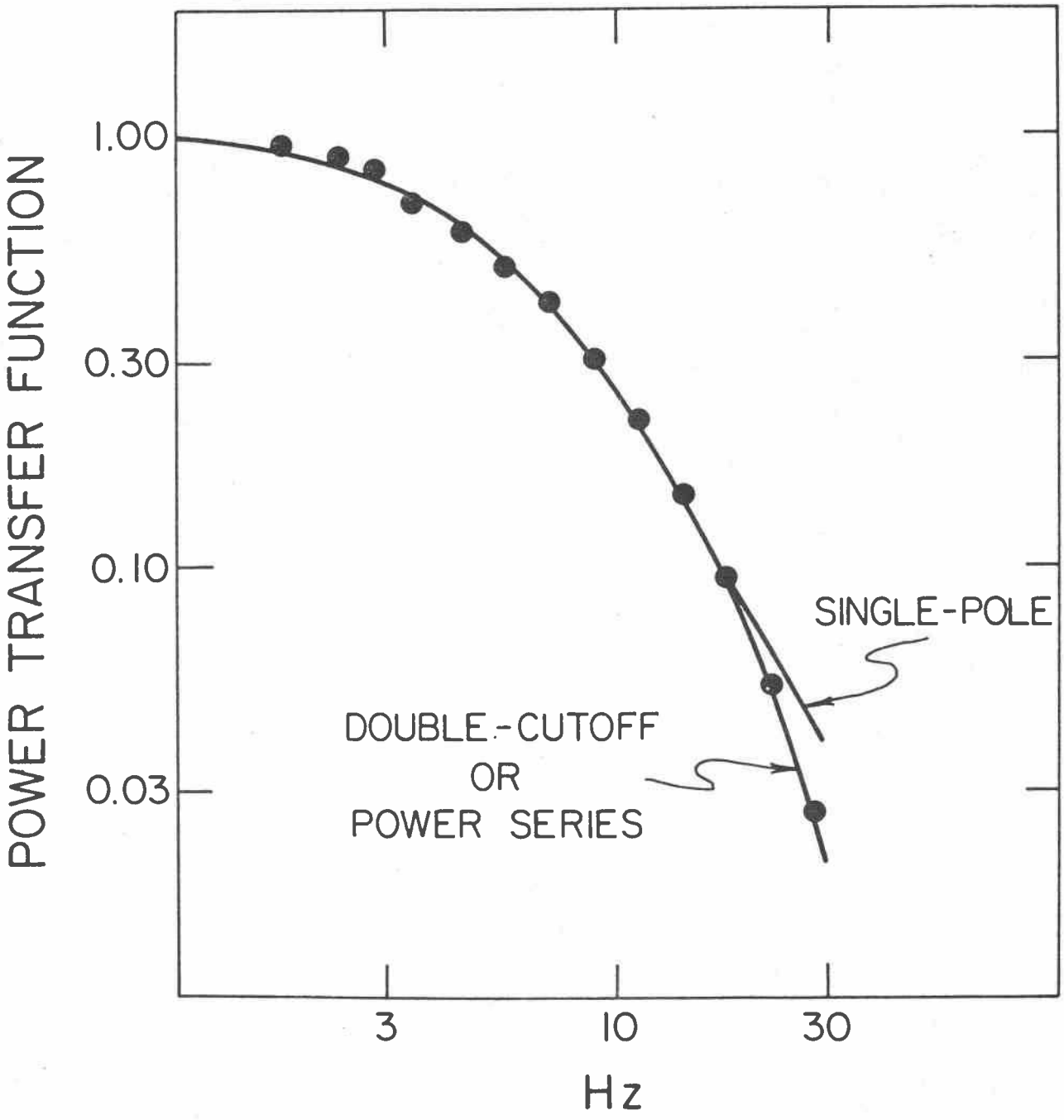

FIGURE V.C.1: Response of a P-85 thermistor as determined by passing it through a thin, warm laminar jet.

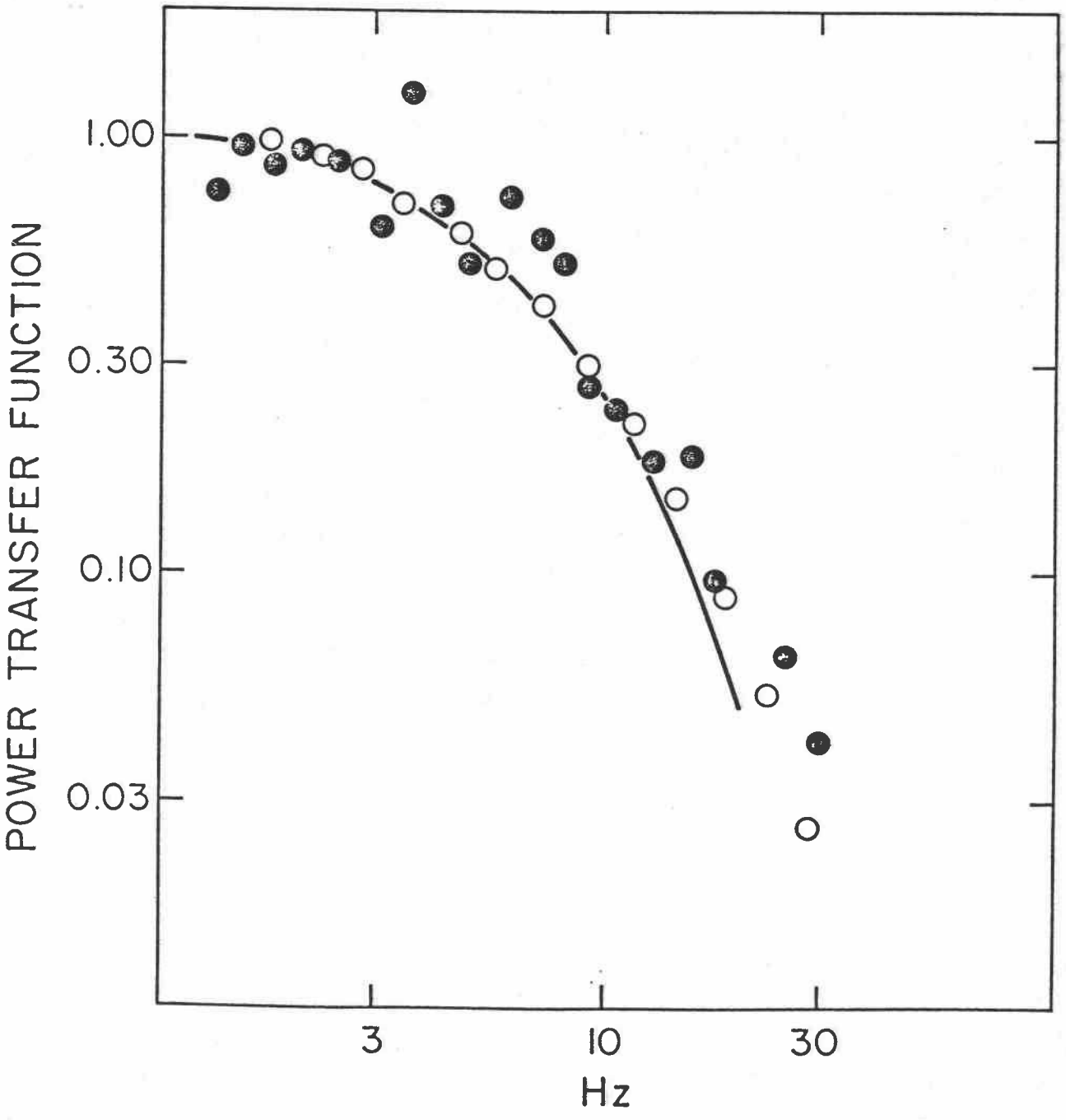

FIGURE V.D.1: Power transfer functions vs. frequency for thermometrics P-85 thermistors as determined in: ● field test vs. thermocouple; ○ laboratory jet test.

encountered at less than 30 Hz will not be attenuated (Appendix D). If this is so, a thermistor's response can be determined by comparing spectra determined from the thermistor signal with spectra determined from the thermojunction signal, if a temperature-gradient signal covering the frequencies of interest is present.

Such a test was made in Lake Tahoe for a (different) P-85 thermistor. It is described in detail in Appendix D. Patches of large dissipation and large gradients in the thermocline supplied the fluctuations. Procedures were exactly those of our usual microstructure casts. Because of the low signal level from the thermocouple, noise dominates the thermocouple channel except in the most active patches. In those patches, however, a comparison between signals could be made. The result cannot be strictly compared with the results of the jet test, because different thermistors (same manufacturer, same model) were used, but the discrepancies are surprisingly small, and certainly lie within the range expected for unit-to-unit variations in the manufacturing process (Fig. V.D.1).

E. Comparison of Estimated Response Functions

We have three sources of data on P-85 thermistor response: (1) the Jet test, (2) the thermocouple comparison, and (3) the result of a Fabula-type test communicated to us by M. C. Gregg. The velocities for all three are within 1 cm s^{-1} of 10 cm s^{-1}. The discrepancies are considered to be consistent with unit-to-unit variations in the manufacturing process (Fig. V.D.1).

Each data-set can be represented fairly well by a single-pole filter for frequencies below 20 Hz. The best estimates for the 3-db frequencies are: (1) 5.83 Hz for the Jet test, (2) 6.5 Hz for the

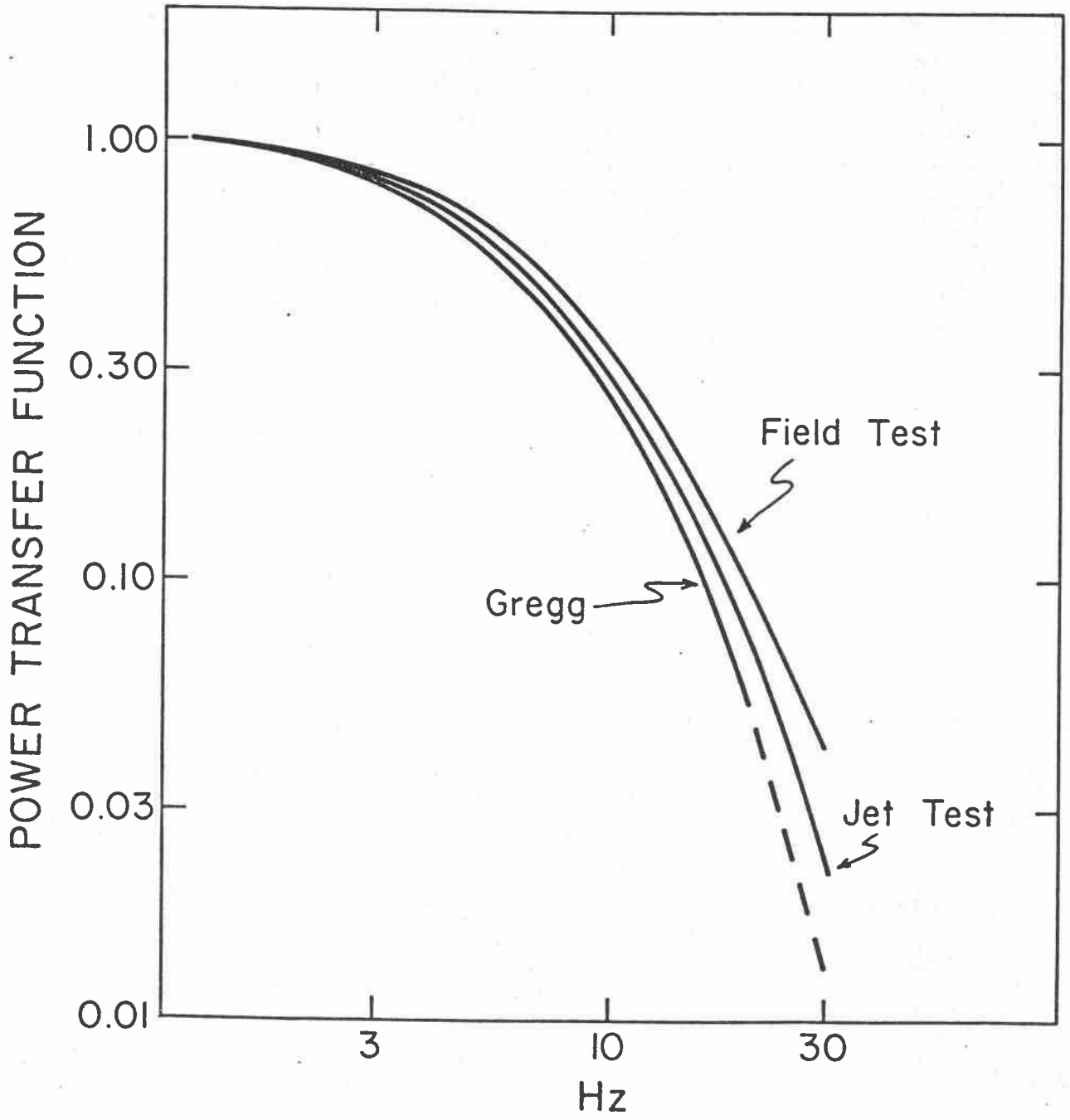

FIGURE V.E.1: Power transfer functions vs. frequency from 3 sources for thermometrics P-85 thermistors.

thermocouple comparison, and (3) 5.2 Hz for Gregg's data. Again note that the single-pole approximation is not to be used in data reduction, but only for comparison purposes, at lower frequencies (see below).

Best fits to the various data sets yield slightly different curves (Fig. V.E.1). The corrections required at 20 Hz are multiplicative factors of (1) 13.0 (Jet test), (2) 10.2 (thermocouple comparison), and (3) 19.23 (Gregg). This variation seems severe, but we are interested in the effect on the temperature-gradient spectra and on quantities calculated from them.

F. Errors Introduced by Misestimation of Response

The cut-off wavenumber, k_c, the wavenumber at which the spectra estimates have fallen to 10% of their peak value, is routinely calculated from the spectra. Its value is used to estimate the kinetic-energy dissipation rate, ε, according to the theory of G. K. Batchelor (Appendix B). Also the integral of the spectrum is calculated to determine χ, the rate of dissipation of temperature fluctuations. The Cox number, $<(\frac{\partial T}{\partial z})^2>/<\frac{\partial T}{\partial z}>^2$ is also calculated from the integral. We have at times been interested in the shape of the spectrum as well, although we are not routinely concerned with it.

The effect of error in determination of the thermistor response on the spectra is assessed by asking what range of results would be given by assuming extreme values for the response if the time response is the mean of the measurements available. The procedure is to assume the existence of a Batchelor spectrum in the water with a given value of ε (for this exercise setting the Batchelor parameter q equal to 3 and the descent rate at 10 cm s^{-1}). Then the thermistor response is applied to

the Batchelor form, to calculate the spectrum "observed" if no corrections are made (single-pole response with f_o = 5.8 is assumed). To find out what the effect of misestimating the response would be, the "observed" spectrum is corrected with f_o equal to 5.2 Hz (overcorrecting) and f_o = 6.5 Hz (undercorrecting). The discrepancy between the overcorrecting and undercorrecting curves is an estimate of the error introduced by misestimating the response.

The results of these calculations are shown in Figs. V.F.1, V.F.2, V.F.3 and V.F.4. We see that for $\varepsilon = 10^{-6}$ cm^2 s^{-3} the spectral estimates are not seriously affected by the thermistor's attenuation, and correction is unnecessary. For $\varepsilon = 10^{-5}$, the attenuation is quite significant, but the corrections produce spectra that differ only slightly from the original spectrum. For $\varepsilon = 10^{-4}$ and $e = 10^{-3}$ the corrected spectra diverge somewhat more.

What are the effects on estimates of ε and χ of over- and undercorrecting? The error induced in ε is $\pm$20% of the true value, even for $\varepsilon = 10^{-3}$. The reason the error in ε is no larger is that ε is calculated from k_c^4, and k_c is determined as the wavenumber at which the spectral estimates have dropped to 10% of their peak value. Therefore it is only the difference in over- or undercorrecting between the frequency at the peak and the frequencies 3 to 4 times larger that induces errors. Note that if no corrections were made, the estimate of ε would be only 13% of the true value if the true value were 10^{-3}. Even for a true value of 10^{-5}, the uncorrected spectrum would yield a value only half as large as it should.

Errors in χ and the Cox number vary with ε, increasing from $\pm$7% for $\varepsilon = 10^{-5}$ to $\pm$16% for $\varepsilon = 10^{-3}$. Again these are not serious errors; sampling errors far exceed them.

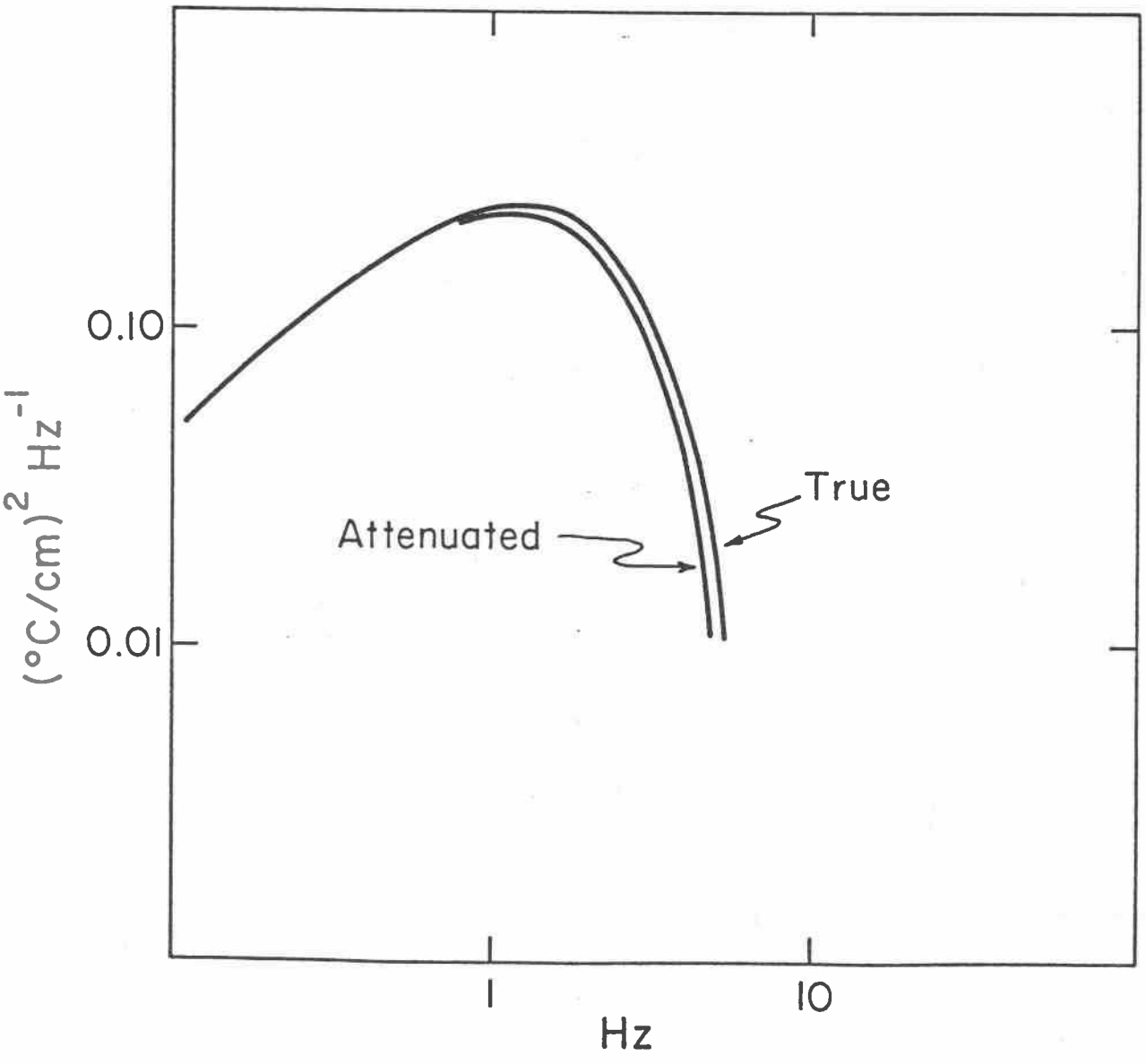

FIGURE V.F.1: For $\epsilon = 10^{-6}$ cm^2 sec^{-3} and a drop speed of 10 cm sec^{-1}, the curves represent a calculated Batchelor spectrum (q=3) as it would be seen by a perfectly responding sensor (the "true" spectrum), and as it would be seen by a thermistor with a single-pole response, with a 3dB point of 5.8 Hz, the mid-value of the three determinations ("attenuated").

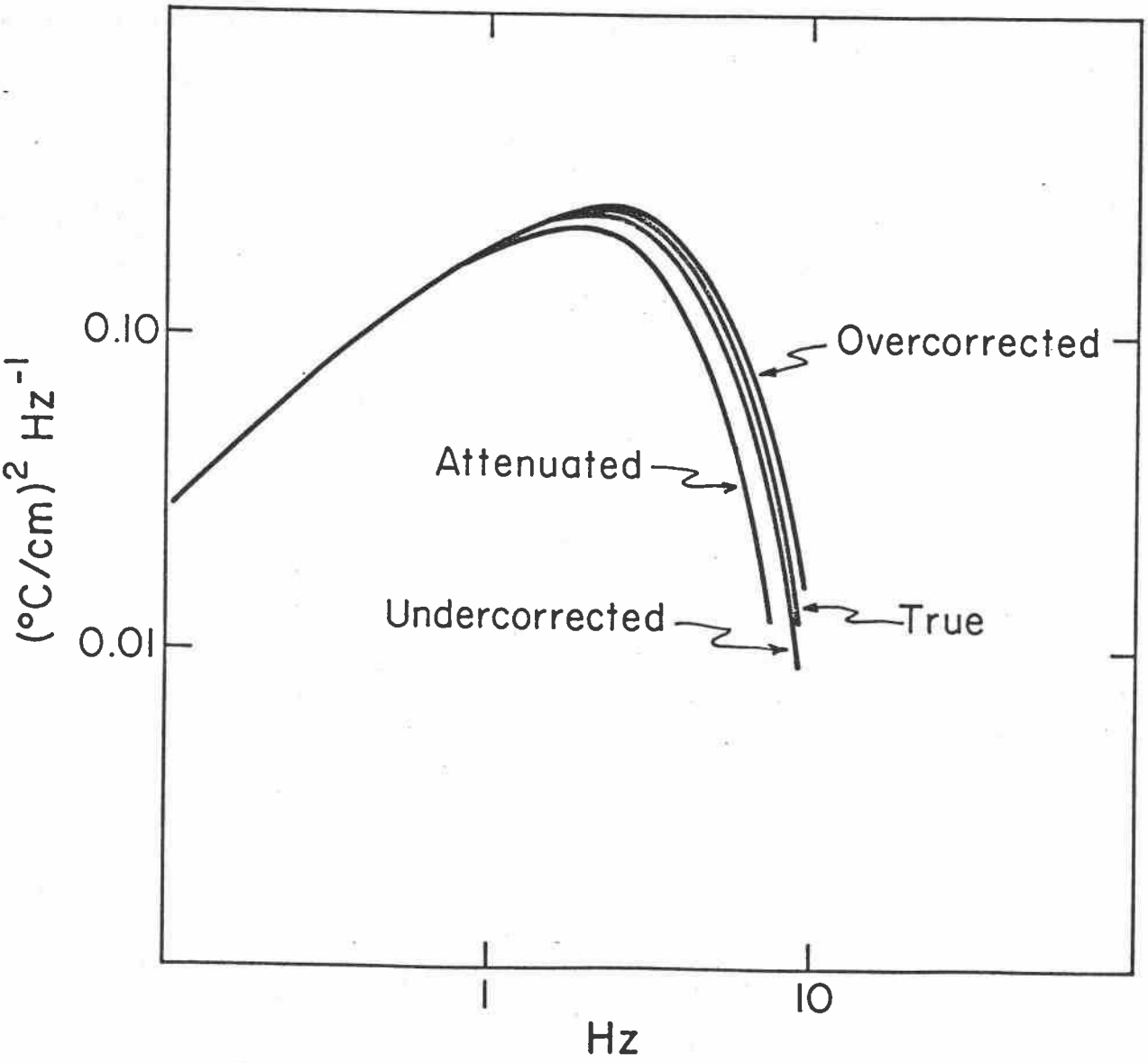

FIGURE V.F.2: For $\varepsilon = 10^{-5}$ cm^2 sec^{-3} and a drop speed of 10 cm sec^{-1}, the "true" curve represents the assumed spectrum as in the previous figure and the "attenuated" curve represents the spectrum as observed by a thermistor with a single-pole response with 3dB frequency at 5.8 Hz. The "attenuated" spectrum is corrected assuming a 3dB frequency of 5.2 Hz (the lowest value measured) to calculate the "overcorrected" curve. The "attenuated" spectrum is corrected assuming a 3dB frequency of 6.5 Hz (the highest value measured) to calculate the "undercorrected" curve. The difference between the "undercorrected" and "overcorrected" curves represents the error caused by uncertainty in the correction.

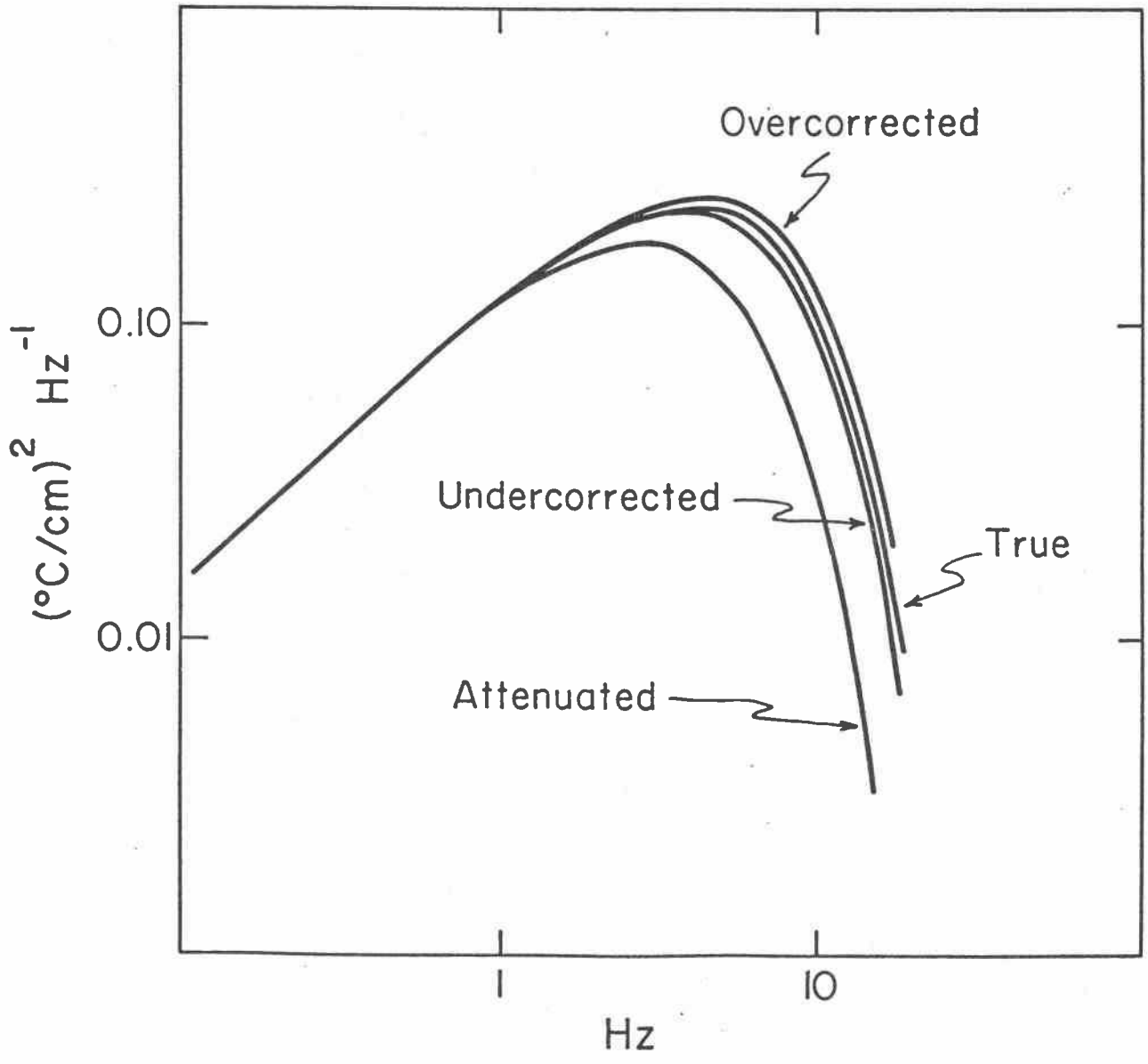

FIGURE V.F.3: As in previous, but for $\varepsilon = 10^{-4}$ cm^2 sec^{-3}.

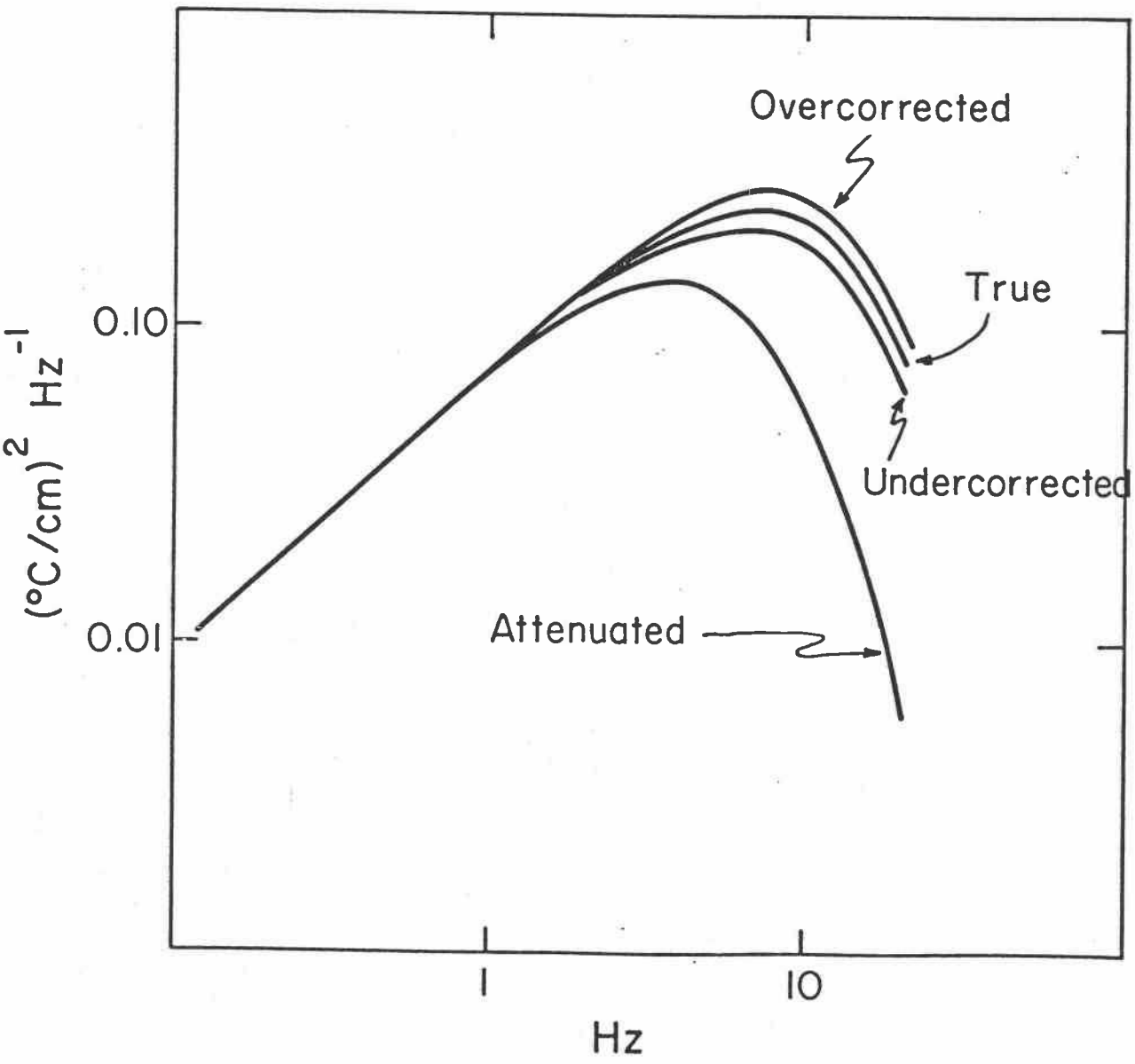

FIGURE V.F.4: As in previous, but for $\varepsilon = 10^{-3}$ cm^{-2} sec^{-3}.

G. Circuitry Transfer Function

Frequency-dependent modifications of the signal are made chiefly by the differentiator and the filter. Their effects are considered separately above. An overall amplitude transfer function was measured by introducing a signal at the transducer input and measuring the amplitude at the data-acquisition-system input (Fig. V.G.1). The system functions as an ideal differentiator to 30 Hz, with rapid attenuations due to the filters above 40 Hz. Some further details will be given in a later section concerned with data analysis.

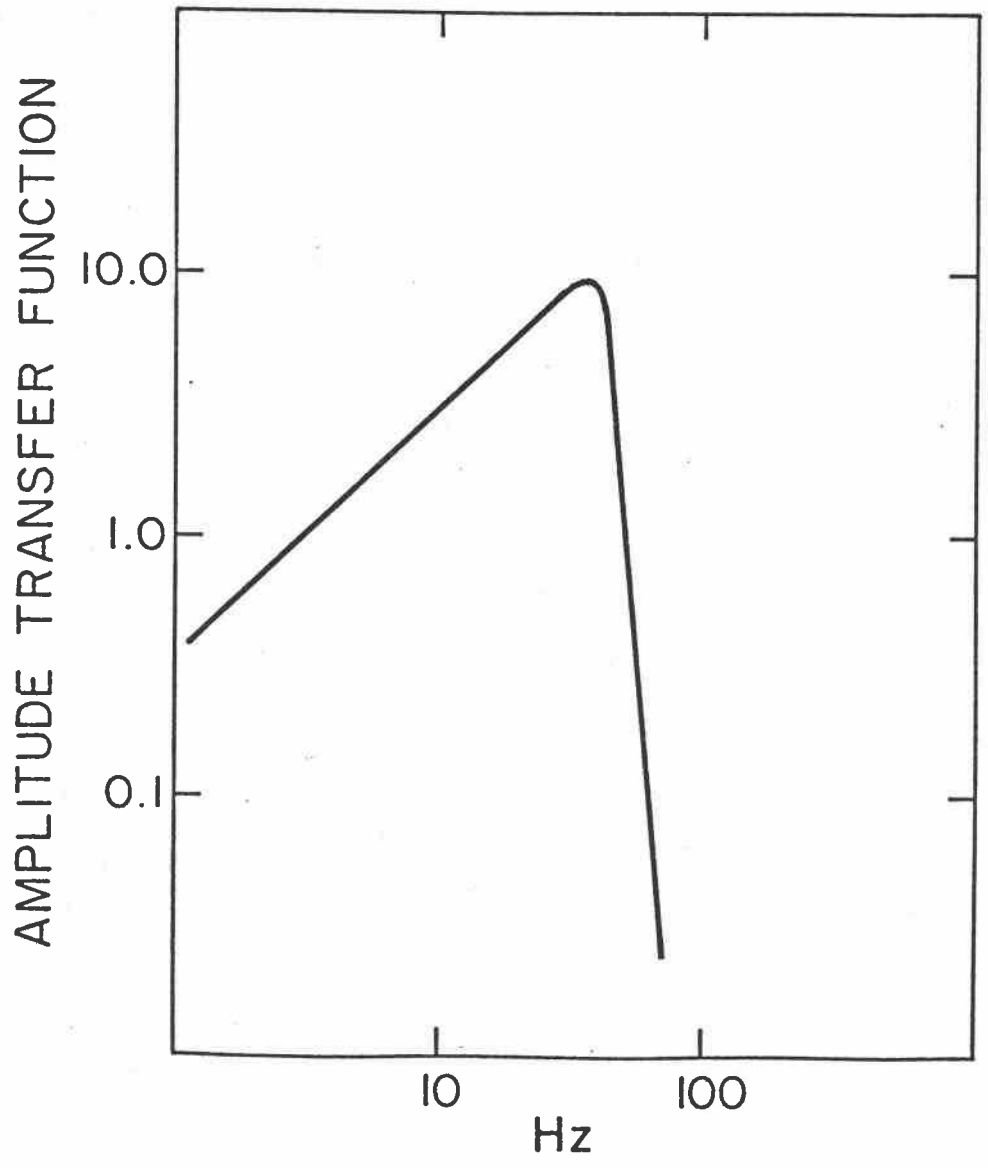

FIGURE V.G.1: Measured amplitude response function of on-board electronics system.

VI. ESTIMATION OF SPECTRA

Much of the information learned from microstructure profiles is obtained through vertical wavenumber spectra. From these, ε, χ, and the Cox number are calculated. Also the shapes of the spectra can tell us about the processes. Correction for sensor-response and removal of noise are much more easily accomplished in the wavenumber domain. Some techniques for data manipulation would be very difficult to implement using the signals themselves.

A. The Basic Calculation

We would like to have the spectra calculated for segments in which the basic parameters ε and χ do not vary excessively, so the segments chosen are relatively short. For each transform a segment of data 512 points in length is used. With a descent rate of 10 cm s^{-1} and a data rate of 90 per second, this means that only 57 cm of the water column is covered in each spectra. To avoid spectral leakage problems, a Gaussian window that weights the endpoints at only 13% of the weight of the central points is applied before transforming. To avoid losing the information contained near the endpoints, the segments are 50% overlapped. Thus the endpoint of one segment is the central point of the next.

A complex Fast Fourier Transform is applied. It transforms two series at once, so that coherence between channels is easily computed.

The spectra calculated in this manner take on quite different appearances, depending on the signal present. If the signal is strong, even such a short segment may have the form of a Batchelor spectrum (Fig. VI.A.1). With so few degrees of freedom, however, one cannot expect estimates to be very stable, especially in the lower-frequency

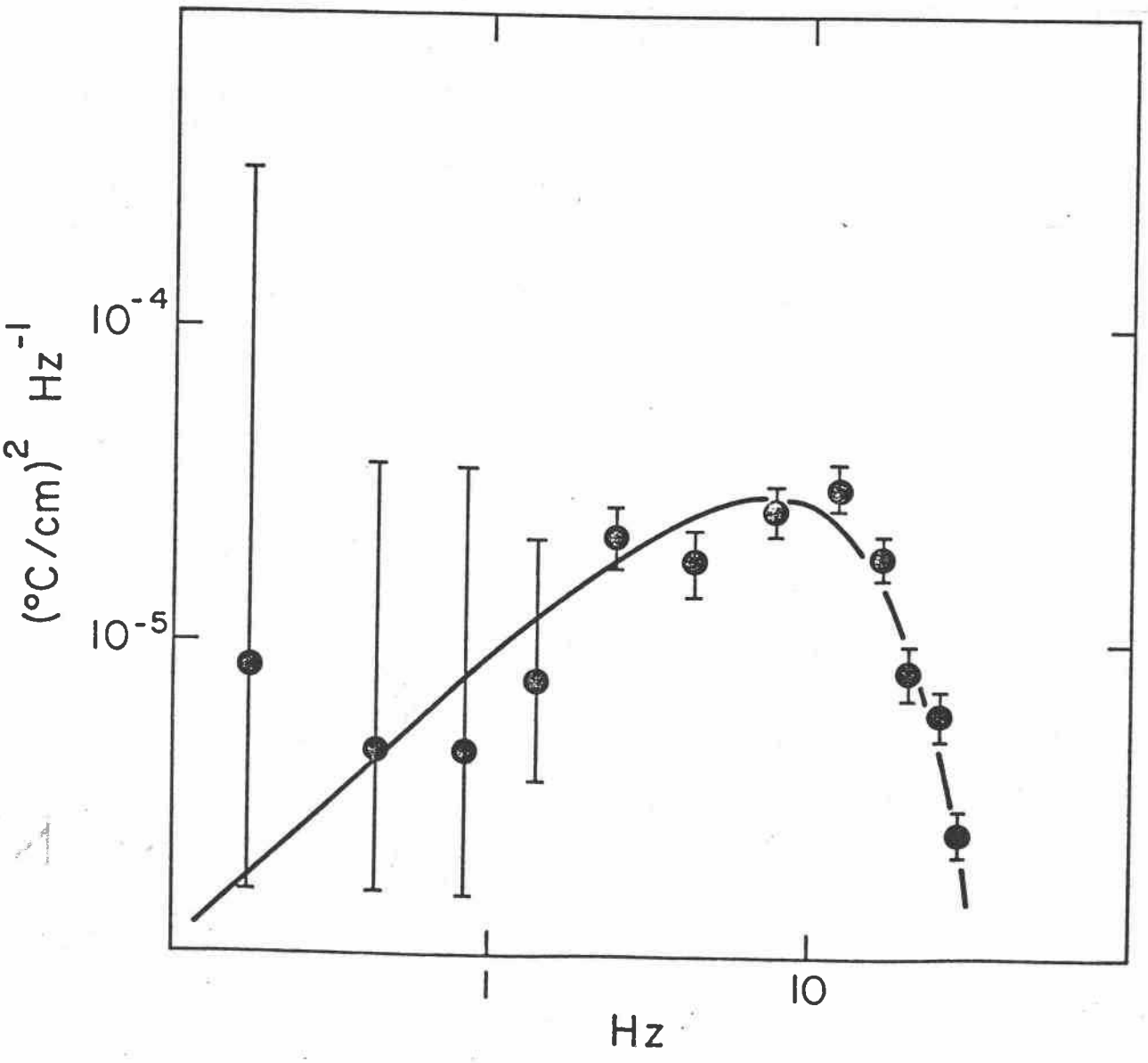

FIGURE VI.A.1: Band-averaged spectral estimates for one noise-free segment, with error bars representing 95% confidence limits.

bands, in which only a few estimates are averaged. The lowest band used only a single estimate, and the next two average only two. The highest 6 bands average 25 estimates, and of course are more stable.

If a few (4) adjacent, overlapping spectra are plotted together (Fig. VI.A.2), no pattern is evident, except that all rise from low frequencies, peak broadly, and cut off somewhere between 15 and 30 Hz. If, however, each spectrum is scaled by its integral and the 4 estimates in each frequency band are averaged, a pattern emerges that resembles the Batchelor spectrum quite closely (Fig. VI.A.3). (If ε varies greatly from spectrum to spectrum, it is necessary to scale k by k_c as well. This is done in standard processing.)

B. Noise Seen in Data

Often noise enters significantly into the spectra. It is readily identified because the coherence between the two channels originating in the same transducer drops significantly below 1.00 when noise enters (Fig. VI.A.4). In this example, noise has entered only into the highest frequency bands. Coherence drops, and the estimates of in-phase power are significantly lower than the estimates from either channel. The computed phase difference does not vary greatly from zero.

In other, quieter regions the noise enters even more seriously (Fig. VI.A.5). In this case if the spectral estimates from Channel 1 (or Channel 2) alone were the only evidence, the spectrum would have to be judged as unresolved. But it is only a bit of noise entering at high frequencies that causes this appearance. The in-phase power shows that the spectrum is resolved, and is as close an approximation to the Batchelor spectrum as we can expect from an individual 512-point segment.

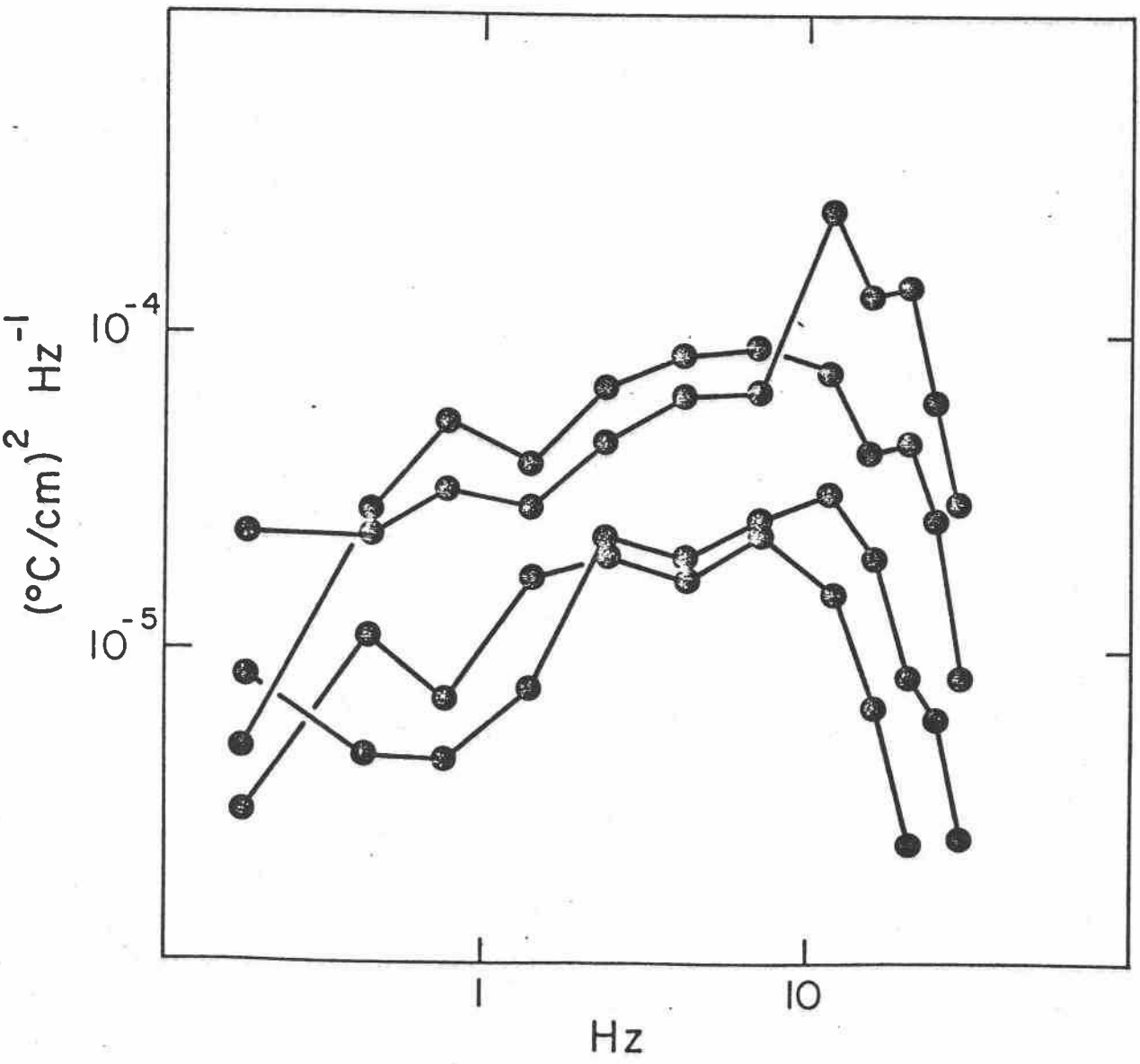

FIGURE VI.A.2: Band-averaged spectral estimates for four neighboring segments.

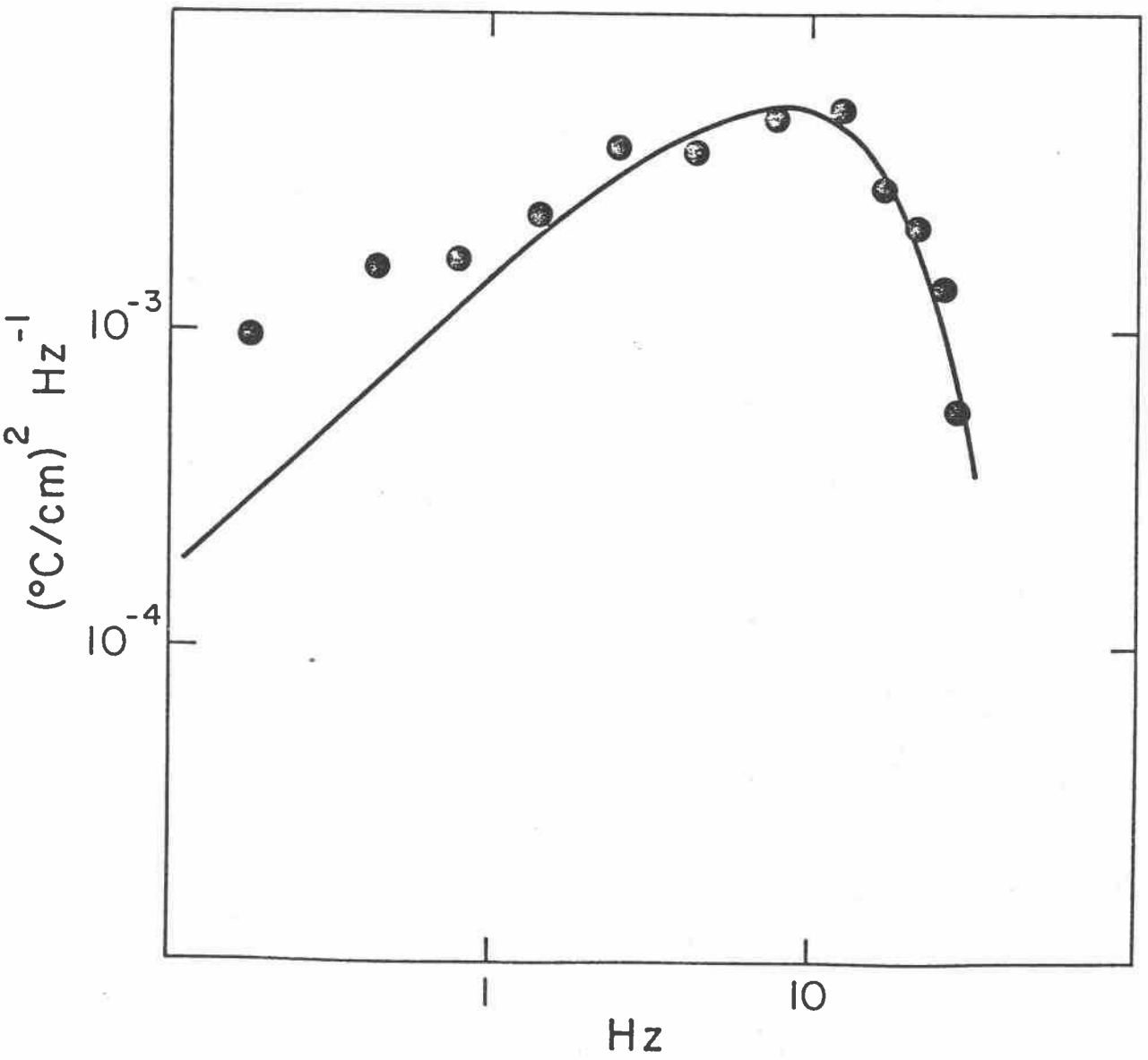

FIGURE VI.A.3: Ensemble average of the four spectral shown in the previous figure.

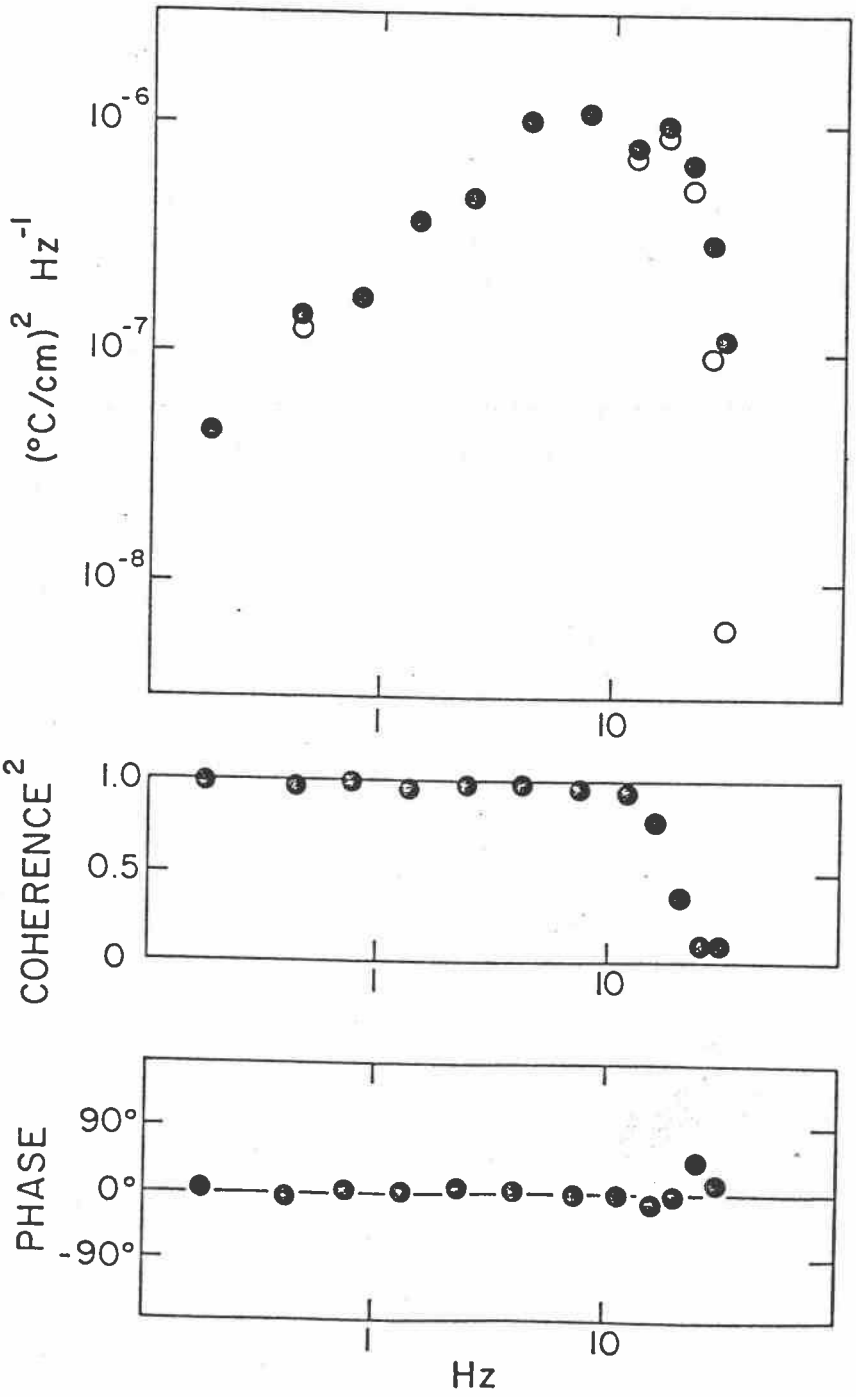

FIGURE VI.A.4: The top plot shows band-averaged spectral estimates for a case in which noise enters at high frequencies. ● Band averaged spectral estimates, Q in-phase power. The middle plot shows the coherence-squared for the same record of 512 numbers and the lowest plot shows the phase difference between the redundant signals.

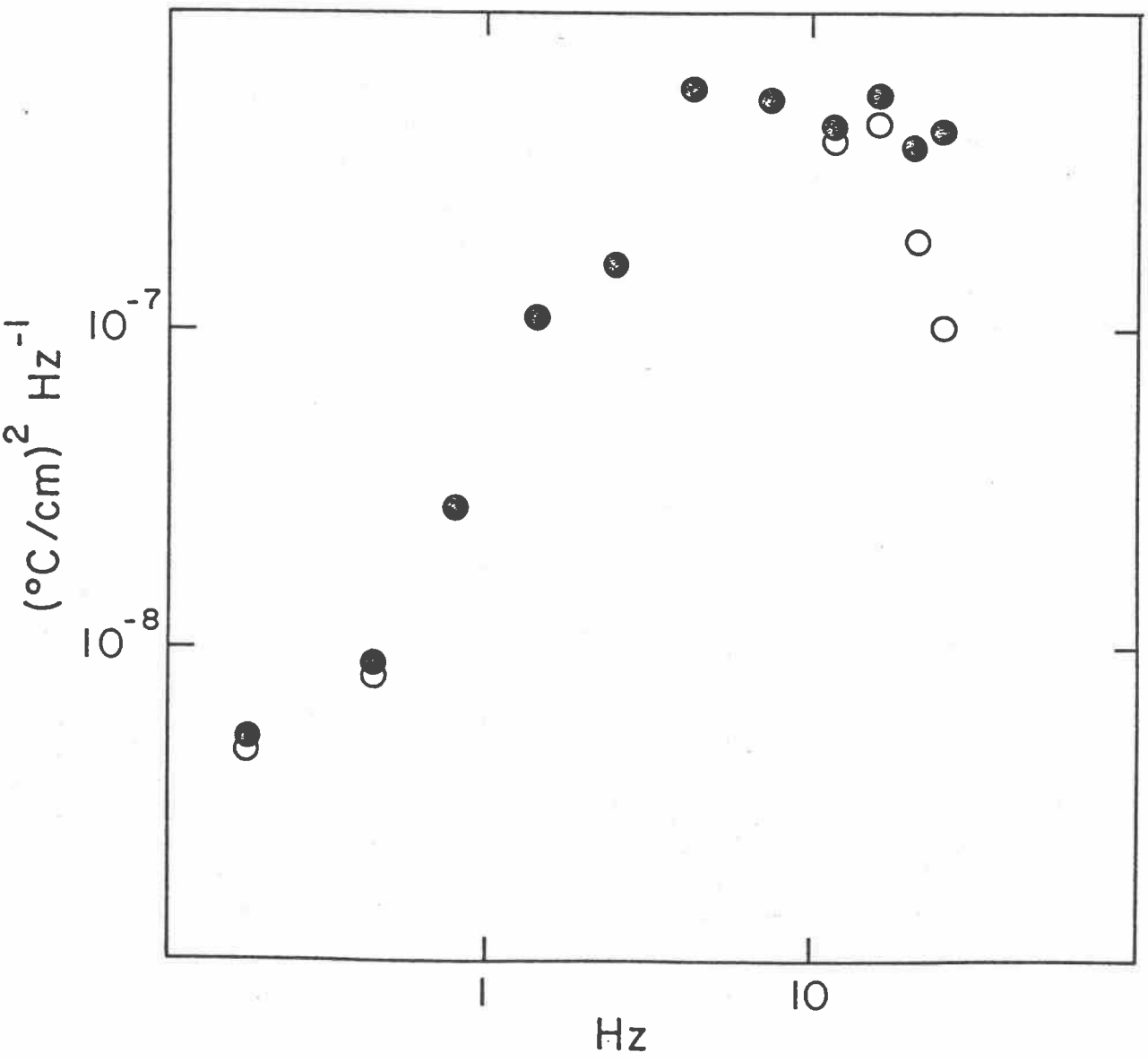

FIGURE VI.A.5: Spectrum of differentiated temperature record for case in which just a bit of noise enters at the highest frequencies, but in-phase power calculation reveals the cut-off. ● Band-averaged spectral estimates, ○ in-phase power.

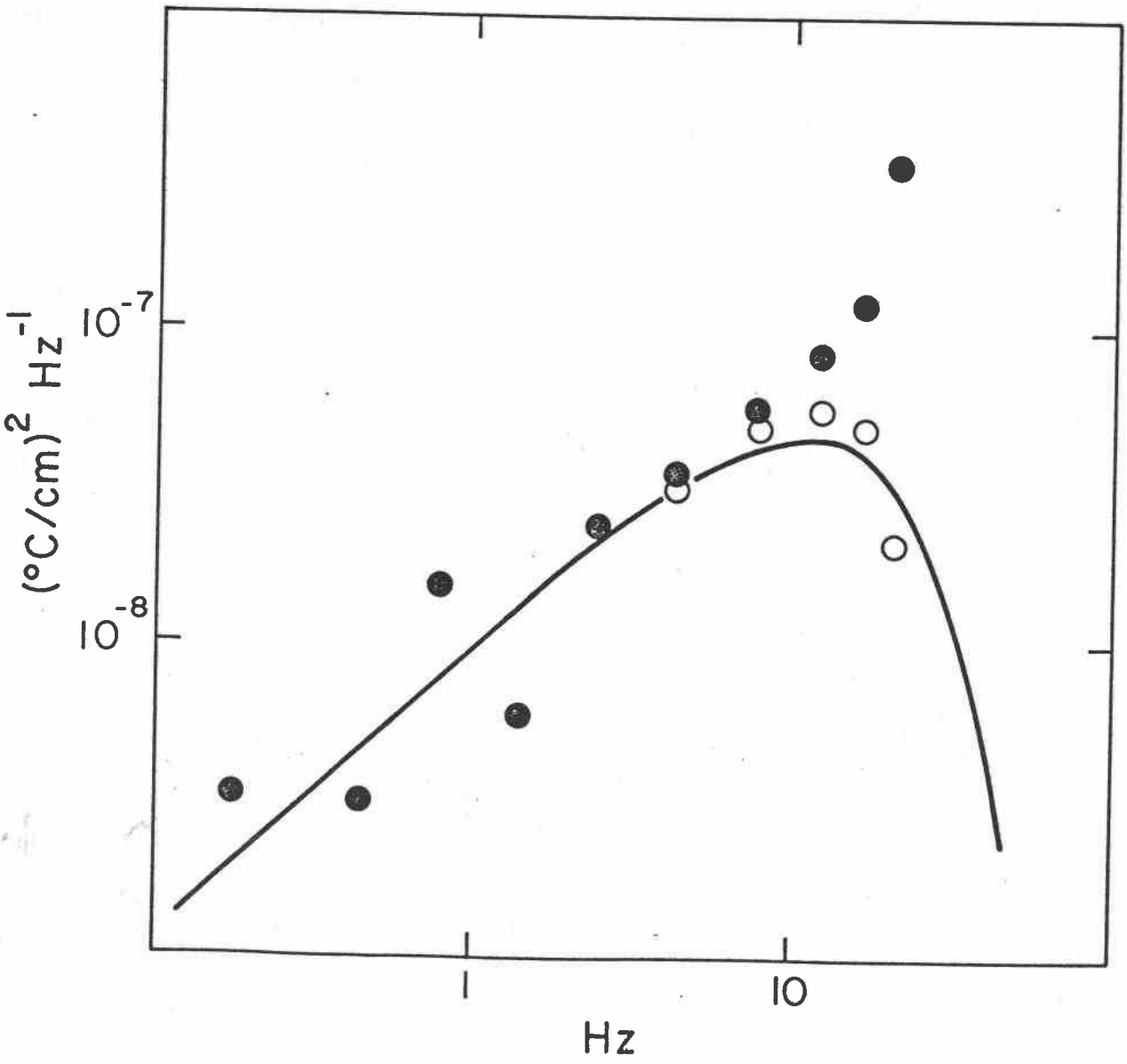

FIGURE VI.A.6: Spectrum of differentiated temperature record for case in which in-phase power calculation reveals the cut-off in spite of the noise. ● Band-averaged spectral estimates, O in-phase power.

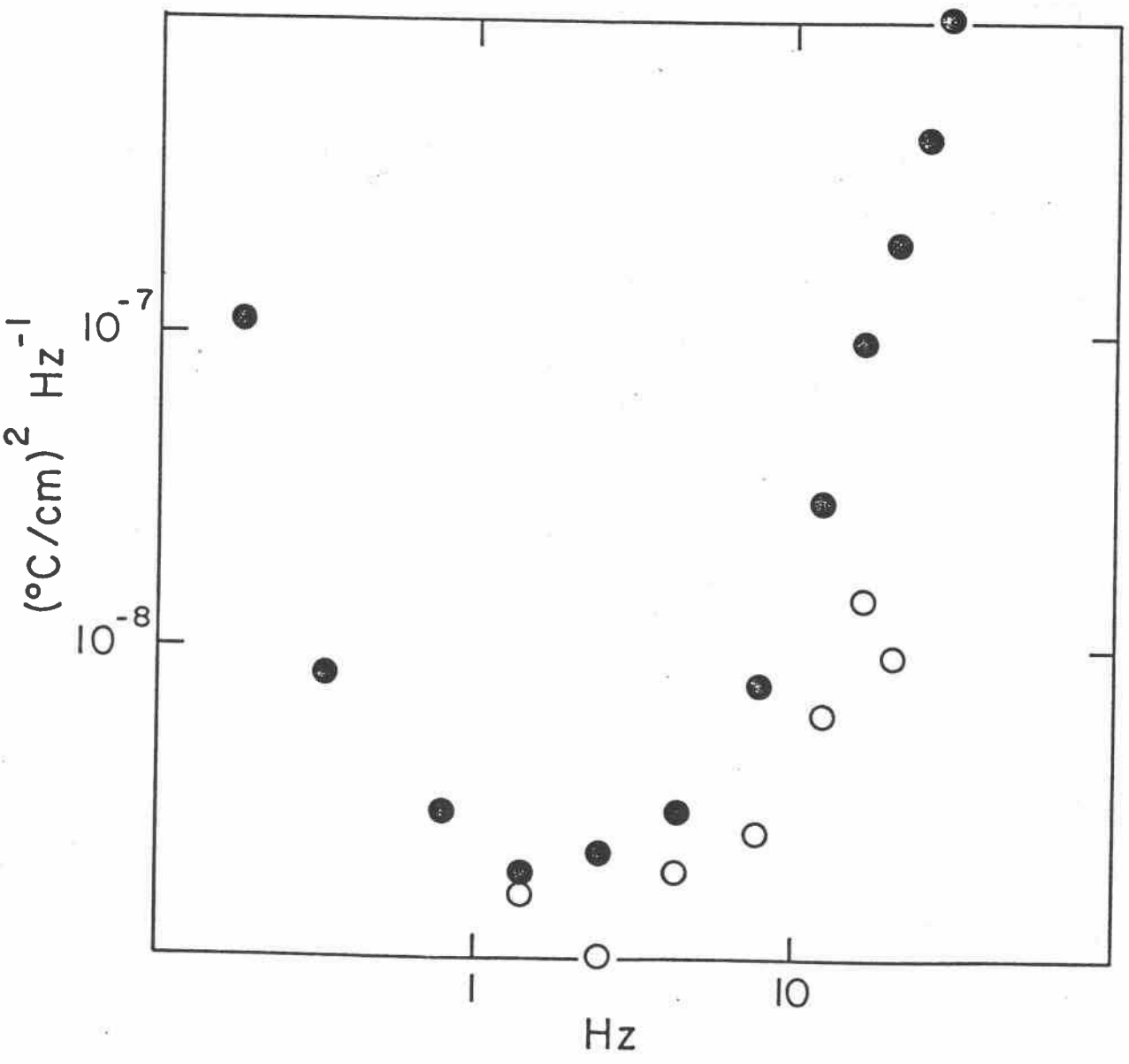

FIGURE VI.A.7: Spectrum of differentiated temperature record for case in which noise dominates at all but the lowest frequencies. ● Band-averaged spectral estimate, O in-phase power.

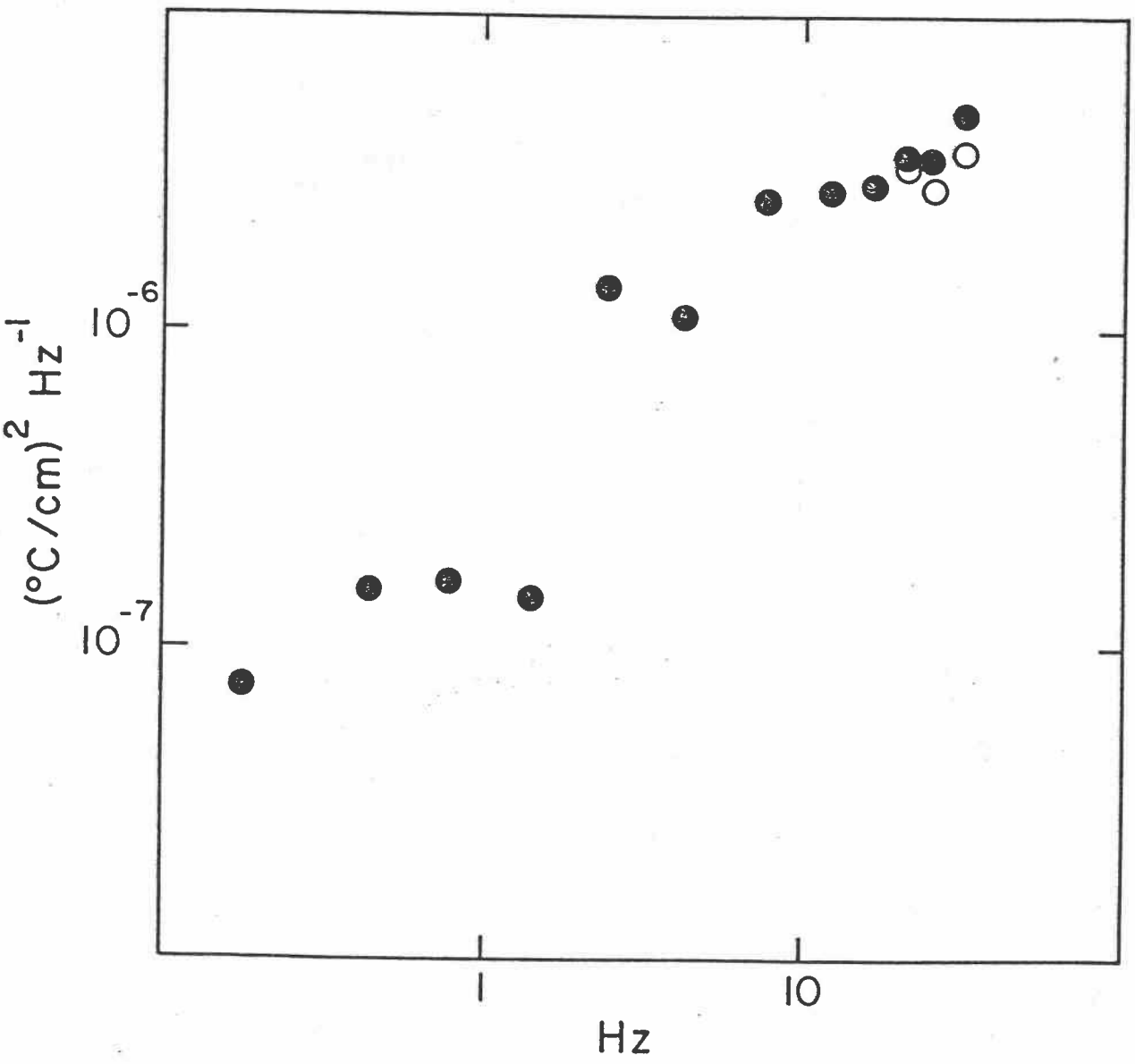

FIGURE VI.A.8: Spectrum of differentiated temperature record for a case in which the incoming signal had bandwidth wider than our system can resolve. ● Band-averaged spectral estimate; ○ in-phase power.

Noise enters even more significantly in another example (Fig. VI.A.6). Here the spectral estimates from Channel 1 are increasing rapidly with frequency, but the coherence is falling and the in-phase power shows a cut-off. The plot is cut off at 20 Hz because the coherence drops so low at higher frequencies that its estimation cannot be trusted, and the estimation of in-phase power becomes highly imprecise. The computation of in-phase power and its statistics will be discussed later.

Sometimes signal is small at high frequencies in well-mixed layers. This will happen in a well-mixed but nonenergetic region, usually below the thermocline (Fig. VI.A.7). Here the spectral estimates above 2 Hz represent mainly noise, and the statistics are not good enough for the in-phase power calculation to pick a significant signal out of the noise. This segment can only be ignored in further processing.

Another example in which the spectral estimates rise monotonically with frequency represents a real process in the water (Fig. VI.A.8). In this case the high coherence shows that the estimates represent mainly signal; the in-phase power estimates differ only slightly from the Channel 1 estimates. Without the redundant channel and the coherence calculation it would be impossible to prove that the estimates of Fig. 46 represent signal while those of Fig. 45 do not. Examples like this where the signal is unresolved are encountered near the surface in stormy weather. The dissipation in this particular case must be above 10^{-2} cm^2 s^{-3}.

C. Formulae

The quantity called the in-phase power is very nearly the same as the cospectrum. As its name indicates it is the part of the power in Channel 1 that is coherent and in-phase with Channel 2. For the purpose of this calculation, Channel 2 need not be calibrated, sometimes an advantage. We define the transforms in terms of the signals T1(t) and T2(t):

$$T1(t) = \sum_n A_n \cos(\frac{2\pi nt}{T}) + B_n \sin(\frac{2\pi nt}{T})$$

$$T2(t) = \sum_n a_n \cos(\frac{2\pi nt}{T}) + b_n \sin(\frac{2\pi nt}{T})$$

where T is the total time for the segment. Then quantities to be calculated are the spectral estimates (here <> refers to an average over a band of frequencies):

$$S1 = \frac{1}{2} < A_n^2 + B_n^2 > F(f)$$

$$S2 = \frac{1}{2} < a_n^2 + b_n^2 > F(f)$$

Here F(f) is the correction factor for thermistor response and f is the center frequency of the band.

The cospectral and quadrature-spectrum estimates are:

$$P = \frac{1}{2} < A_n a_n + B_n b_n > \times F(f)$$

$$Q = \frac{1}{2} < a_n B_n - b_n A_n > \times F(f)$$

and the phase and coherence-squared estimates are:

$$PHASE = \tan^{-1}[Q/P]$$

$$COH2 = (P^2 + Q^2)/(S1 \cdot S2)$$

The in-phase power is then defined as

$$PWRIPH = S1 \cdot (P^2/(S1 \cdot S2))$$

$$= P^2/S2$$

The statistics of the in-phase power will be those of the spectral estimates themselves as long as the coherence is high, but share in the characteristic instability of a phase calculation when coherence is low. Only that power in S1 which is coherent and in phase with S2 will be represented in PWRIPH. So the estimates of PWRIPH contain only the signal (and whatever noise is coherent and in phase), within statistical limits.

D. Tests

To confirm the expectations of system operation, tests were run in which a broadband source was applied to the system input (and recorded), and the system response was found by comparing input and output in the frequency domain. These tests were run in 1976 when the filter bandwidth were set somewhat narrower than now. At that time the system's response was ideal to 22 Hz only, and severe filtering had set in by 30 Hz. Nevertheless the tests indicate the system's performance, and the applicability of the Fourier processing.

A simple test is to compare the differentiated channel's output with its input. In this case we use amplitude transfer functions, the square root of the ratio of the mean spectral estimates in each band (Fig. VI.D.1).

Comparing the coherence and phase difference between two differentiated channels, we see that coherence is near perfect and the phase difference is near zero (Fig. VI.D.2). In fact the coherence squared is

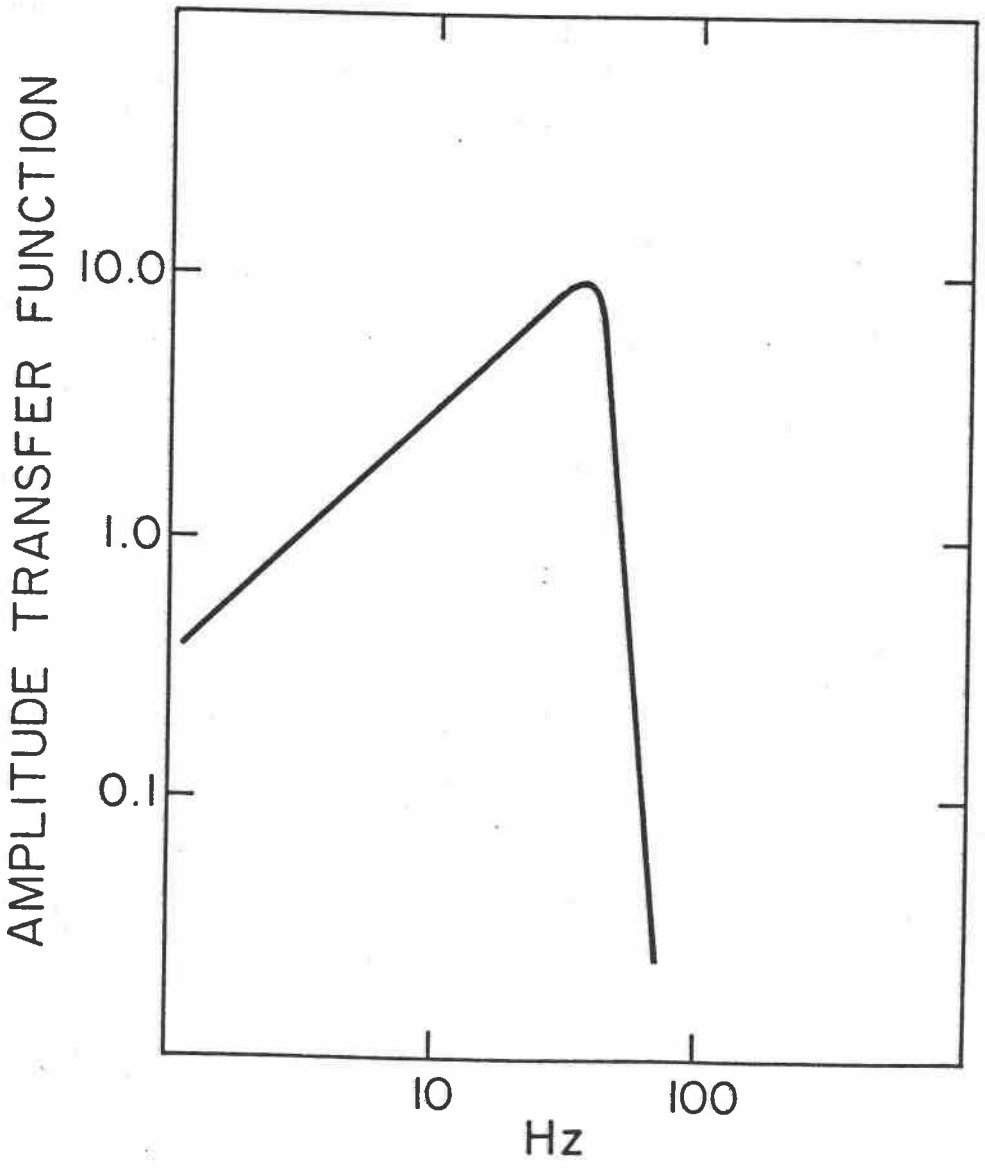

FIGURE VI.D.1: Test of system amplitude response.

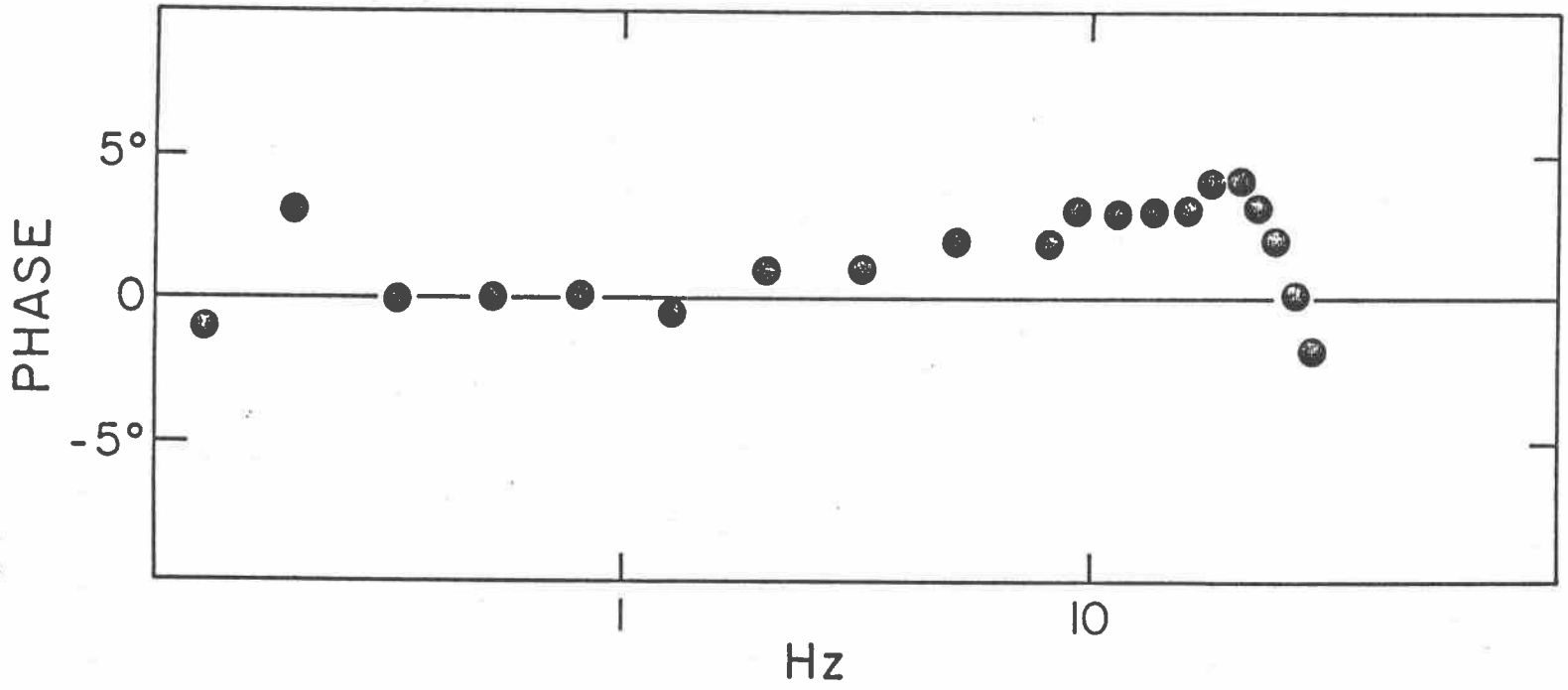

FIGURE VI.D.2: Phase difference between redundant temperature signals. The linear trend in the 30 Hz signal band is caused by the time lag (1/900 secs) between recording times. This lag is removed in normal processing.

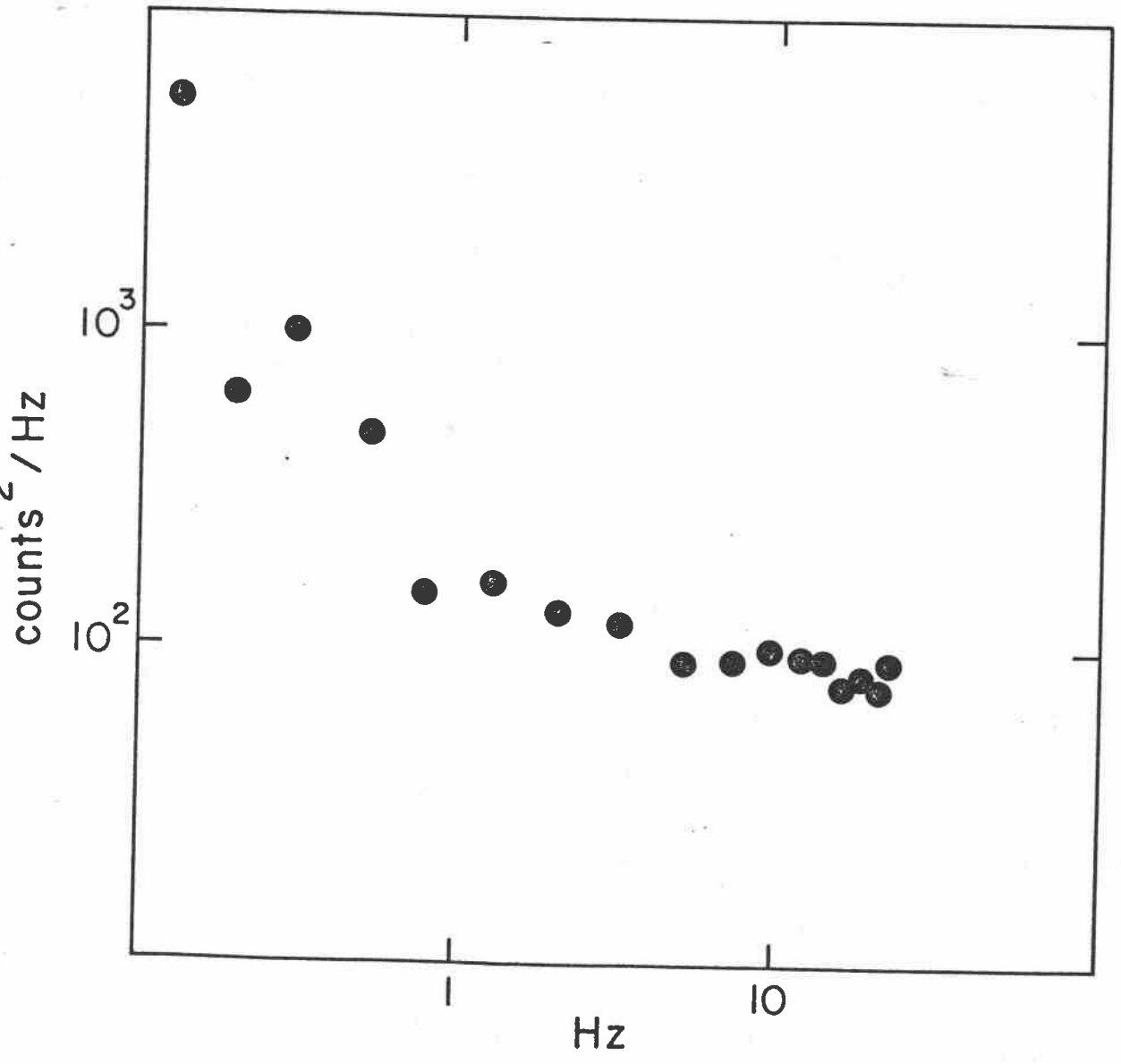

FIGURE VI.E.1: Noise spectrum of undifferentiated temperature signal (with dummy thermistor), showing its nearly-flat character above 1 Hz.

greater than 0.998 to 35 Hz and the phase error between the two channels (compensated for time displacement at recording time) is well within 5°. Even a 5° phase error would cause only 0.4% error in the in-phase power.

E. Noise

Most of the noise originates in the first operational amplifier of the bridge module. Its variation with frequency is seen in a lab test (Fig. VI.E.1). Through much of the signal band (1-25 Hz) the noise is fairly independent of frequency. When this noise is run through the differentiator and then corrected, along with the signal, for thermistor response, the calculated spectrum would be expected to rise rapidly with frequency.

On each cruise casts of the instrument are made with the thermistors shrouded with small plastic tubes. The tubes prevent high frequency signals from reaching the thermistor, so that the "signal" received is mainly noise. When differentiated and corrected for thermistor response the spectrum does indeed rise rapidly with frequency (Fig. VI.E.2).

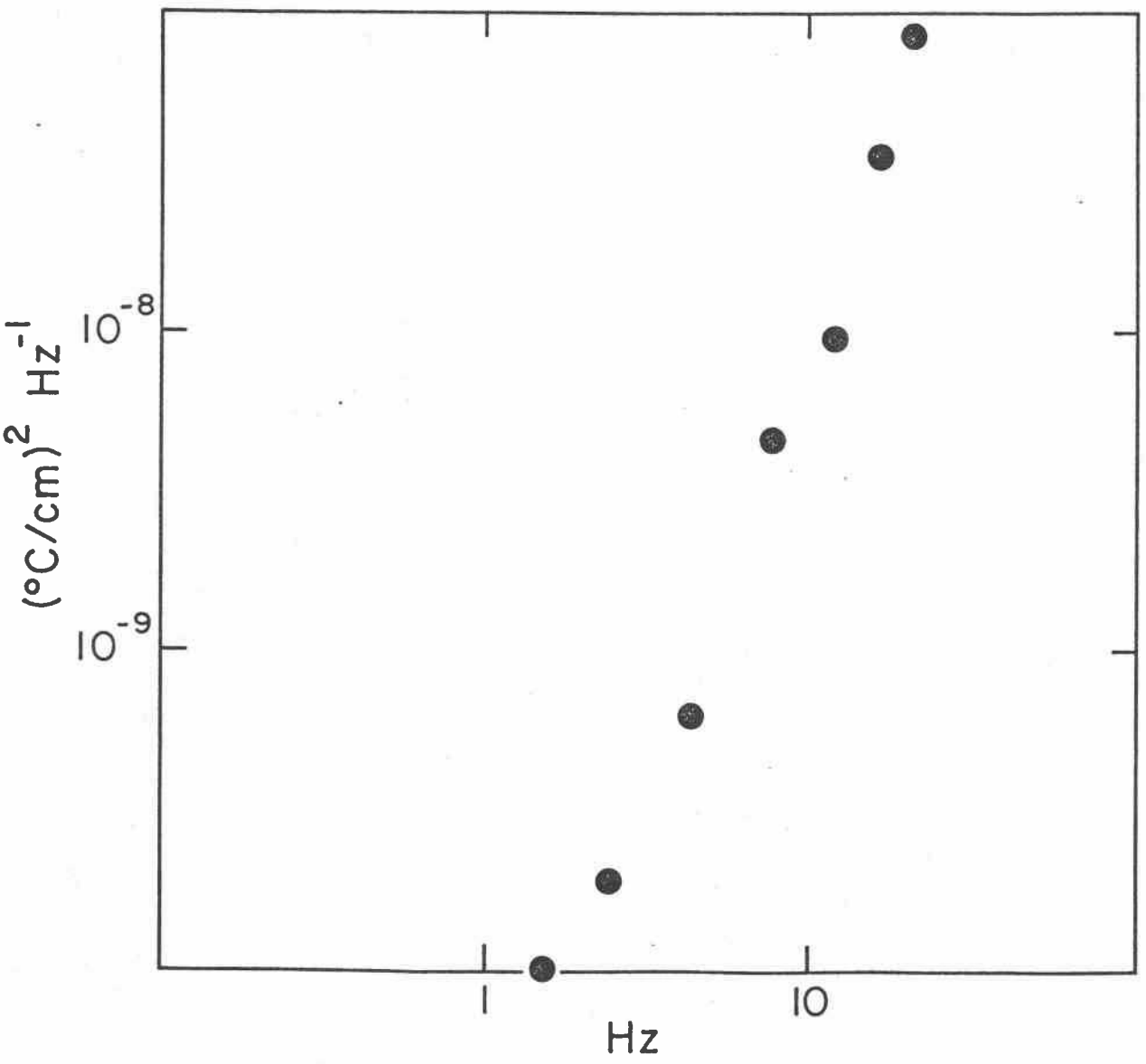

FIGURE VI.E.2: Spectrum of differentiated temperature signal obtained when thermistor was shrouded to suppress true temperature signals, therefore a noise spectrum. The correction for frequency-dependent thermistor response has been made.

VII. FURTHER CALCULATIONS

For each spectrum, the cut-off wavenumber, k_c, and the integral $<(\frac{dT}{dz})^2>$ is estimated. From k_c the kinetic-energy dissipation rate, ε, is calculated, as

$$\varepsilon = \frac{4q^2\nu D^2}{(2.225)^4}(2\pi k_c)^4$$

Here ν is the kinematic viscosity, D is the thermal diffusivity, and q is the Batchelor constant (see Appendix B for details). From $<(\frac{dT}{dz})^2>$ the dissipation rate of temperature fluctuations is calculated, as

$$\chi = 6D<(\frac{dT}{dz})^2>$$

and also the Cox number, as

$$Cox = \frac{<(\frac{dT}{dz})^2>}{<\frac{dT}{dz}>^2}$$

where <> denotes an average over a segment, so $<\frac{dT}{dz}>$ is the mean vertical temperature gradient over the 60-cm segment.

Another required quantity is the buoyancy frequency, N. In the ocean the salinity gradient must be taken into account as well as the temperature gradient.

Another quantity we sometimes calculate is the "isotropy index." By finding the vertical wavenumber at which thermistors separated in the horizontal lose coherence, the shape of the temperature features of one horizontal scale can be determined, and thus the degree of isotropy at that scale.

A. Cut-Off Wavenumber, k_c, and ε

To estimate k_c, defined as the wavenumber at which temperature-gradient spectral estimates have decreased to 10% of their peak value, the spectral estimates are fit to the Batchelor form. Before this is done, a decision must be made for each spectrum as to whether noise is entering and if so which estimates of in-phase power can be trusted to represent signal. Usually estimates for which the coherence-squared between the redundant channels is greater than 0.2 are trusted. Estimates at frequencies higher than the first for which coherence-squared is lower than 0.2 are rejected. The remaining estimates are fit to the Batchelor form, weighted with the degrees of freedom in each. Because of this weighting, the estimates at the lower frequencies have little effect on this calculation. From the fit, k_c is calculated, and then ε.

The errors involved in the final determination of ε come mainly from three sources. First, there are random errors due to sampling. A systematic error caused by error in the determintion of the thermistor's response function is discussed in Section V.F. Finally uncertainty as to the correct value of the constant q introduces another systematic error. It is difficult to even assess the range of values q might have. Grant et al. (1968) estimated 3.9 ± 1.5; Gibson (1968) suggested on theoretical grounds that $\sqrt{3} < q < 2\sqrt{3}$. So values from 1.7 to 5.4 are within possiblity. We are using $2\sqrt{3} = 3.46$ at present. Because q enters the calculation of ε as q^2, we are overestimating ε by a factor of 4 if q is truly $\sqrt{3}$, Gibson's lower bound. If the true value of q is Grant's upper bound, 5.4, we are underestimating ε by a factor of 2.4.

Random errors are difficult to assess also. An upper bound could be set by the scatter in plots involving ε such as Fig. 6 of Caldwell et

al. (1980). Points scatter by a factor of 3 in ε, but it is not known whether this scatter represents a statistical error in the application of the Batchelor form, or represents real variations in ε. It must be remembered that the Batchelor theory is only statistical; a single fluctuation need not have the Batchelor form as its spectrum.

B. Cox Number and χ

To calculate the variance for a segment the non-noise spectral estimates are weighted by their bandwidths and summed. This yields an estimate of the variance of $\frac{dT}{dz}$ which has noise removed and is corrected for thermistor response. At times its value may be somewhat low because some signal has been rejected along with the noise. To find χ this estimate is multiplied by 6D (assuming isotropy, see below for discussion as applied to Cox number).

For a calculation of the Cox number we need to divide by the square of the mean gradient calculated over the same segment. Then there is the question of isotropy. As the Cox number is derived from the equation for turbulent fluctuations of temperature, the variances of the horizontal gradients should be summed with the vertical. We have no way of determining horizontal gradients, and so must make some assumption about isotropy. Some investigators have multiplied $(\frac{\partial T}{\partial z})^2$ by 3, assuming complete isotropy. Others have used a factor 2 ± 1. We choose to make no correcton for the horizontal gradients, but keep the problem in mind.

C. Isotropy

In the nosepiece of the probe, two thermistors are situated 2.54 cm apart. They each sense the fluctuations in the water column, rotating

slowly about a common center. One rotation of the probe takes at least a meter, so they sense on a slightly twisted line. Comparing the records, we expect to find some features common to both. Features with horizontal scales exceeding the separation will be seen by both. We can ask what is the vertical extent of these features? In other words, what is the average vertical extent of features which have horizontal scales on the order of the separation distance. Mathematically we ask at what vertical wavenumber is coherence lost between the series. Then a shape factor is defined as $w/(2\pi f_c d)$, where w is the descent rate of the probe, f_c is the frequency at which coherence is lost, and d is the separation. This factor pertains only to features of horizontal extent of order d. Narrower features are not defined.

VIII. REFERENCES

Caldwell, D. R., S. Wilcox and M. Matsler (1975) A relatively simple and inexpensive probe for fine-scale temperature measurements. Limnology and Oceanography, 20,1034-1042.

Caldwell, D. R. (1976) Fine-scale temperature structure in the bottom mixed-layer on the Oregon shelf. Deep-Sea Research, 23,1025-1036.

Caldwell, D. R., J. M. Brubaker and V. T. Neal (1978) Thermal-microstructure on a lake slope. Limnology and Oceanography, 23,372-374.

Caldwell, D. R. (1978) Variability of the bottom mixed-layer on the Oregon shelf. Deep-Sea Research, 25,1235-1244.

Caldwell, D. R. and T. M. Chriss (1979) The viscous sublayer at the sea floor. Science, 205,1131-1132.

Caldwell, D. R., T. M. Dillon, J. M. Brubaker, P. A. Newberger and C. A. Paulson (1980) The scaling of vertical temperature-gradient spectra. Journal of Geophysical Research, 85,1917-1924.

Caldwell, D. R., T. M. Chriss, P. A. Newberger and T. M. Dillon (1981) The thinness of oceanic temperature gradients. Journal of Geophysical Research, 86,4290-4292.

Chriss, T. M. and D. R. Caldwell (1981a) Universal similarity and the thickness of the viscous sublayer at the ocean floor. Submitted.

Chriss, T. M. and D. R. Caldwell (1981b) Evidence for the influence of form drag on bottom boundary layer flow. Journal of Geophysical Research (submitted).

Dillon, T. M. and D. R. Caldwell (1978) Catastrophic events in a surface mixed layer. Nature, 276,601-602.

Dillon, T. M. and D. R. Caldwell (1980a) High frequency internal waves at Ocean Station P. Journal of Geophysical Research, 85,3277-3284.

Dillon, T. M. and D. R. Caldwell (1980b) The Batchelor spectrum and dissipation in the upper ocean. Journal of Geophysical Research, 85,1910-1916.

Dillon, T. M., J. G. Richman, C. G. Hansen and M. D. Pearson (1981) Near-surface turbulence measurements in a lake. Nature, 290,390-392.

Elliott, J. A. and N. S. Oakey (1975) Horizontal coherence of temperature microstructure. Journal of Physical Oceanography, 5,506-515.

Fabula, A. G. (1968) The dynamic response of towed thermometers. Journal of Fluid Mechanics, 34,449-464.

Marmorino, G. O. and D. R. Caldwell (1978a) Horizontal variation of vertical temperature gradients measured by thermocouple arrays. Deep-Sea Research, 25,175-181.

Marmorino, G. O. and D. R. Caldwell (1978b) Temperature fine structure and microstructure observations in a coastal upwelling region during a period of variable winds. Deep-Sea Research, 25,1073-1106.

Newberger, P. A. and D. R. Caldwell (1981a) Mixing and the bottom nepheloid layer. Marine Geology, in press.

Newberger, P. A. and D. R. Caldwell (1981b) An inertial subrange in microstructure spectra. Journal of Geophysical Research, 86,4265-4268.

A Transformerless Conductivity Circuit

Douglas R. Caldwell
School of Oceanography
Oregon State University
Corvallis, Oregon 97331

15 Aug. 1980

ABSTRACT

A transformerless circuit for use with a 4-electrode conductivity cell is described which is relatively small, consumes as little as 50 milliwatts power and if necessary will operate under pressures to 300 decibars in a liquid Freon environment. Sensitivity to circuit temperature is reduced, by careful selection of components and by temperature compensation, to approximately 1 ppM apparent salinity change for a circuit temperature change of 20°C. Over a few seconds, rms output noise is less than 0.1 ppM salinity equivalent. Drift of circuit-transducer system corresponds to less than 3 ppM apparent salinity change in a week, and may be much less.

INTRODUCTION

For our microstructure instrument and for the new Rapid Sampling Vertical Profiler (RSVP), a circuit must be small, have low power comsumption, operate under pressures to 300 decibars in a Freon environment, and yet have a small temperature sensitivity. Also the circuit must tolerate occasional exposure to seawater. An earlier version did not satisfy the requirements because of its transformers; transformers of high enough quality could not be found that were small enough.

CIRCUIT PRINCIPLE

The principle is similar to some previous circuits, in that a feedback loop keeps the voltage across the receiver electrodes constant, the driver electrodes supplying whatever current is required. The output is proportional to the driver current. This arrangement will, with large enough input impedance of the receiver circuit, reduce sensitivity to surface polarization impedance changes at the electrodes to a negligible amount.

The equivalent circuit of a four-electrode transducer (Fig. 1) shows complex impedances Z_p in series with each electrode. If the circuit is not carefully designed, changes in these impedances will not be distinguished from changes in the conductivity of the water. These impedances do drift, with temperature, pressure, salinity, and time, even if platinized platinum electrodes are used to reduce their values. If the electrodes can be regarded as points, Fig. 1 can be used to deduce formulas for the operation of the cell. (Minimizing current short-circuiting by the electrodes and other problems in cell design are not addressed here.) The voltage across the receiver electrodes, V_w, is just the ohmic drop in the water if the cell is properly designed, so

$$V_w = I \frac{Z_2 \cdot (Z_A + 2Z_p)}{Z_2 + Z_A + Z_p} \tag{1}$$

and the voltage V_A seen by the amplifier is related to V_w by

$$V_A = \frac{Z_A}{Z_A + 2Z_p} V_w. \tag{2}$$

Combining these relations, we can see that

$$V_A = \frac{Z_A Z_2}{Z_A + Z_2 + 2Z_p} I. \tag{3}$$

If we make $Z_A >> Z_2$ and $Z_A >> Z_p$, then

$$I \cong \frac{V_A}{Z_2} (1 + \frac{Z_2 + 2Z_p}{Z_A})$$

so for constant V_A, I is proportional to Z_2^{-1}, the conductance of the water between the receiver electrodes, except for an error given by $(Z_2 + 2Z_p)/Z_A$. Deviations from linearity are caused by Z_2/Z_A, drifts due to polarization layer changes by $2A_p/Z_A$. With the cell we use (Neil Brown Instrument Co.), Z_2 is approximately 120Ω, and Z_p is approximately 100Ω at the operating frequency, 3kHz. In our circuit, Z_A is 10^6 ohms, and Z_2 changes by ±30% over usual oceanic conditions, so nonlinearity is 0.003%. As to drifts, even if Z_p changes by 50%, the output will change by only 0.01% as a result, so I is indeed a good measure of conductivity of the water with this circuit, as long as the geometry of the cell is not changed by fouling or mechanical effects.

CIRCUIT OPERATION

Direct current is prevented from passing through the electrodes and degrading them by capacitors in series with each (Fig. 2). The cell is driven by current from a 3kHz oscillator passing from electrode A to electrode D. After passing through electrode D the current is sensed by an operational amplifier in a current-sensing mode. The voltage across the receiver electrodes (approximately 0.4 v. peak to peak) is amplified × 9 by a high-impedance differential amplifier. After capacitor C_3 removes any dc offset, the signal is rectified and compared to a reference voltage. The output of the rectifier-comparer controls the amplitude of the oscillator. Thus the oscillator supplies whatever current is required to maintain the amplified output of the receiver electrodes at a level determined by the reference.

The output of the current-to-voltage circuit is rectified, amplified and offset to yield a dc output centered about zero in ocean waters. A voltage change of 0.2 volts corresponds roughly to a salinity change of 1 $^{o}/_{oo}$ or a temperature change of 1°C.

DETAILED DISCUSSION

The oscillator (Fig. 3) is controlled by an FET current sink. Adjustment of R24-R25 for marginal oscillation with grounded control input (Jumper #1) sets the operating point such that the error voltage is near zero, the condition of greatest sensitivity of the control circuit. The seemingly purposeless resistor R28 is required to forestall oscillation.

The input circuit for the differential amplifier is critical. The voltage drop across C1 and C2 must vary negligibly with temperature, pressure, etc. Electrocube series 652A capacitors are compact and have

a temperature coefficient at oceanic temperatures of about 100 ppM/°C. Pressure sensitivity is more serious, 1% in 300 decibars. The impedances of C1 and C2 at 3kHz are about 50Ω so the voltage drops across them, as they are in series with the 1 m bias-current resistors. R1, R2, are only 0.005% of the voltages seen by the amplifier, so changes with temperature and pressure are negligible. Capacitors of this type are used throughout wherever the value of capacitance is important.

The differential amplifier precedes comparison of voltage level with the reference, so its gain stability and the stability of the rectifier-comparer are critical. Low-drift resistors (Vishay S 1025P) must be used. The blocking capacitor between amplifier and rectifier is critical also. The diodes in the rectifier are a serious source of temperature sensitivity. Their effect is minimized with this configuration and these component values. Also an identical rectifier circuit is used in the output, so that with identically drifting components the effects would compensate.

The same reference zener supplies the reference voltage to which the rectified receiver voltage is compared in the output offset, so any drifts in it compensate to some extent. A current derived from this reference is summed with the rectified receiver current in IC5 and amplified with a frequency-dependent gain that is approximately × 1000 at the highest frequency of the signal band, 1Hz. The gain is inversely proportional to the frequency. The sensitivity of the oscillator control circuit is approximately 2000 v/v, and the × 9 gain of the differential amplifier just compensates for the voltage divider effects caused by R28, C7, and C8, so the loop gain is greater than 10^6 at 1Hz. Therefore a change in cell impedance of 30%, typical in oceanic conditions, corresponds

to a proportional change in receiver voltage of only 0.3×10^{-6} and an apparent change in output due to finite gain of 0.01 ppM salinity, negligible.

The driving current is transformed to a voltage, rectified, offset, and amplified. Also in the output circuit a temperature-compensating thermistor is included, to take out residual temperature sensitivity of the circuit. This thermistor is mounted on the circuit board and is potted with it. It may not be required for many applications.

The operational amplifiers are of two types, OP-7 and OP-12, both from Precision Monolithics. The OP-7 is a precision dc amplifier for use where dc drifts are damaging. Its power drain corresponds roughly to that of a 10 KΩ resistor connected from + supply to - supply. The OP-12 has poorer dc drift properties, but consumes much less current, 0.3 to 0.4 mA regardless of supply voltage. A version of this circuit with OP-12's throughout consumed much less current, but was less stable. This trade-off will be discussed below under TESTS.

The circuit is assembled on a printed-circuit board 7"" long and 1.5 inches wide and expoxy-cast in a half-cylinder mold so that it fits on a mother board within our instrument case (Fig. 4). The cast circuit can be damaged only by corrosion or breakage of its pins.

LABORATORY TESTS

The range of supply voltages for operation is ±4.5 to ±18 volts. The usual power source is a "transistor" 9v alkaline battery. At 8.4 volts the current drain is approximately 10 mA from the + battery and 9 mA from the - battery. With the OP-7 operational amplifiers replaced with OP-12's, the current drain is reduced to 6 mA on the + side and 5 mA on the minus side with this supply voltage. The circuit's sensitivity to changes in supply voltage

is such that a 1 volt change in supply produces an output change corresponding to approximately 0.0005°/$_{oo}$ salinity change.

Routine checking of circuit operation is performed with a dummy which roughly simulates a four element transducer (Fig. 3). If the circuit performs up to expectations, shorting of point A to point B should have little effect on the output. In fact a change in output corresponding to 3 ppM salinity change is seen, so if drifts in electrode polarization impedances are no worse than 30% of their nominal values, drifts of less than 1 ppM salinity-equivalent will result.

The sensitivity and linearity of the circuit are tested by varying the resistance, R, between terminals B and C and plotting the result vs. R^{-1}. The resulting plot cannot be distinguised from a straight line. Calculated deviations from a least-squares straight line fitted over a ± 30% range in R correspond to 2 ppM salinity.

The sensitivity of the circuit to temperature changes is critical, because in use it will be cycled from deck to several hundred meters depth, a temperature shock of 20°C which in the RSVP will be accomplished in only a minute, but will take 10-20 minutes in the microstructure instrument. Temperature sensitivity is measured by placing the circuit, without batteries or transducer, into a container filled with liquid Freon and then placing the container in a refrigerated controlled-temperature bath. The dummy transducer is connected, but remains outside the bath. The temperature coefficient is approximately 0.3 ppM salinity equivalent per °C circuit-temperature change (Fig. 5). With the temperature-compensating circuit connected and adjusted, the variation nearly disappears (Fig. 6). A test which simulates the temperature cycling involved in

casts of the microstructure instrument shows apparent salinity variations of approximately 1 ppM induced by the temperature cycling (Fig. 7). Adjustment of the temperature componsation, if required, must be performed individually for each circuit, apparently because of variations in the properties of individual components.

With OP-12 replacing the OP-7's, hysteresis in the temperature sensitivity is found (Fig. 8). Such a circuit would be satisfactory in an application where its temperature does not change much, or where precision of 5 ppM is sufficient. It draws much less power, as discussed above.

Noise level is approximately 0.4 ppM salinity equivalent peak-to-peak, therefore less than 0.1 ppM salinity equivalent rms (Fig. 9). Long term drift of the combination of circuit and transducer were measured by placing both in a constant-temperature bath for a week and measuring the output each day (Fig. 10). The indicated drift was roughly 3 ppM salinity-equivalent per week, which could well have been a real change in sample salinity due to evaporation.

CALIBRATION

The calibrations of the combination of circuit and transducer are done in two steps: (1) The properties of each circuit are determined by determining its output with each of two high-quality dummies of different resistance, resulting in a formula relating conductance, C, and output, V:

$$C = a_I + b_I V, \qquad (1)$$

where a_I and b_I are characteristic of the circuit numbered I.

(2) Each transducer is calibrated with one standard circuit (circuit 1), retained for that purpose, yielding a relation between output for this circuit and conductivity, λ;

$$\lambda = A_{1J} + B_{1J} V \tag{2}$$

where A_{1J} and B_{1J} are characteristic of the combination of circuit 1 and transducer J.

Combining (1) and (2), a relation specific to transducer J can be derived, relating the conductance of the effective water path between its receivers to the conductivity of the water:

$$C = (a_1 - \frac{b_1}{B_{1J}} A_{1J}) + \frac{b_1}{B_{1J}} \lambda. \tag{3}$$

Now by combining (1) and (3) the calibration for any combination of transducer and circuit is derived as:

$$\lambda = A_{IJ} + B_{IJ} V \tag{4}$$

where

$$A_{IJ} = A_{1J} + B_{1J} \frac{a_I - a_1}{b_1}$$

$$B_{IJ} = \frac{b_I}{b_1} B_{IJ}.$$

The calibrations are performed using Copenhagen water, varying the temperature to get different values of conductivity. Conductivity is also measured with an Autosal salinometer. Calibrations are reproduced within

about 9 ppM salinity in several repetitions. It was found to be very important to conduct the calibration in a well stirred sample with evaporation minimized.

FIELD TEST

The circuit was installed in a microstructure instrument and a dummy transducer was connected. A standard microstructure cast was carried out, with a drop speed of 15 cm/sec, at 31°N 154°W in January 1980. At this time the temperature in the water column was nearly constant to 120m depth, then decreased quite suddenly in the seasonal thermocline. The variation in the output, caused presumably by thermal shock, was approximately $0.001°/_{oo}$ apparent salinity variation, with noise in a bandwidth equivalent to the transducer response length of approximately $0.0002°/_{oo}$ (Fig. 11).

Acknowledgement: This development was sponsored by the Oceanic Processes Branch, National Aeronautics and Space Administration.

FIGURE CAPTIONS

Fig. 1. Equivalent circuit of 4-electrode conductivity cell. The electrode polarization impedance are all denoted by Z_p, although they will each have different values. The input circuit of the differential amplifier is represented in a simplified way. The driving current, I, passes through one driver electrode to the other, past the receiver electrodes. The voltage senses by the receiver electrodes is V_w, that seen by the amplifier is much larger than any other impedence.

Fig. 2. Block diagram. The cell electrodes are labeled A, B, C, D. The reference and temperature compensation circuits are shown in detail (R16, R37, R39, T1).

Fig. 3. Schematic. IC 1, 2, 3, 6, 7, 8 are Precision Monolithics OP-12 FJ's. IC 4, 5, 9, 10 are OP-07CJ's in the more precise version of the circuit, but are OP-12FJ's in the lower-power version. Resistances with values underlined are Vishay S 102SP, others are RN55C metal film resistors. The reference diode Z1 is a Zener ICL 8069 CCQ. Thermistor T1 is a 500 k unit, Fenwal PT55D1. Capacitors are Electrocube series 652A except for C11 and C12 which are solid tantalytics. Resistors R6, R7, R8, and R9 are match to ± Ω to minimize amplification of common-mode signals. Operating frequency is 3 kHz. Jumper #1 is removed after R24 and R25 are selected for marginal oscillation, and jumper #2 is connected for feedback operation.

Fig. 4. The circuit board before and after plotting.

Fig. 5. Typical sensitivity of output to circuit temperature without temperature compensation. Unit-to-unit variation is considerable.

Fig. 6. Sensitivity of output to circuit temperature, with temperature

compensation circuit added. A slightly more complex circuit would be required to achieve perfect compensation.

Fig. 7. Variation of output while circuit temperature is varied to simulate a microstructure cast through the seasonal thermocline.

Fig. 8. Sensitivity of output to circuit temperature with OP-12 operational amplifiers throughout and no temperature compensation.

Fig. 9. Sample record of noise in a 30 Hz bandwidth.

Fig. 10. Drift of combined circuit-transducer system in 8 days at constant temperature ± 0.002°C. The error bars on the point for DAY1 represent the standard deviation for 10 readings on that day. The trend is toward larger conductivity and could be caused by very slight evaporation of the seawater sample. Loss of approximately 0.0003 cm of water from the surface would accomplish this change.

Fig. 11. Output of circuit with dummy transducer vs. depth of instrument on microstructure cast with 15 cm/sec fall speed. The bandwidth for the signal is 0.3 Hz, which corresponds to the expected response length of the transducer, 8cm. The trace at left represents the temperature profile.

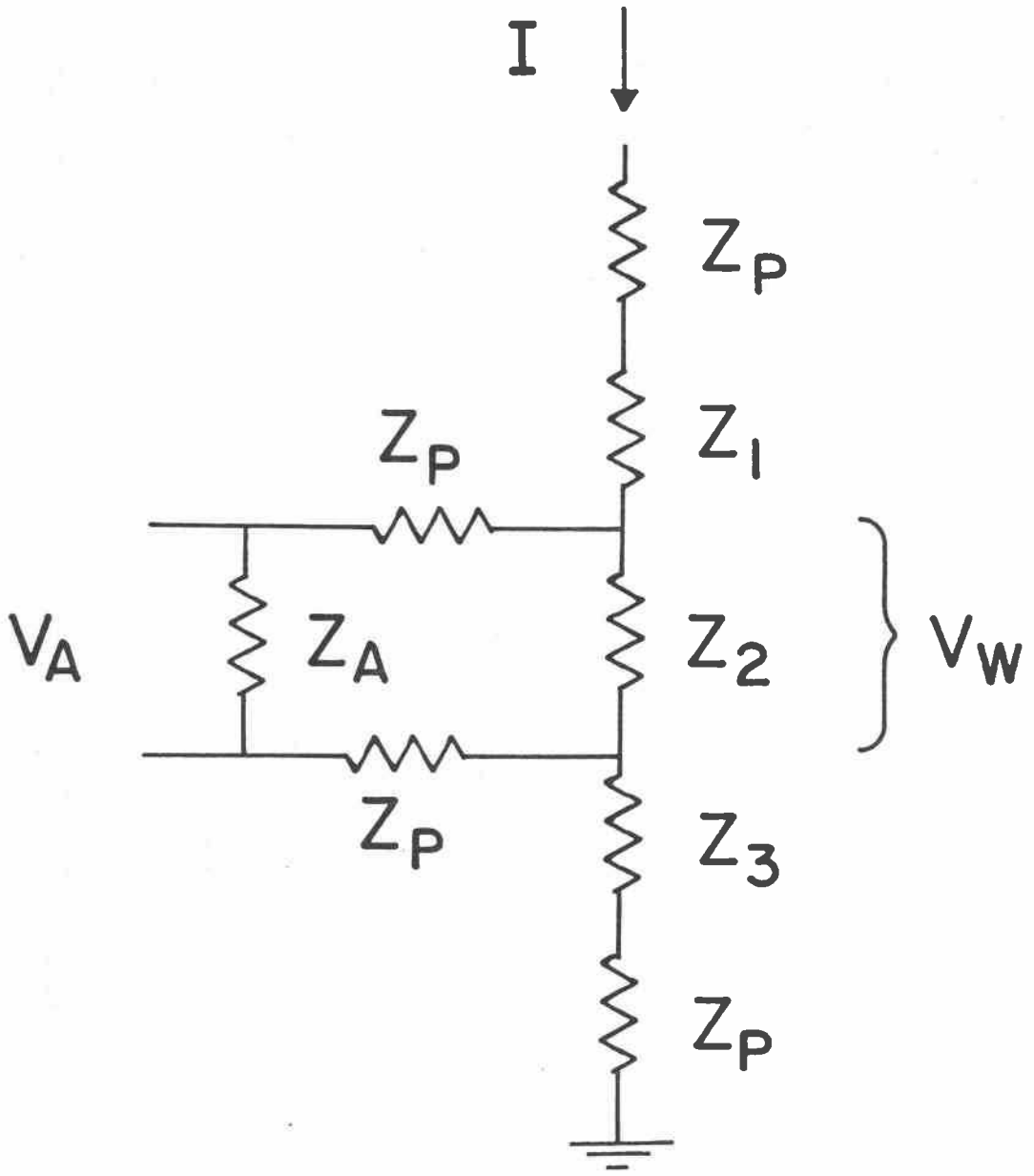

FIGURE 1.

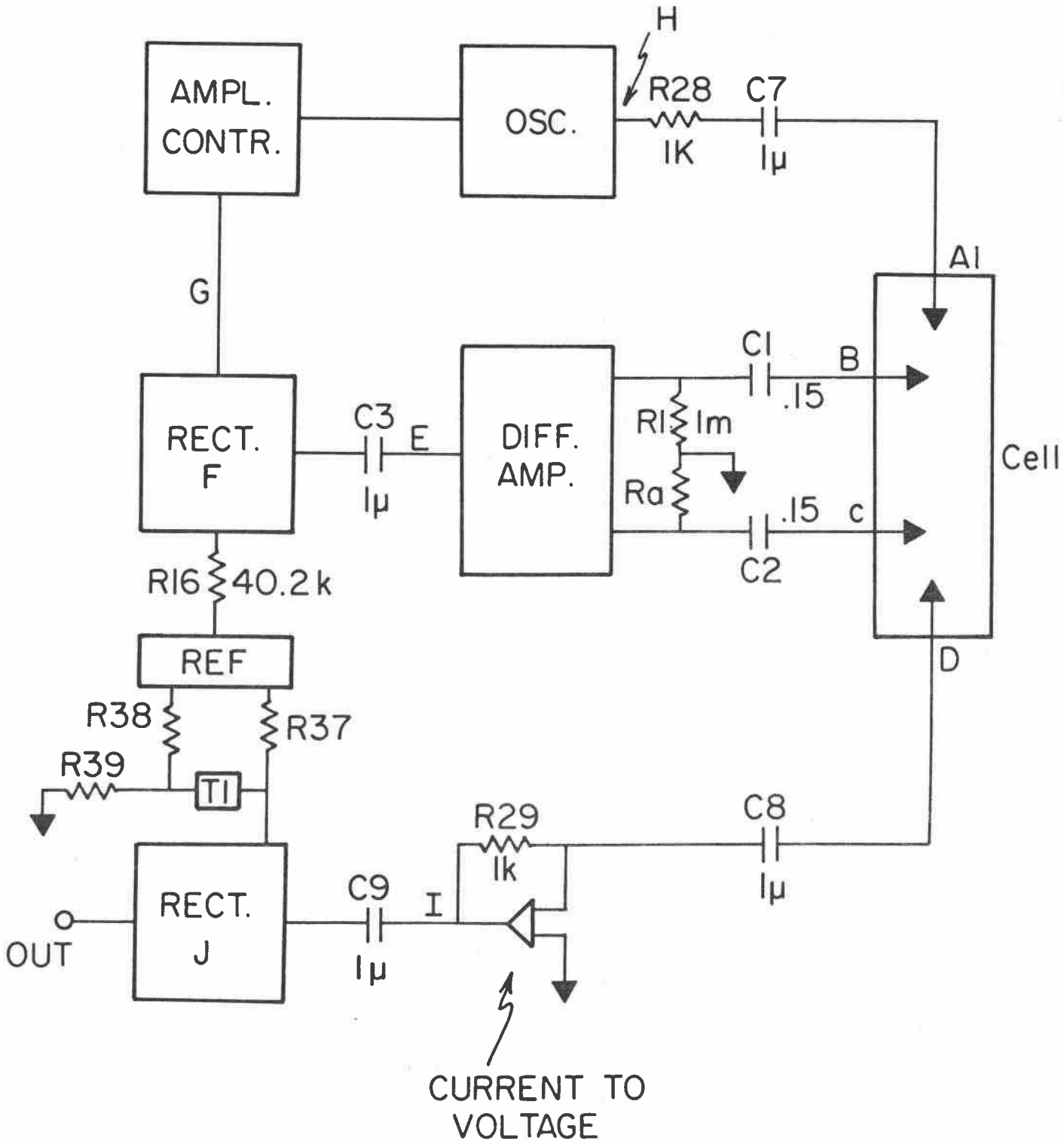
AMPL.
CONTR.
OSC.
H
R28
IK
C7
Iμ
A1
G
C1
.15
B
RECT.
F
C3
Iμ
E
DIFF.
AMP.
RI
Im
Ra
.15
c
C2
Cell
R16
40.2k
REF
D
R38
R37
R39
TI
R29
Ik
C8
Iμ
RECT.
J
C9
Iμ
I
OUT
CURRENT TO
VOLTAGE

FIGURE 2.

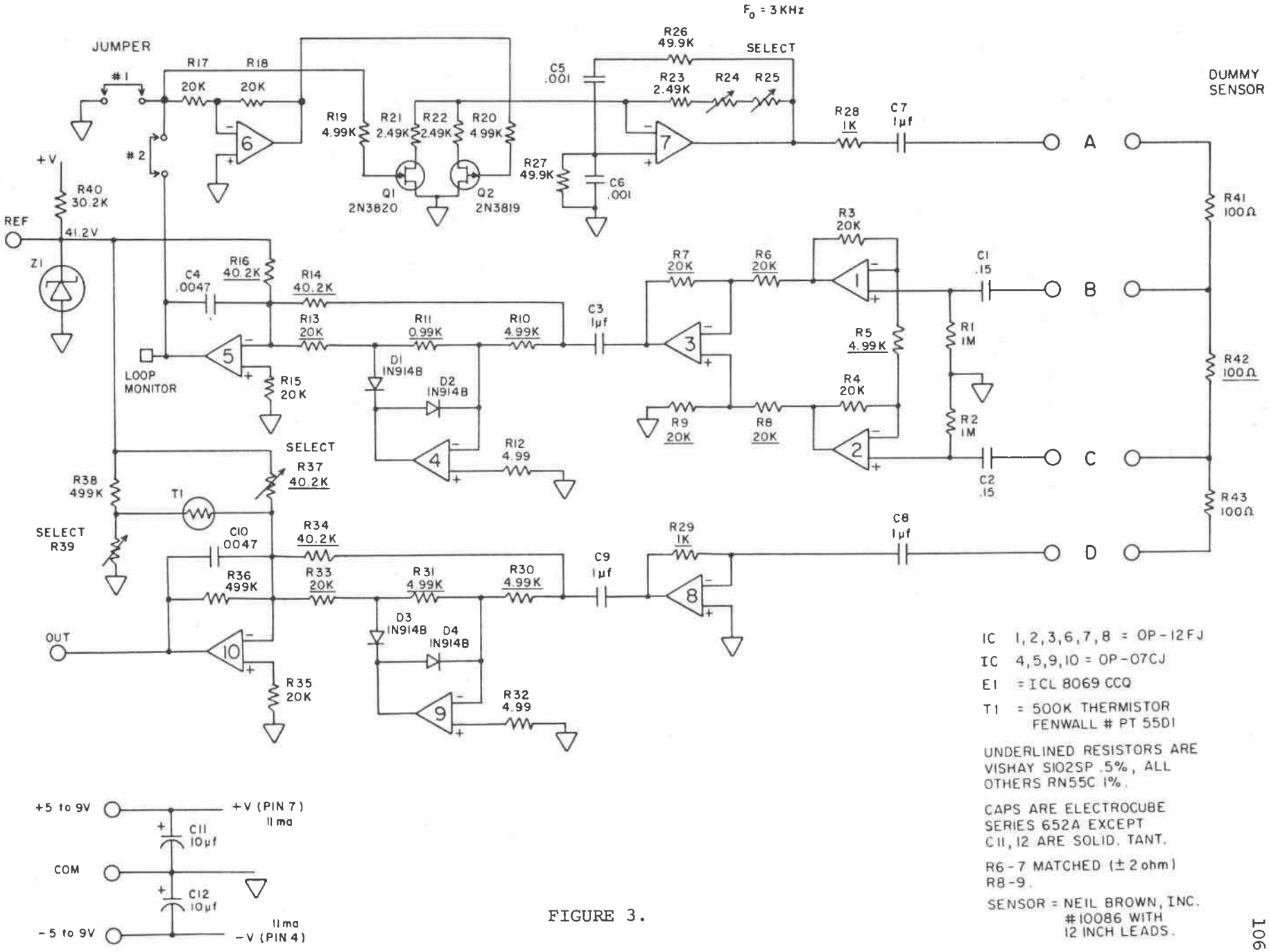

IC 1,2,3,6,7,8 = OP-12FJ

IC 4,5,9,10 = OP-07CJ

E1 = ICL 8069 CCQ

T1 = 500K THERMISTOR
FENWALL # PT 55D1

UNDERLINED RESISTORS ARE VISHAY S102SP .5%, ALL OTHERS RN55C 1%.

CAPS ARE ELECTROCUBE SERIES 652A EXCEPT C11, 12 ARE SOLID. TANT.

R6-7 MATCHED (±2 ohm) R8-9.

SENSOR = NEIL BROWN, INC. #10086 WITH 12 INCH LEADS.

FIGURE 3.

FIGURE 4.

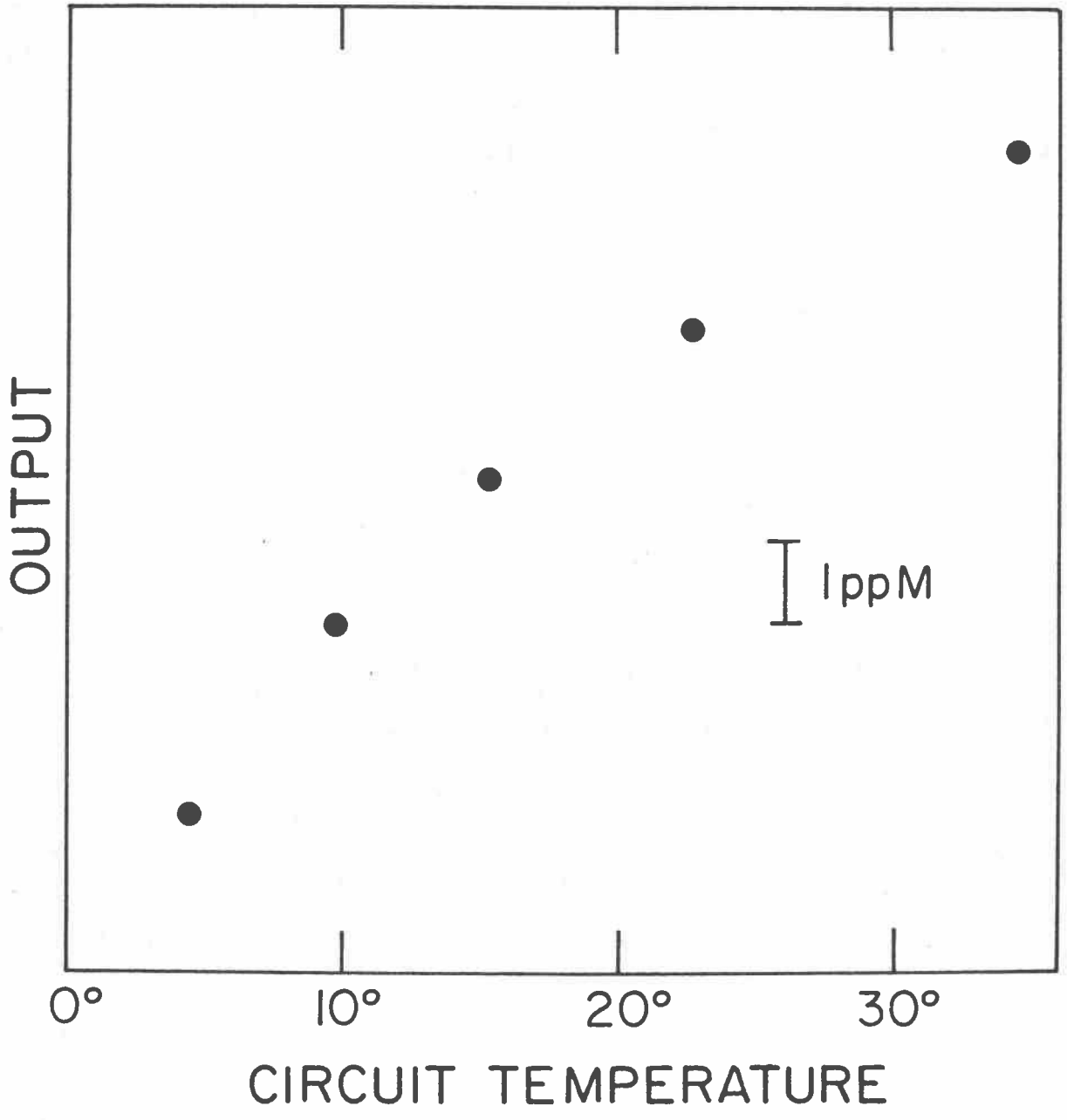

FIGURE 5.

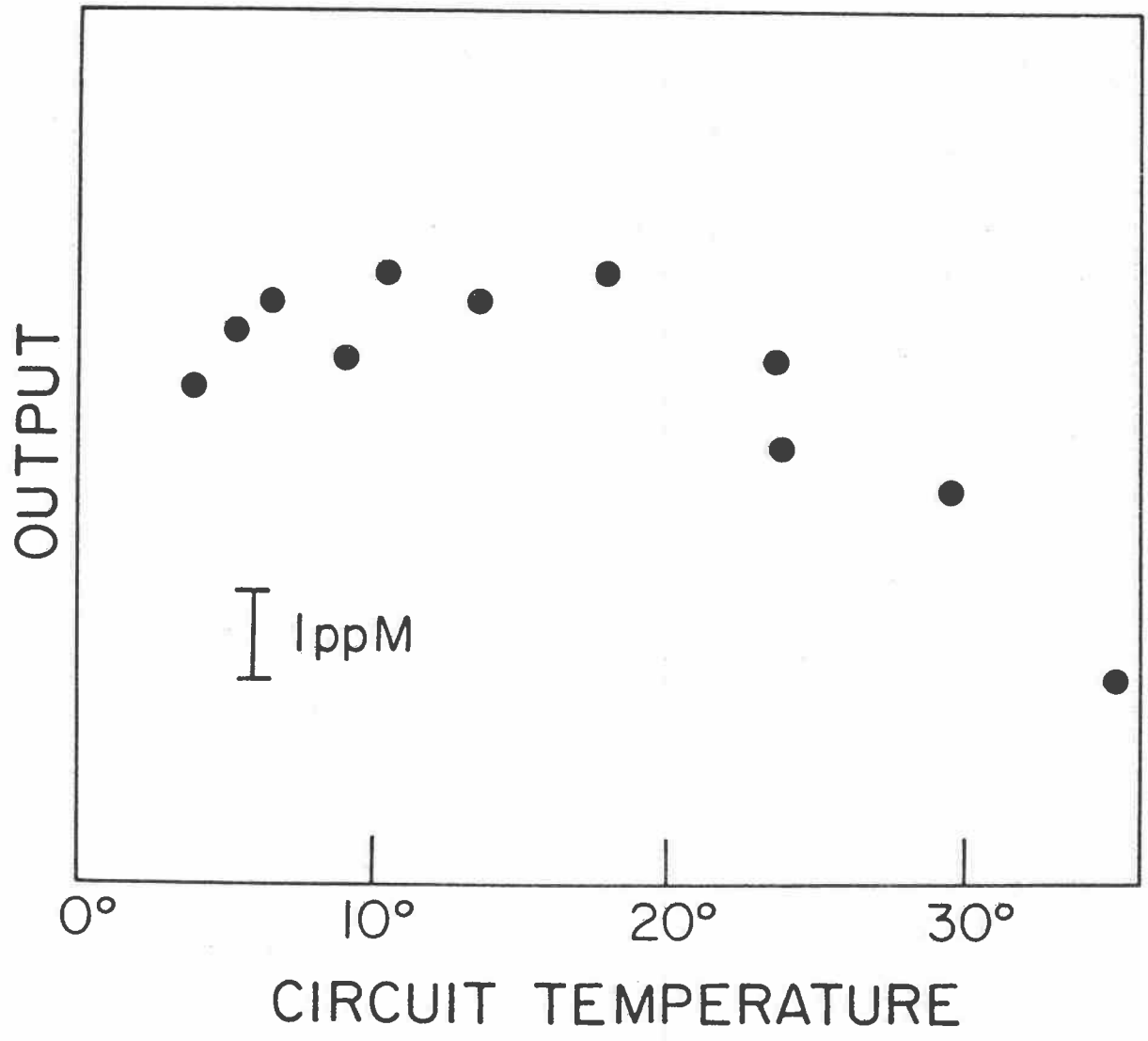

FIGURE 6.

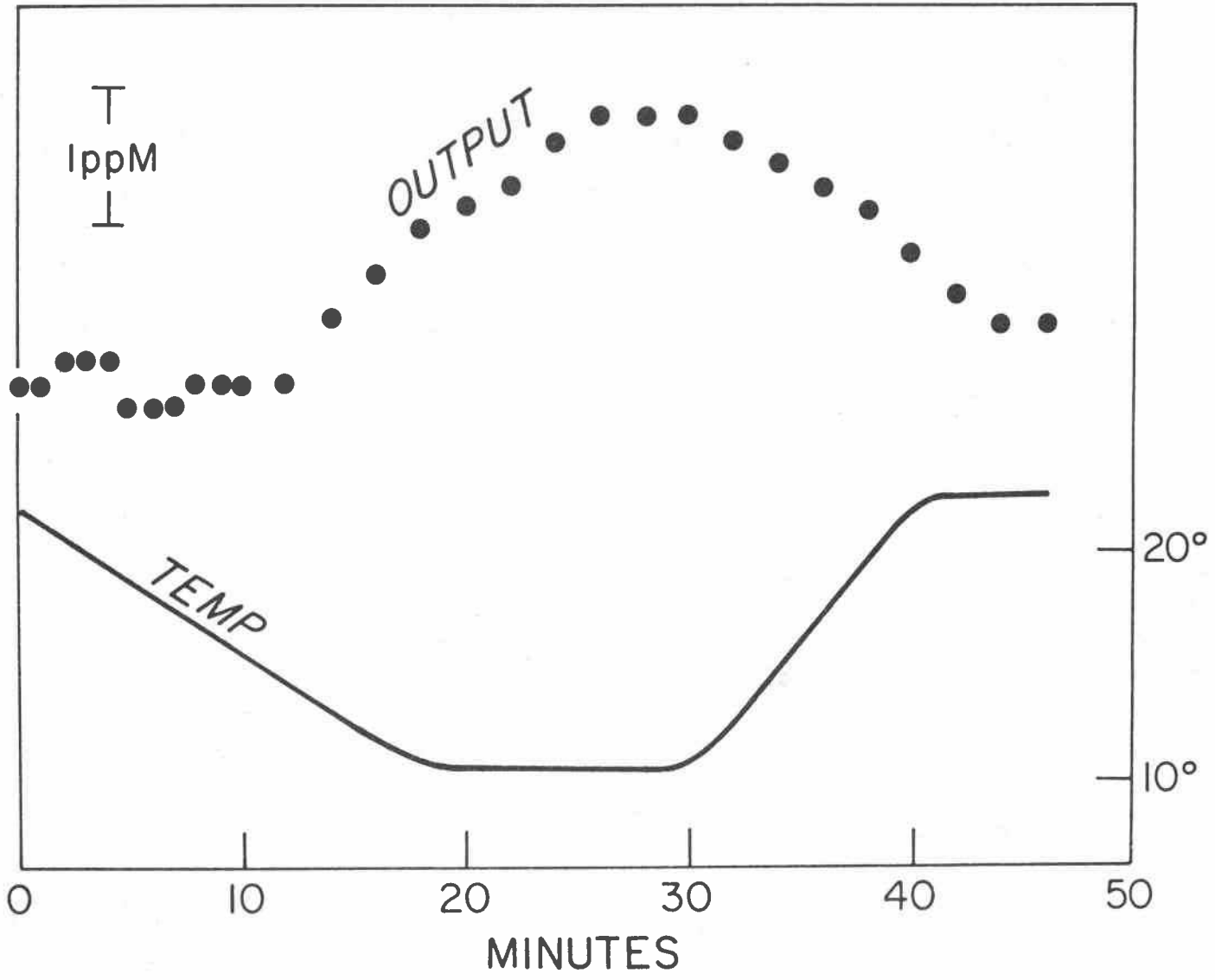

FIGURE 7.

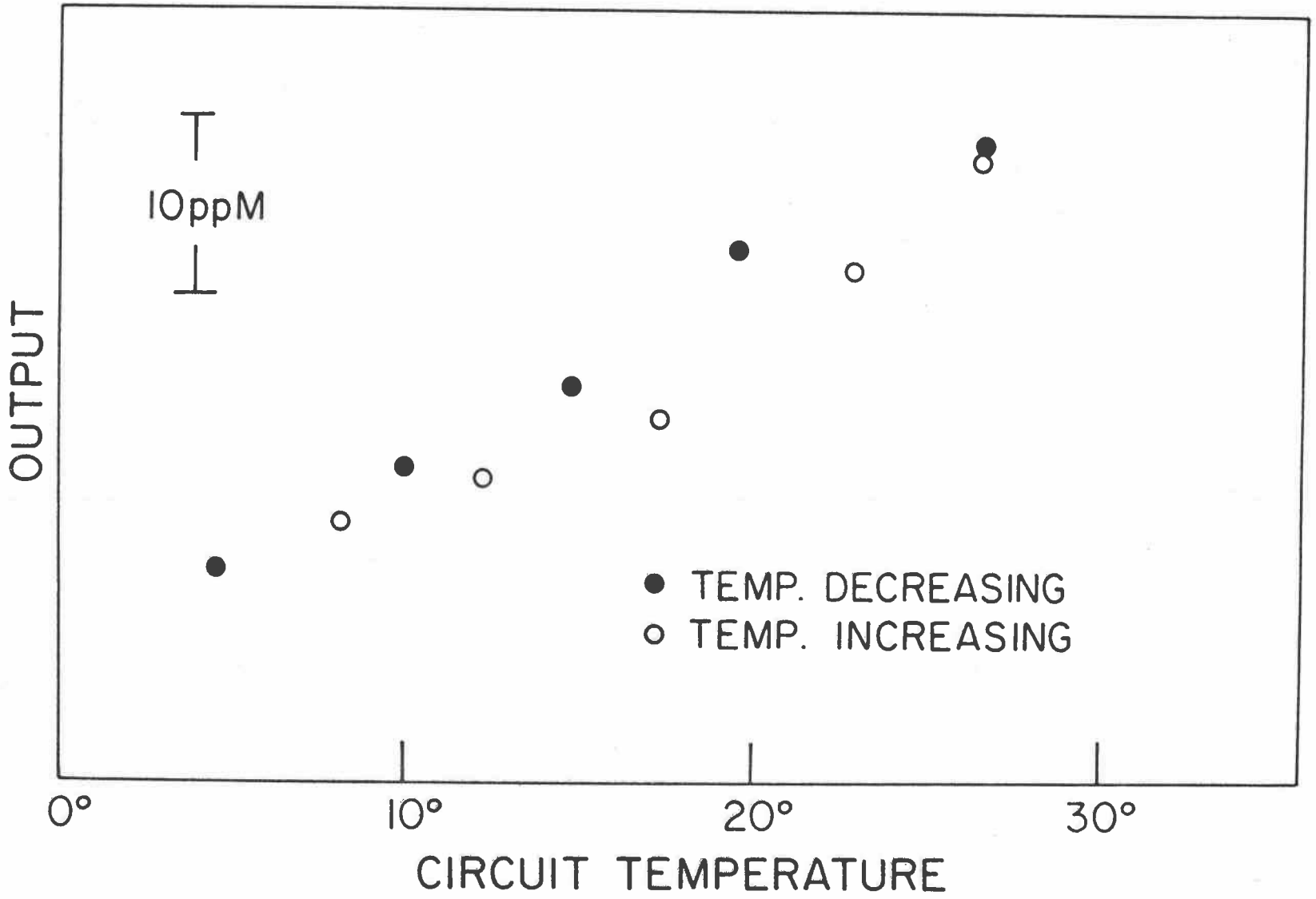
10ppM
OUTPUT
TEMP. DECREASING
TEMP. INCREASING
0°
10°
20°
30°
CIRCUIT TEMPERATURE

FIGURE 8.

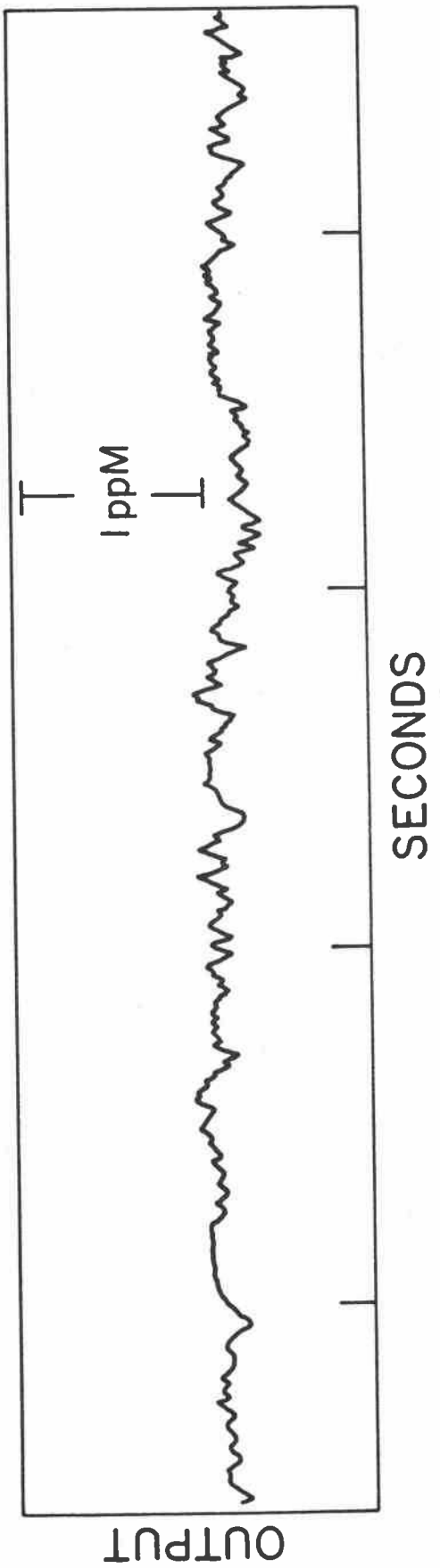

FIGURE 9.

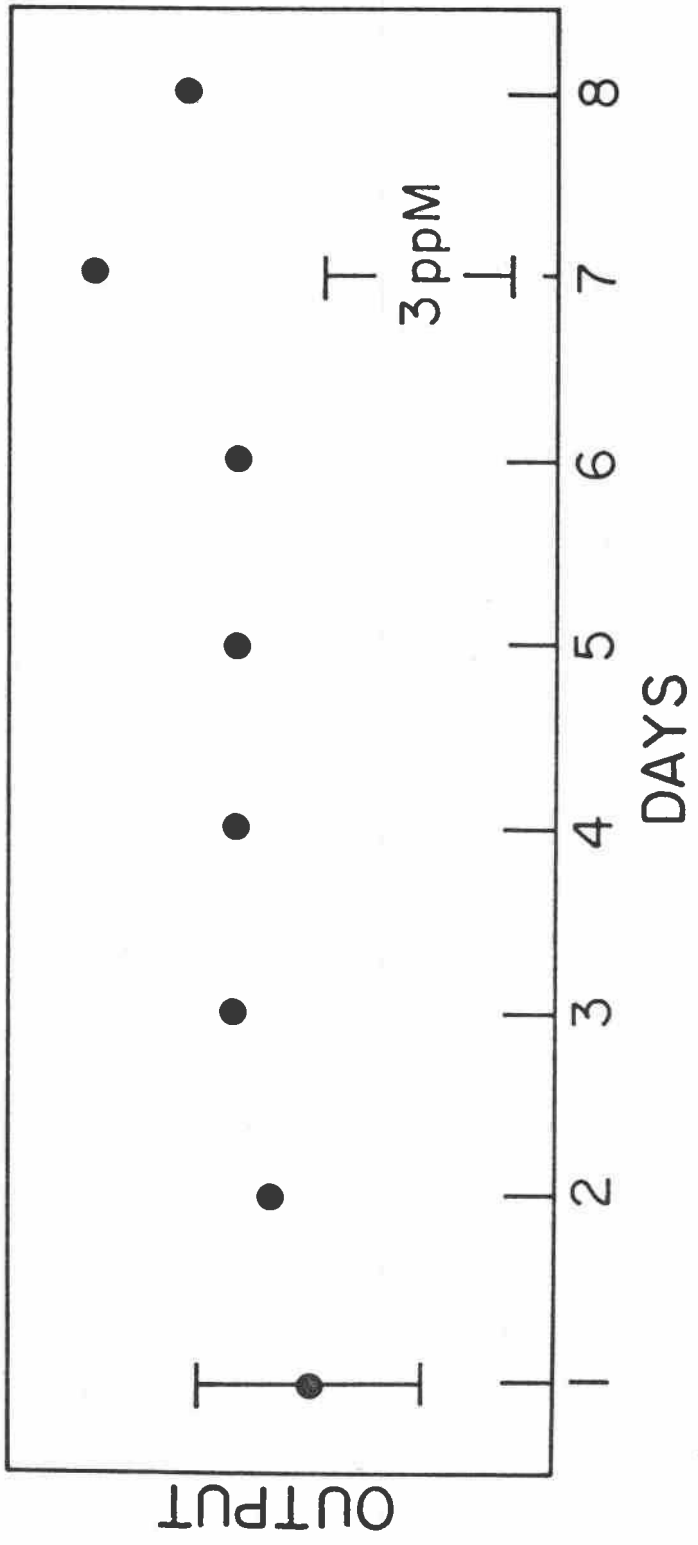

FIGURE 10.

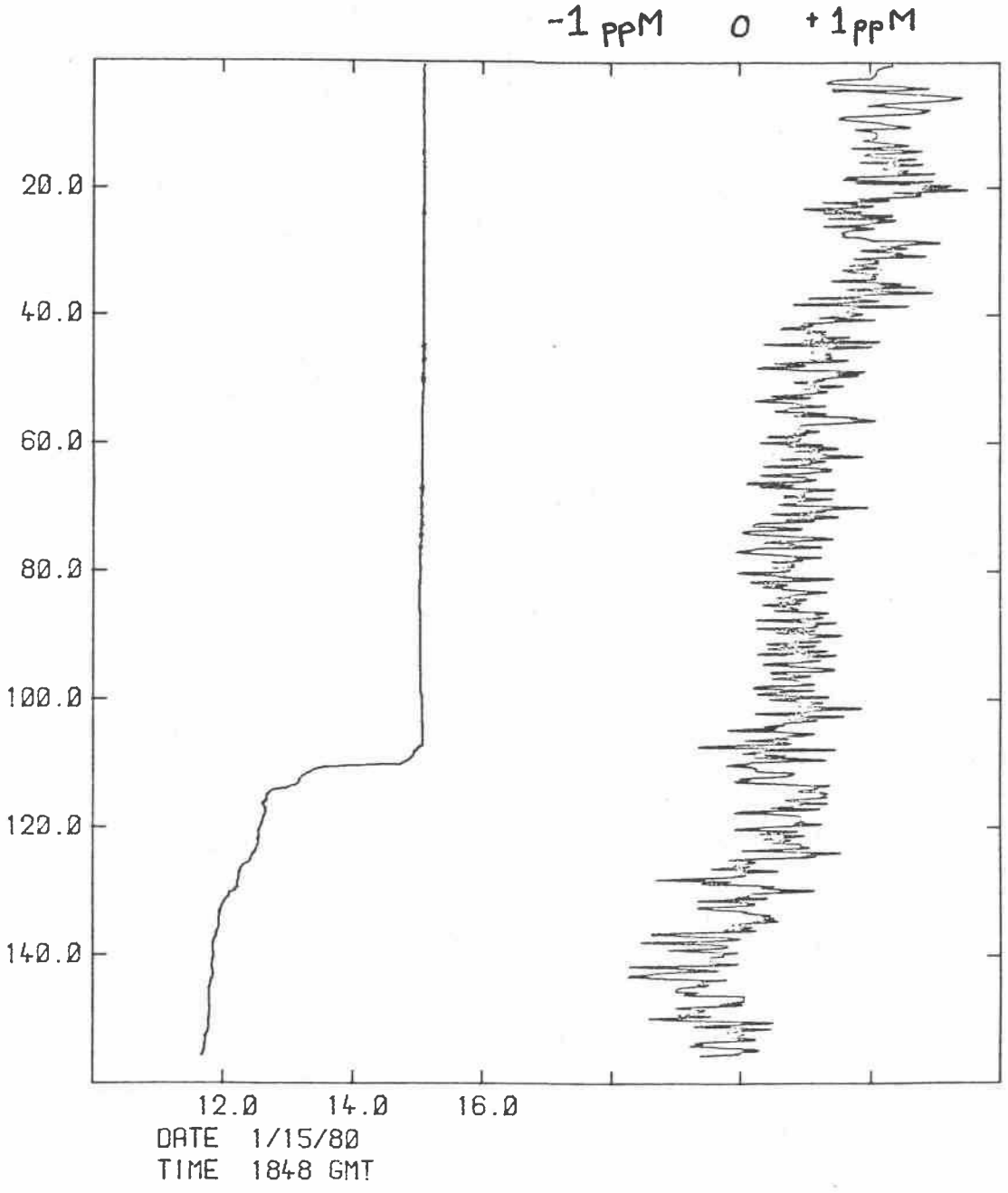
TAPE F1J FILE 3
UNIT 2.79
-1 ppM 0 +1 ppM
20.0
40.0
60.0
80.0
100.0
120.0
140.0
12.0
14.0
16.0
DATE 1/15/80
TIME 1848 GMT

FIGURE 11.

The Batchelor Spectrum and Oceanic Microstructure

Interim Report, 1980

D. R. Caldwell
T. M. Dillon

School of Oceanography
Oregon State University
Corvallis, Oregon 97331

ABSTRACT

In the past three years we have been occupied with an attempt to discover whether "microstructure" data, small-scale temperature-gradients, can be fit by a theory put forward by G. K. Batchelor in the context of high Reynolds number, homogeneous, isotropic flow. In this collection are gathered six papers detailing our progress in this enterprise, as well as some insights we have gained into energy dissipation in various regimes of the ocean. An overview is included as an introduction.

INTRODUCTION

We present a series of manuscripts dealing with the application to the ocean of a theory for the small-scale variation of temperature in a turbulent fluid. The essential results of this theory were put forward by G. K. Batchelor (1959), and the one-dimensional form was derived by Gibson and Schwartz (1963). We compare Batchelor's predictions with vertical wavenumber spectra calculated from vertical temperature-gradient profiles taken with a freely-falling instrument package, using data from several regimes in natural waters. The first object of this enterprise was to discover whether Batchelor's results are relevant to oceanic flows. Encouraged by finding their application at least plausible we proceeded to look for situations where quantitative comparisons of theory and field data were possible. At the same time an effort to obtain information of more general interest has been maintained.

In the introduction of Batchelor's (1959) paper, he states:

> "When the temperature of a fluid in turbulent motions is not uniform (although with such small variations that buoyancy forces are negligible), the temperature field is made random by the irregular movements of the fluid and acquires statistical properties which are directly related to those of the turbulent motion... This paper will give a theoretical discussion of the small-scale components of quantities like temperature, "small" being taken here to mean that the components concerned have characteristic length-scales small compared with the length-scale of the eddies containing the bulk of the kinetic energy of the turbulent motion.
>
> The dominant feature of the action of the turbulent motion on the temperature distribution is a continual reduction of the length-scale of temperature variations. The random convection of material elements of the fluid is inevitably accompanied by distortion of these elements, and, in the absence of molecular conduction, a (statistical) increase in the gradients of temperature... Unless temperature variations on some definite length-scale are supplied continually by some external agency, the statistical properties of the temperature distribution cannot be exactly steady; however, the properties of the small-scale components

of the temperature distribution will be approximately steady in general, because the process of convective distortion and increase of temperature gradients takes place much more quickly than the over-all decay of the temperature field. The continual increase in the magnitude of temperature gradients due to random convection will ultimately be checked by the smoothing action of thermal conduction, and no further refinement of the temperature distribution can occur; in this way, a length-scale characterizing the smallest temperature 'eddies' is determined...

The problem to be studied is thus as follows. A quantity $\theta(x,t)$ has a distribution in the fluid which is governed by the equation

$$\frac{\partial \theta}{\partial t} + u \cdot \nabla\theta = D\nabla^2\theta,$$

where u is the velocity of the fluid and is independent of θ. The fluid, taken as incompressible, is in turbulent motion at high Reynolds number, and the length-scale characterizing the energy-containing eddies is L. We wish to determine the statistical properties of those components of the spatial distribution of θ that have a length-scale small compared with L, and in particular to determine the wave-number spectrum of the distribution of θ. This is a familiar kind of objective in the theory of turbulence, although not one which is often achieved convincingly. It will be shown that a reasonably complete description of the spectrum of θ can be obtained, partly by the use of simple new ideas and partly by the use of old ideas in a new context, this success being made possible by the linearity in θ of all terms in (1.1). No measurements appear to be available for comparison with the theoretical results."

Theoretical spectral form Batchelor goes on to develop the form the wavenumber spectrum would be expected to take in high Reynolds number, isotropic, homogeneous turbulence. We are concerned only with the case where the viscosity, ν, is much larger than the diffusivity, D, so that thermal gradients may exist on scales smaller than the smallest eddies of the turbulence. Two formulas then describe the temperature spectrum, one applying to scales smaller than the eddies, the other to larger scales. At the smallest scales the one-dimensional wavenumber spectrum, developed from Batchelor's three-dimensional form by Gibson and Schwartz (1963) is:

$$S(k) = (q/2)^{1/2} \chi (k_B^{-1} D^{-1} f(\alpha)) \qquad (1)$$

in terms of radian wavenumbers. In terms of the cyclical wavenumbers more often used in oceanic work

$$S(k) = (\chi/2D)((2q)^{1/2}/k_B) f(\alpha) \qquad (2)$$

where $S(k)$ is the value of the temperature gradient spectrum in units of $(°C/cm)^2/(\text{cycle per cm})$, k is the wavenumber in cycles per cm, k_B is the Batchelor wavenumber $(1/2\pi)(\varepsilon/\nu D^2)^{1/4}$ in units of cycles per cm, D is the (thermal) diffusivity in cm^2/sec, and α is $(2q)^{1/2} k/k_B$. It is hoped that the dimensionless constant q is universal. The rate of dissipation of temperature variance χ is defined as $6D < (\frac{\partial T'}{\partial z})^2 >$, T' being the temperature fluctuation and the symbol <> denoting an appropriate averaging process. The function $f(\alpha)$ is given by:

$$f(\alpha) = \alpha\{\exp(-\alpha^2/2) - \alpha \int_{\alpha}^{\infty} \exp(-\alpha^2/2)\, dx\}. \qquad (3)$$

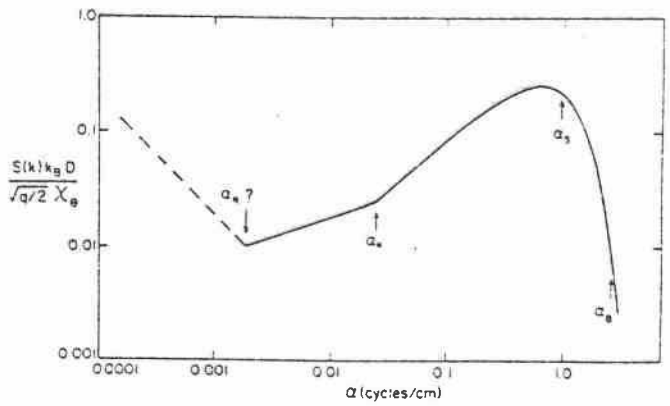

Fig. 1. Nondimensional universal spectrum with a 'fine structure' range for $\alpha < \alpha_R$, the Richardson wave number; an inertial subrange for $\alpha_R < \alpha < \alpha_*$; and a viscous-convective Batchelor spectrum for $\alpha > \alpha_*$. The positions of the Kolmogorov wave number α_s and Batchelor wave number α_B are determined by choice of the universal constant q ($2(3)^{1/2}$ assumed here), while the shape of the spectrum for $\alpha > \alpha_*$ is independent of universal constants. The inertial subrange is rarely observed in vertical microstructure.

At smaller wavenumbers, those of the "inertial subrange" of the turbulent velocity spectrum, the temperature gradient spectrum is given by

$$S(k) = \beta\chi\varepsilon^{-1/3} k^{1/3} \qquad (4)$$

where ε is the kinetic energy dissipation rate in units of cm^2 sec^{-3} and β is another constant. (Because of our choice of units, the value of β will differ from the conventional.) The units of S(k) here are $(°C/cm)^2$/(cycle/cm), those of k are cycles/cm. A schematic drawing of this form is given as Figure 1 of paper #2.

Relevance to the ocean: Because of the vertical stratification common in natural waters the assumptions underlying Batchelor's concepts are not fulfilled at all scales. Whether all, or any, of his conclusions will apply is open to question. Let us break down Batchelor's results into a series of statements and then see what can be concluded about each on the basis of the papers in this collection.

1. A cut-off wavenumber exists at which the spectrum falls rapidly, so that little of the spacial variation occurs at higher wavenumbers: According to the spectrum (2), at a wavenumber k_c of $2.28 \cdot k_B/\sqrt{2q}$ the spectrum has dropped to 10% of its peak value. Finding this cut-off in vertical temperature-gradient spectra presents experimental problems: It has been difficult to deploy in the ocean sensors which respond quickly enough for accurate measurement at frequencies corresponding to this scale. If a vertical section contains a region where ε is so large that k_c lies beyond the resolution of the sensor, then the cut-off is not seen, and the spectrum is "unresolved", in that neither k_c nor χ can be determined

from it. With the fastest sensors we can find, analyzing relatively short segments in the vertical, we do find a cut-off [Figures 2(c) and 2(d) of Paper #1 and Figure 3 of Paper #5] in many cases.

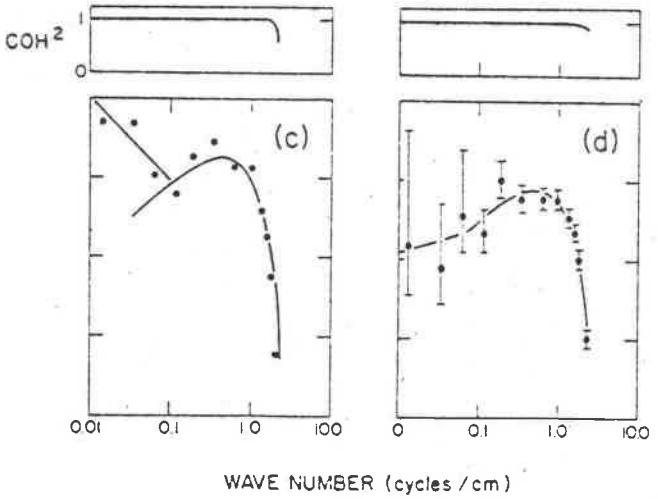

Fig. 2. Examples of observed spectra. Here 512 points at 90 points per second are used. Gaussian windowed. Two signals from the thermistor are amplified and recorded separately, so the coherence between them, shown above each spectrum, discriminates signal from noise (because the noise source lies mainly in the amplifiers). All data were recorded on August 23 in 18 m s^{-1} winds: (*a*) 51-m depth, turbulence level so low that fine structure dominates, noise shows up at right; (*b*) 54-m depth, all three components at comparable levels, turbulence just visible; (*c*) 40-m depth, turbulence signal dominates noise, fine structure just visible at left; (*d*) 32-m depth, only the turbulence signal is visible. The 95% confidence limits in Figure 2*d* apply to Figures 2*a*–2*c* also.

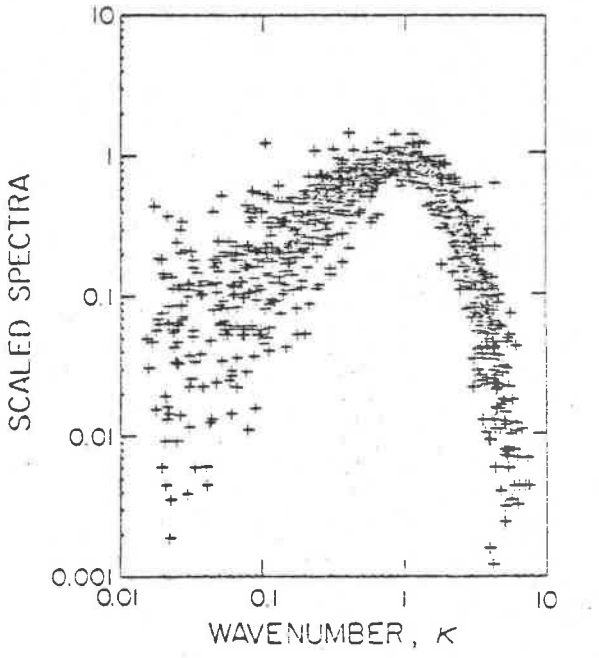

Figure 3. The seventy-seven non-dimensionalized spectra

Scaling such spectra and ensemble-averaging, the form of the spectrum in the cut-off region becomes apparent (Figures 4, 5 and 6 of Paper #2 and Figure 4 of Paper #5).

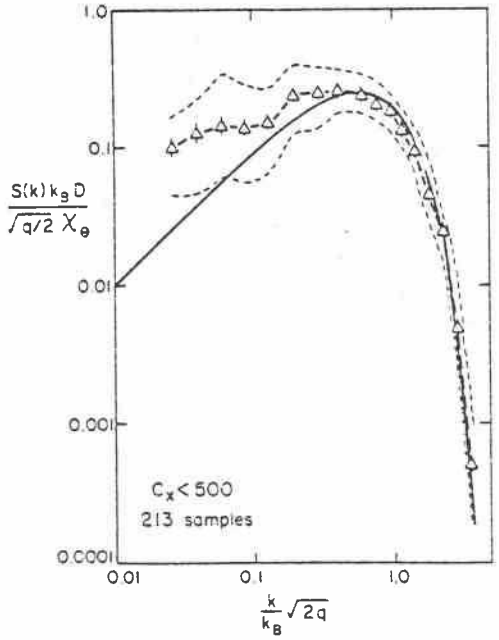

Fig. 4. Ensemble-averaged nondimensional spectrum for Cox numbers less than 500. The lower wave number portion of the spectrum departs significantly from the Batchelor spectrum (solid curve). Error bars are the standard error of the mean based on the standard deviation. The dashed envelope shows the average positive and negative deviation from the mean; that is, half of the spectral estimates lie within the envelope. Thus although the mean of the spectral values has a small uncertainty (the bars), the estimates in an individual spectrum may lie quite far from the mean.

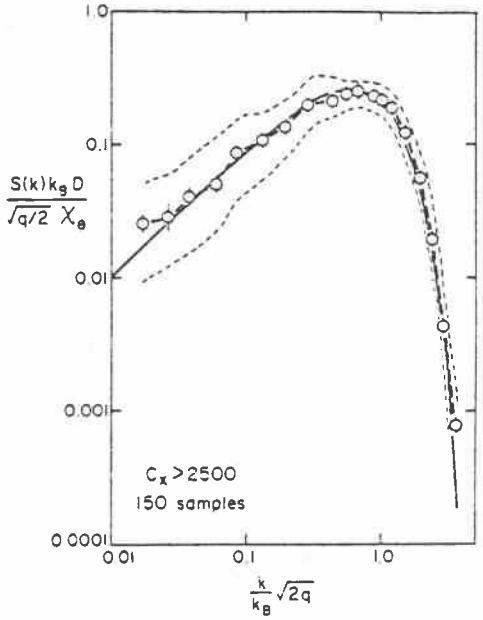

Fig. 6. Ensemble-averaged nondimensional spectrum for large Cox numbers. The low wave number portion of the spectrum is in remarkably close agreement with the Batchelor spectrum. Thus although the mean of the spectral values has a small uncertainty (the bars), the estimates in an individual spectrum may lie quite far from the mean.

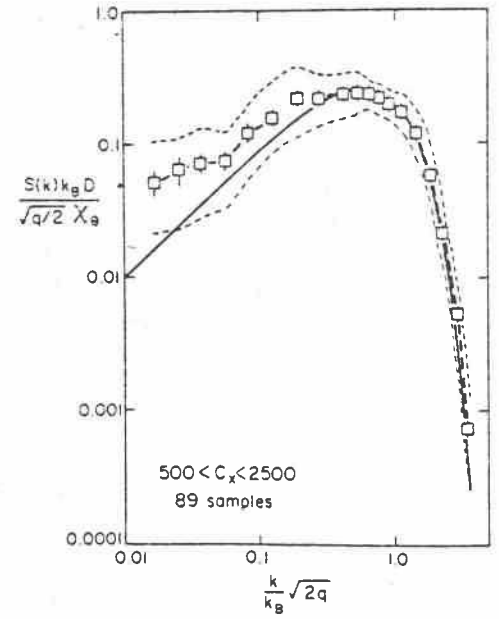

Fig. 5. Ensemble-averaged nondimensional spectrum for intermediate Cox numbers. The low wave number portion of the spectrum is closer to the Batchelor spectrum than the low Cox number spectrum but still is significantly different. Thus although the mean of the spectral values has a small uncertainty (the bars), the estimates in an individual spectrum may lie quite far from the mean.

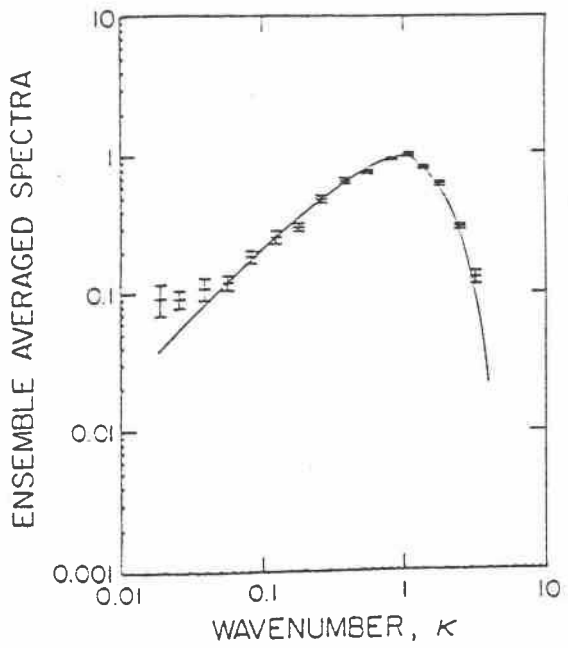

Figure 4. The ensemble averaged spectrum. The bars represent the standard error of the mean; the solid line is the Batchelor spectrum.

In some spectra a cut-off cannot be seen. Examination of these cases reveals several reasons: (1) The turbulence signal is too weak relative to the "fine-structure" signal or the instrumental noise [Figure 2(a) of Paper #1] or (2) The dissipation in that segment of the water column is so large that the cut-off lies beyond the sensor's resolution. We conclude that the cut-off does exist.

2. The cut-off wavenumber is related to the Batchelor wavenumber: Once it is established that the cut-off wavenumber k_c does exist and that it can be seen in spectra produced by our instrument system, the next step in testing the applicability of the Batchelor spectrum is to determine whether k_c is related to k_B. Two problems are presented in calculating k_B: (1) a value for ε is required and (2) considerable uncertainty exists as to the value of the "universal constant" q. We have used data from various regimes in the water column, and used different means of estimating values of ε. Each time, a close relation between k_c and k_B has been found. In principle the constant q should be calculable from these results, but statistical variations are too great for us to improve previous estimations. The evidence for the relationship between k_c and k_B follows:

(a) MILE thermocline The first evidence, which rendered the relationship at least plausible, came from data taken in August 1977 at Ocean Station P as part of the Mixed Layer Experiment (Paper 1). The temperature-gradient profiles came from the mixed layer, the seasonal thermocline, and the halocline. Values of ε were estimated from the rate of work, $\dot{E}$,

done against the density gradient. A formula for $\dot{E}$ was derived by following atmospheric work in relating $\dot{E}$ and the eddy diffusivity, and then calculating the eddy viscosity by the usual Osborn-Cox method. The utility of $\dot{E}$ as an indication of ε is based on the hope that the efficiency of the mixing process does not vary greatly. The formulas involved are:

$$k_c = \frac{2.28}{\sqrt{2q}} k_B, \tag{5}$$

derived from the Batchelor spectrum and the definition of k_c,

$$K_\rho = I \cdot D \cdot Cox, \tag{6}$$

the Osborn-Cox relation (assuming the eddy diffusivity for buoyancy, K_ρ, is the same as that for heat), where Cox is defined as $\langle(\frac{dT'}{dz})^2\rangle/(\langle\frac{dT}{dz}\rangle)^2$ and I is the isotropy factor, which varies from 1 for vertical stratification to 3 for isotropy,

$$\dot{E} = N^2 K_\rho \tag{7}$$

the relation between rate of work and eddy diffusivity in the presence of stratification represented by buoyancy frequency N, and the definition of the efficiency of mixing

$$\lambda \equiv \frac{\dot{E}}{\varepsilon + \dot{E}}. \tag{8}$$

Combining all these, we obtain

$$k_c = 2.28 \left\{\frac{I(1-\lambda)/\lambda}{4q^2}\right\}^{1/4} \cdot \frac{1}{2\pi} \left(\frac{\dot{E}}{\nu D^2}\right)^{1/4} \tag{9}$$

so that, except as affected by variations in λ and I, k_c and $\dot{E}$ will be correlated. The result from analyzing data selected

from the "mixed layer," seasonal thermocline, and halocline at Station P (Paper 1) was that this correlation is quite good

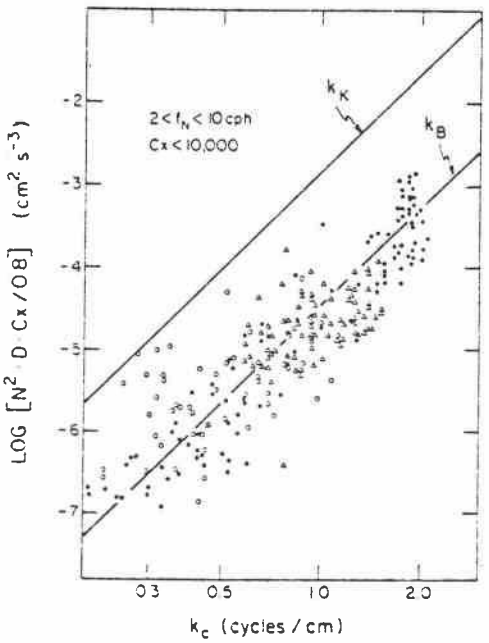

Fig. 6. Dissipation calculated as prescribed versus cutoff wave number. Cases with Cox number less than 10^4 and f_N between 2 and 10 cph are included. The data are those of Figure 4 (solid circles), together with data from the mixed layer on September 1 in 14 m s^{-1} winds (triangles) and data from various casts through the halocline (open circles). Lines are drawn to represent the Kolmogorov (k_K) and Batchelor (k_B) wave numbers.

(Paper 1, Figure 6), and that the coefficient $2.28 \cdot (I(1 - \lambda)/4q^2\lambda]^{1/4}$ is near 1, for cases where the Cox number was less than 1000. The coefficient turned out to be 1.2 ± 0.2 (Paper 1, Figure 5). We might note that reasonable choices of the parameters might be

$\lambda = 0.2$ Osborn (1980)

$I = 2 \pm 1$

$q = 3.9 \pm 1.5$ Grant, et al. (1962).

With these choices we might have expected the coefficient to lie between 0.98 and 1.94, so the value of 1.2 is reasonable. The scatter (e.g. Paper 1, Figure 6) may be caused by any of a number of factors, but probably principally results from either the statistical nature of the Batchelor theory or local variations in λ or I. A segment represented by a dot in this figure uses data from only 60 cm of the water column, so the effective number of degrees of freedom represented in k_c are few. The decrease in k_c/k_B as the Cox number increases above 1000 can be ascribed to a decrease in mixing efficiency; for very small mean gradients N becomes irrelevant and our scheme breaks down. Encouraged by these results, but wishing to find a more reliable way of estimating ε we proceeded to:

(b) The bottom boundary layer. In the classical turbulent boundary layer, the dissipation at distance z from the wall is $(\tau/\rho)^{3/2}/(0.41z)$ where τ is the stress exerted on the wall and ρ is the density of the fluid. If the layer of water near the sea bed often observed to be well mixed is such a layer, and if τ can be measured, then ε is known as a function of z and k_B can be computed for comparison with values of k_c observed in free-fall data. A bottom-mounted velocity profiler has given evidence that the bottom layer closely resembles laboratory turbulent layers as well as measurements of τ (Caldwell and Chriss, 1979). On several cruises in the spring of 1979

on the Oregon coast in 100 and 200 m water depth, profiles were taken with the microstructure instrument while the velocity profiler was recording. The results relevant to the question of the cut-off wavenumber are presented in Paper 3, further results concerning the bottom layer being given in Paper 6. The essential result is contained in Figure 1 of Paper 3, which shows that the ratios of k_c/k_B obtained in the bottom layer are indistinguishable from those obtained by the procedures described above. The Cox numbers in the bottom layer were much larger than 1000; thus our hypothesis that k_c is determined by k_B holds up regardless of Cox number. The mean value of k_c/k_B is similar to the MILE value, but the precision is not sufficient to calculate an improved value of q. The scatter is similar, leading us to believe that it is due to the statistical nature of the process.

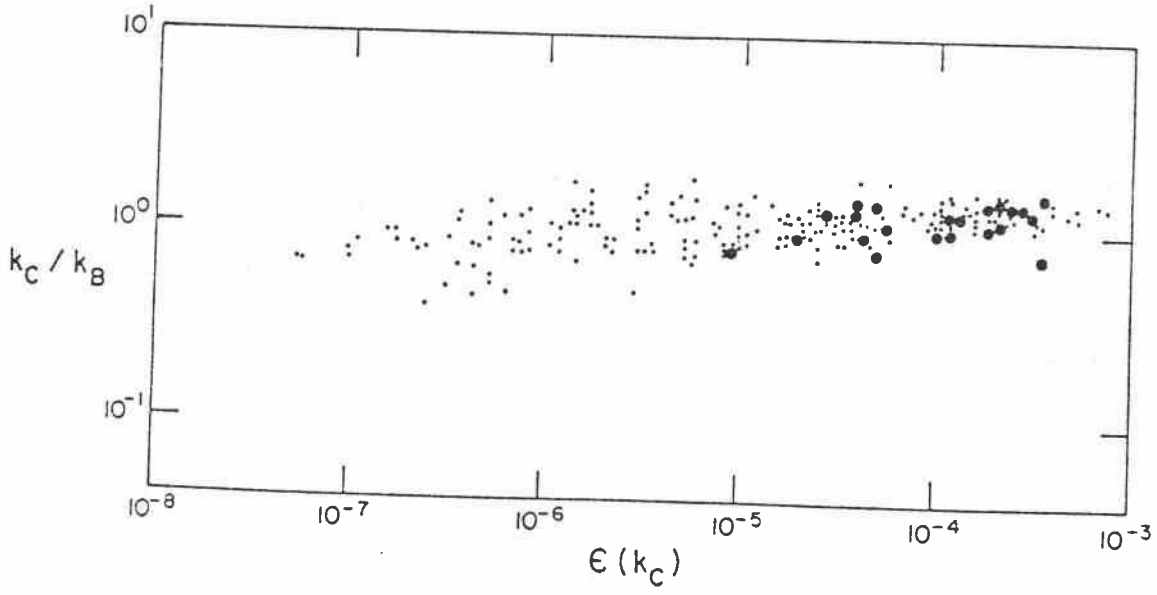

1. Large dots represent the ratio of cutoff wavenumber in vertical temperature gradient spectra to the Batchelor wave number calculated from boundary layer assumptions and sublayer measurements, plotted vs. dissipation. Small dots represent upper layer data with Cox number < 1000, for which ε was calculated by an entirely different method (Caldwell et al., 1980). The units of ε are $cm^2\ sec^{-3}$.

3. The shape of the spectrum near cut-off: Even if it is granted that the cut-off wavenumber of the spectrum is that predicted by Batchelor, it does not follow that the shape of the spectrum follows his predicted form. A separate investigation was undertaken to see under what conditions, if ever, the spectra take on the predicted shape. We must keep in mind that extensive averaging may be required before the form emerges; its derivation is statistical. In the averaging process we must be cognizant of the spacial variation in the turbulence parameters, ε and χ. Their distribution functions in the ocean are known to resemble the log-normal, with decades of variance. Therefore to average properly care must be taken to calculate the spectra over regions in which χ and ε have restricted variation. The averaging should then be done on scaled spectra, scaled in wavenumber by k_c and in power by χ/k_c. (Averaging in this manner maintains the effective number of degrees of freedom; otherwise the averaged spectrum is inevitably dominated by the individual spectrum with the largest χ.) The results, calculated from selected data from the MILE experiment, are summarized in Figures 4, 5 and 6 of Paper 2. Spectra with large Cox number ensemble-average to the Batchelor form (2); deviations become larger as the Cox number decreases. Only a hint of the "inertial subrange" (4) is seen (Figure 6, Paper 2). A similar procedure for bottom-layer data produces similar results (Paper 5, Figure 4). We conclude that vertical temperature-gradient spectra average to the Batchelor form above the inertial subrange only if the Cox number is larger than 1000 or so, and only if many samples are averaged.

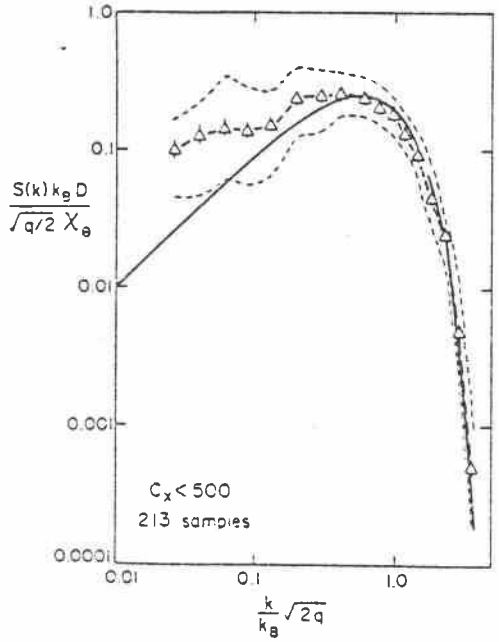

Fig. 4. Ensemble-averaged nondimensional spectrum for Cox numbers less than 500. The lower wave number portion of the spectrum departs significantly from the Batchelor spectrum (solid curve). Error bars are the standard error of the mean based on the standard deviation. The dashed envelope shows the average positive and negative deviation from the mean; that is, half of the spectral estimates lie within the envelope. Thus although the mean of the spectral values has a small uncertainty (the bars), the estimates in an individual spectrum may lie quite far from the mean.

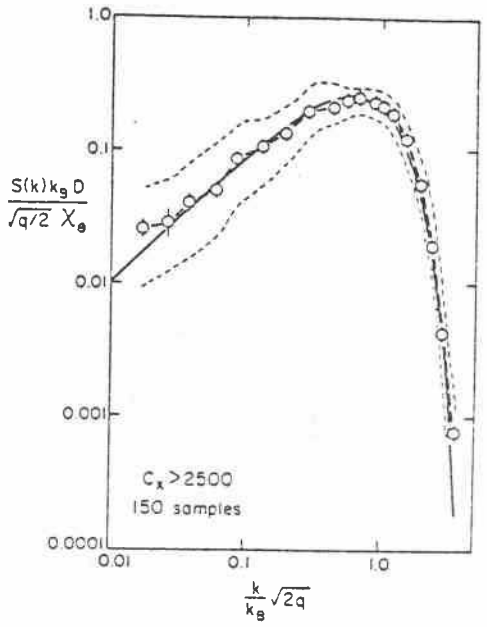

Fig. 6. Ensemble-averaged nondimensional spectrum for large Cox numbers. The low wave number portion of the spectrum is in remarkably close agreement with the Batchelor spectrum. Thus although the mean of the spectral values has a small uncertainty (the bars), the estimates in an individual spectrum may lie quite far from the mean.

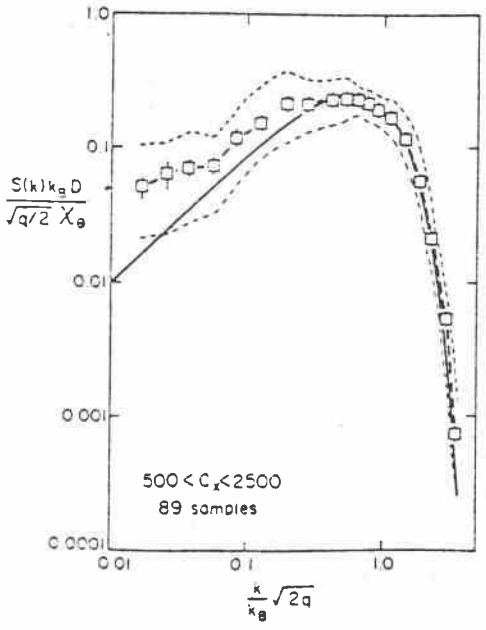

Fig. 5. Ensemble-averaged nondimensional spectrum for intermediate Cox numbers. The low wave number portion of the spectrum is closer to the Batchelor spectrum than the low Cox number spectrum but still is significantly different. Thus although the mean of the spectral values has a small uncertainty (the bars), the estimates in an individual spectrum may lie quite far from the mean.

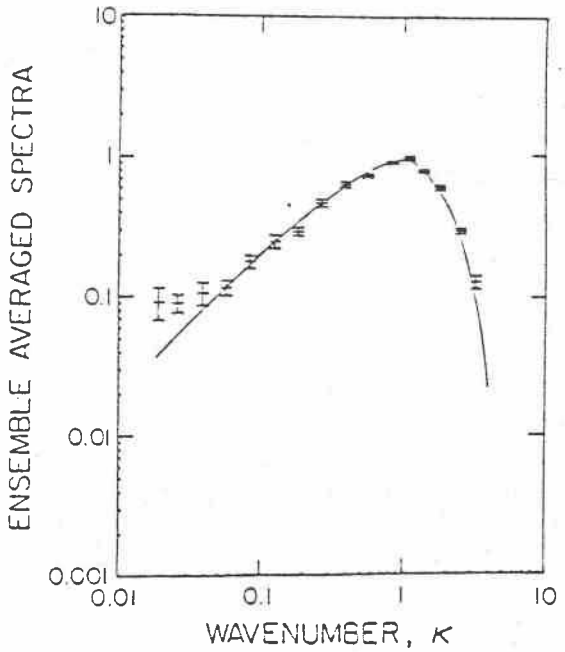

Figure 4. The ensemble averaged spectrum. The bars represent standard error of the mean; the solid line is the Batchel trum.

Finding the spectral form at all must increase our confidence in the relation between the cut-off wavenumber and k_B.

4. The inertial subrange: In the bottom layer, stratification is imperceptable at times and ε is relatively large. The stratification length scales, e.g. $(\varepsilon/N^3)^{1/2}$, become very large, so isotropic turbulence may be expected even in the wavenumbers of the inertial subrange [Equation (4)]. An average of 77 spectra does show a few points at what might be the top of the inertial subrange (Paper 5, Figure 4). The uncertainties in our knowledge of the constants q and β frustrate precise quantitative comparison but the positions of the spectral values lie well within the range predicted from accepted values. Therefore we conclude that in this case the inertial subrange was present. We do not expect to see it often in the ocean; rarely will isotropic regions of great enough extent be found. Gregg and Sanford (1980) seem to have found another one.

Applications If now we may assume that the cut-off wavenumber k_c is related to k_B, observations of k_c may be used to estimate ε. Recall that k_c is defined as the wavenumber at which the spectral values have fallen to 10% of their peak values. Then ε can be calculated as

$$\varepsilon = 4q^2\nu D^2 \left(\frac{2\pi k_c}{2.28}\right)^4 \qquad (10)$$

with the aid of an assumed value of q. Even if q is not precisely known, the variations of ε can be estimated, subject to a multiplicative error. On a single cast through the water column ε varies by several factors-of-ten, so the variations are clearly seen. Some conclusions arise from these profiles:

1. In the wind-mixed layer, dissipation picks up rapidly when a wind event occurs (Paper 2, Figure 10). In light winds shear production at the base of the "mixed layer" may be important in generating turbulence, in heavy winds strong turbulence descends from the surface.

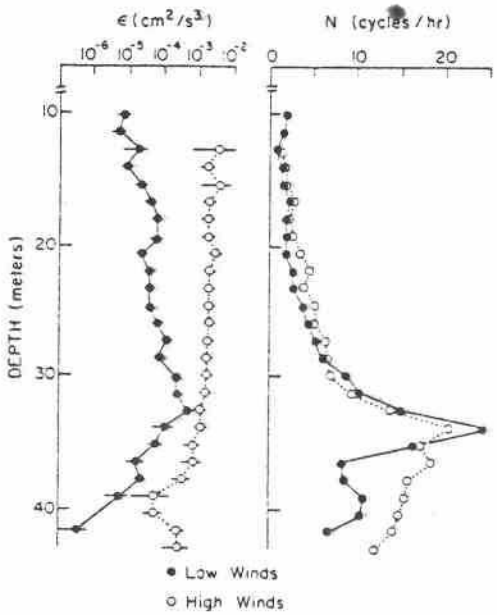

Fig. 10. Average of ϵ_B and buoyancy frequency in low (solid circle) and high (open circle) wind speed. During low winds, ϵ_B increases with depth until the thermocline is reached and shows two regions of high dissipation associated with the top of the transition zone near 20 m and the top of the thermocline at 33 m. During high winds, ϵ_B is nearly constant with depth and is much larger than during low winds. The volume average of ϵ_B should not be attempted below 30 m.

2. The wind-mixed layer may exhibit a turbulence structure similar to a laboratory boundary layer (Paper 4). The microstructure probe was adapted to near-surface measurements by changing its weight-balance to make it stable with the transducers at the top, as well as making it buoyant. A weight heavy enough to sink the instrument

is released when the instrument reaches a predetermined depth, after which it "free-falls" upward. Profiles begin at depth and terminate when the transducers break the surface. An experiment was run at Green Peter reservoir in Oregon in a moderate wind. Dissipation was calculated as a function of depth as in the bottom layer, using the wind stress to predict the dissipations calculated from the microstructure instrument's gradient data by assuming $k_c = k_B$. Good agreement (Paper 4, Figure 2) increases our confidence in the relationship between k_c and k_B.

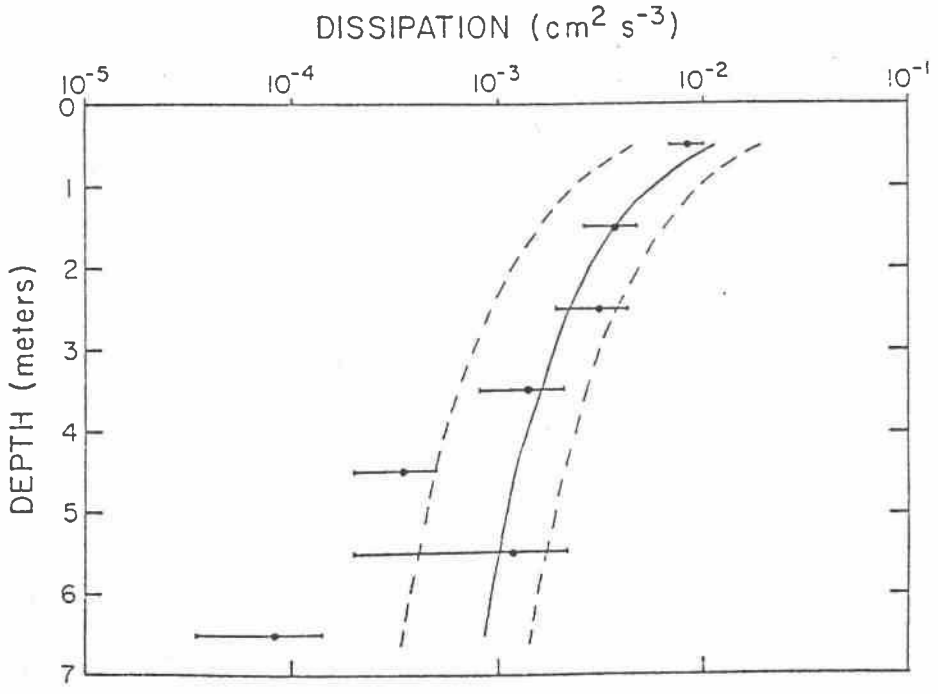

2. Kinetic energy dissipation rate per unit mass in the near-surface layer (solid circles). Error bars are the standard error of the mean. Solid line is $(\tau/\rho)^{3/2} \kappa^{-1} Z^{-1}$ calculated from mean winds, dotted lines are $(\tau/\rho)^{3/2} \kappa^{-1} Z^{-1}$ calculated from highest and lowest winds. Dissipation falls dramatically in the thermocline at 6m.

3. In the thermocline, dissipation is often localized and intermittant (Paper 1, Figure 7).

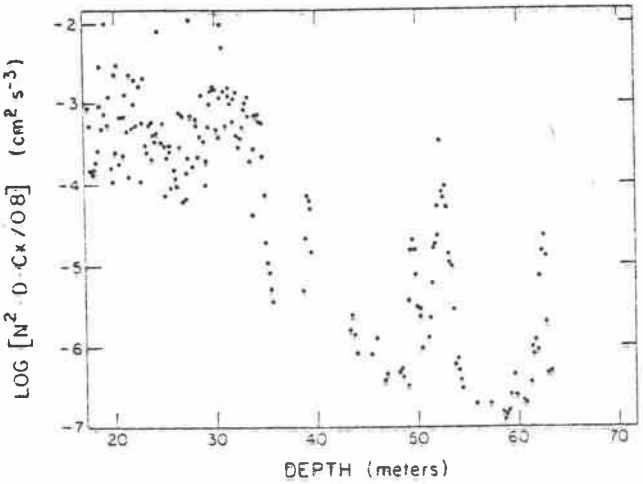

Fig. 7. Dissipation calculated as prescribed versus depth for the cast on August 23, 1977.

4. Bottom layer turbulence is at times very similar to laboratory boundary layer turbulence. Occasionally stratification caused by suspended material may be important (Paper 6).

References

Batchelor, G. K. (1959) Small-scale variation of convected quantities like temperature in a turbulent fluid. J. Fluid Mech. 5,113-133.

Caldwell, D. R. and T. M. Chriss (1979) The viscous sublayer at the sea floor. Science 205,1131-1132.

Gibson, C. H. and W. H. Schwarz (1963) The universal equilibrium spectra of turbulent velocity and scalar fields. J. Fluid Mech. 16,365-384.

Grant, H. L., B. A. Hughes, W. M. Vogel and A. Moilliet (1968) The spectrum of temperature fluctuations in turbulent flow. J. Fluid Mech. 34,423-442.

Gregg, M. C. and T. B. Sanford (1980) Signatures of mixing from the Bermuda Slope, the Sargasso Sea and the Gulf Stream. J. Phys. Oceaogr. 10,105-127.

Osborn, T. R. (1980) Estimates of the local rate of vertical diffusion from dissipation measurements. J. Phys. Oceanogr. 10,83-89.

Determining the Dynamic Response of a Thermistor to Thin Temperature Features

T. M. Dillon

D. R. Caldwell

J. M. Brubaker

V. T. Neal

School of Oceanography

Oregon State University

Corvallis, Oregon 97331

ABSTRACT

Two techniques for measuring the dynamic response to thin gradients of a fast-responding temperature sensor moving at slow (10 cm s^{-1}) speeds are described. One is a modified Fabula test in which the thin temperature signal is provided by a gentle laminar jet. In the other method an in-situ comparison is made with the signal in the water column as seen by a faster sensor, a thermojunction. The response function of Thermometrics P-85 thermistors are determined by both procedures. Good agreement is found.

INTRODUCTION

Turbulence produces temperature fluctuations in the oceans so thin that for their accurate measurement the dynamic response of the sensor must be taken into account. Slowly-descending sensor vehicles, free of the ship and its motion, give the sensor as much time to respond as possible, but the requirement that probe motion be rapid compared to motions in the water limits the slowness. Descent-rates have been maintained above 8 cm s^{-1} by all investigators.

The distribution of temperature fluctuations extends to a spatial frequency of $k_B \equiv (2\pi)^{-1}(\varepsilon/\nu D^2)^{1/4}$, insofar as heat can be regarded as a passive contaminant and insofar as the flow at these scales can be regarded as homogeneous, isotropic turbulence (Batchelor, 1959; Caldwell, Chriss, Newberger and Dillon, 1981; Dillon and Caldwell, 1980). Here k_B is the Batchelor wavenumber, ε is the kinetic-energy dissipation rate, ν the kinematic viscosity and D the thermal diffusivity. Values as high as 10^{-3} cm^2 s^{-3} are not unusual for ε, especially in surface layers, and ν and D can be taken as 10^{-2} and 10^{-3} cm^2 s^{-1}, respectively, so k_B can be as large as 2.8 cycles cm^{-1}. If fluctuations of this wavenumber were encountered by a sensor moving at a speed of only 8 cm s^{-1}, their apparent frequency would be 23 Hz. The temperature sensor most commonly used for this purpose is the glass-rod thermistor. In previous studies its response has proved to remain unattenuated only to frequencies well below 10 Hz, so it cannot respond fully to these signals. If it is to resolve the gradients, its response must be measured as a function of frequency (wavenumber). Thus we set as our goal the measurement of the dynamic response to 30 Hz.

Previous measurements at low speeds, on sensors somewhat slower than the Thermometrics P-85 glass-rod thermistors used in our work, have used the method of Fabula (1968) (Gregg, Cox and Hacker, 1973; Gregg and Meagher, 1980). In this method, the sensor is traversed across the plume generated above a heated wire or series of wires. The shape of the plume is first mapped by passing the sensor very slowly through it. Then the sensor is assumed to see the same signal when traversing the plume at the speed of measurement. The response function of the sensor is calculated as the ratio of the power-spectral estimate of the sensor to that of the plume at each wavenumber. The result is usually expressed in terms of frequency rather than wavenumber because the frequency function varies less with traverse speed.

The largest wavenumber to which the response can be determined is determined by the thickness of the plume and the accuracy and reproducibility of its mapping. The plumes used have a thickness of approximately 1 cm at the height of probe traverse (Gregg and Meagher, 1980). Their wavenumber spectrum rolls off near 1 cycle/cm. Thus the signal present in the water will be much reduced at 3 cycles/cm, and even if the plume is mapped to this wavenumber, a high degree of reproducibility uncharacteristic of thermal plumes would be required. So a thinner signal is needed.

In our first technique a stream of heated water thinner than the heated-wire plume is used. A thin, gentle laminar jet of warm water is injected upward into the tank from a nozzle only 0.05 cm wide. Otherwise the procedure is quite conventional. To confirm the results of the jet test, comparison is made with response-function estimates made from data taken on a descending instrument. The response of the thermistor is

determined by comparison with the signal from a thermojunction only 0.0088 cm thick. This comparison can only be made in patches of high signal because of the poor signal-to-noise characteristic of the thermojunction, so statistics are harder to gather than in the laboratory, but the comparison is remarkably favorable within its limits.

JET TESTS

For measurement of the response of the Thermometrics P-85 glass-rod thermistor, heated-wire plumes are too wide, as discussed above. A heated-water signal that is much narrower is generated by a small, gentle, laminar jet. The jet nozzle, a slit 1.3 cm long by 0.05 cm wide, is submerged in an annular tank of outer diameter 2 m and channel cross-section 30 cm x 30 cm. The nozzle is pointed upward and connected to a reservoir of warm, dyed water. For operation the reservoir is raised slightly above the tank water-level, forcing water through the nozzle. The sensor is mounted on an arm projecting from a rotating table centered within the annular tank, so the sensor travels around the tank as the table is driven by a variable-speed motor, which is adjustable for sensor speeds of 0.1 to 30 cm s^{-1}. The speed is optically sensed. The nozzle is submerged 20 cm, and the sensor passes through the jet 0.2 cm above the nozzle.

The jet is mapped by passing through it a 0.03 cm diameter thermistor at 0.1 cm s^{-1}. The spectrum of the map fits a Gaussian form well, with a 3-dB wavenumber of 5.3 cycles cm^{-1}. Variation of the 3-dB wavenumber by 10% were found on replication. The discrepancy between the map spectrum and an ideal white-noise spectrum is only 17% to 25% even at the maximum wavenumber of interest, 3 cycles cm^{-1} (corresponding to 30

Hz at 10 cm s^{-1} traverse speed). Therefore only the highest-frequency estimates require correction for map shape.

The jet's temperature was 2-3° above the tank temperature. The speed was determined from plume cross-section and reservoir depletion-rate to be 2.5 cm s^{-1}. The Reynolds number is approximately 10, so the flow is laminar.

The major source of uncertainty in the computed response function was large-scale temperature anomalies in the tank. They cause uncertainty in the low-frequency spectral estimates, discrepancies between the results of replicates, as discussed by Gregg and Meagher (1980). To avoid these anomalies the water is carefully homogenized before a run; then, after the motion in the tank ceases, the nozzle is opened. The jet is visually monitored through a window in the tank's side to ensure that no circulations induced by the probe motion deform the plume. When deformations are observed, the data are discarded. Also the run's data must be discarded if large-scale anomalies are large.

Spectral estimates from five runs at a sensor speed, U, of 10 cm s^{-1} were averaged to determine the P-85's response. The transfer function H(f) was calculated from the map spectrum $S_m(f) = \exp\{-[\pi fa/U]^2\}$, where a = 0.051 cm, and the average thermistor spectral estimate S_p, as

$$H(f) = S_p(f)\ S_m^{-1}(f).$$

Several forms can be used to represent H(f). A least-squares fit of data to 30 Hz to the form

$$H(f) = [1 + Af^2 + Bf^4 + Cf^6]^{-1}$$

yields the coefficients A = 2.635 x 10^{-2}, B = -2.19 x 10^{-6}, and C = 3.256 x 10^{-8}. A combination of two single-pole filters also yields a good fit, to the form:

$$H(f) = [(1 + (\frac{f}{f_1})^2)(1 + (\frac{f}{f_2})^2)]^{-1}$$

Here f_1 = 6.6 Hz and f_2 = 30.5 Hz. The estimates of the response are within 15% of this function for $f \leq 30$ Hz.

A single-pole response can be fit to the estimates for $f \leq 20$ Hz, but fails at higher frequencies:

$$H(f) = [1 + (\frac{f}{f_o})^2]^{-1}$$

A value of 5.83 Hz for f_o gives the best fit ($f \leq 20$ Hz).

FIELD TESTS

For confirmation of the laboratory tests, comparisons with an entirely different sort of test were made. It is similar to a procedure that has been used to determine dynamic response at much higher velocities in the laboratory (Lueck, Hertzman and Osborn, 1977).

In this method, the signal from an extremely small thermocouple (0.0088 cm at the bimetallic junction, Fig. 2) is compared to the signal from the thermistor. Both sensors are mounted on the microstructure instrument and dropped through the seasonal thermocline. The vertical wavenumber spectrum of temperature-gradient is determined in very active patches in the thermocline, and spectral estimates are calculated independently from thermistor and thermocouple. The ratio of the spectral estimates from the thermistor and the thermojunction, at a given frequency, is just H(f) if: (1) the thermojunction's response is unattenuated at that frequency, (2) the noise in neither transducer is significant, and (3) the two signals can be regarded as realizations of the same process. Note that coherence of the signals is not required, only statistical similarity.

How can the above assumptions be tested? For (1), the thermocouple attenuation, we can first argue that for such a small sensor the fluid boundary layer is larger than the transducer and therefore controls the response. The Reynolds number, R, is Ud/ν, U being the drop speed, d the diameter and ν the kinematic viscosity of water. R is approximately $10 \cdot 0.0088/0.01 \sim 9$, so the flow is fairly laminar and we can use the Blasius formula, $\delta = 5(\nu d/U)^{1/2}$, to determine δ, the boundary layer thickness. For the thermojunction $\delta \sim 5(0.01 \cdot 0.0088/10)^{1/2} = 0.015$ cm, much larger than d = 0.0088 cm. Thus, most of the material that must be cooled or heated to effect a temperature change of the transducer is water. By the usual dimensional analysis it can be seen that τ should depend on δ as $\tau \sim \delta^2/D$. Therefore τ is linearly dependent on d. (To the extent that the thermal capacity of the sensor itself has influence, the d-dependence is stronger.) Aagaard (1969) compares τ for .05 and .25 cm thermistors, and finds the ratio of time constants to be 4.3, so in that case at least, τ was roughly proportional to d. So we conclude that the thermojunction's rolloff in response occurs at a frequency higher than that of the thermistor by at least a factor of the ratio of their diameters (thermistor ÷ thermojunction). This ratio is approximately 3 (0.028/0.0088) so there is a range of frequencies between the thermistor's rolloff and the thermocouple's rolloff, where assumption (1) will be satisfied and a useful response function can be calculated.

Noise in the thermocouple signal presents a problem (Assumption #2). Throughout most of the water column the signal from a single junction is so small that even the best amplifiers bury the signal in noise. Our amplifiers introduce noise equivalent to about 0.002°C, but we usually find a few patches, typically 1 to 2 m in thickness, in the

thermocline where the signal does emerge from the noise. These patches can be identified on a chart record and isolated from the digital tape record for computations. Sections between active patches were used for computation of the noise spectrum, which was subtracted from the thermocouple spectral estimates. The noise in the thermistor signal is 30-dB lower, and not detectable in the active patches.

To examine assumption (3) we can only look at ensemble averages of response functions, assuming that if the averaging process leads to values that "make sense" in terms of our intuitive ideas of the form of the response, and seem to have standard deviations comparable with those of a chi-squared distribution with the same number of degrees of freedom, then this assumption is validated.

The thermocouple transducer comprises two butt-welded junctions between 0.0025-cm copper and constantan wires. One junction is supported only by its wires and extends about 0.3 cm from a 0.31 cm diameter PVC tube into which it is epoxy-potted. The reference junction is approximately 1 cm up the tube. Because it is potted into the epoxy inside the PVC tube, its response time, relative to water temperature changes, is more than 1 minute. Therefore, the couple responds to changes in ambient water temperature which occur faster than the reference junction's response, but slower than the "active" junction's response. We are interested only in frequencies at which the thermistor's response is frequency-dependent, so the characteristics of the reference junction are not significant, as long as signals above 1 Hz are not affected.

The thermistor protrudes from a similar 0.31 cm PVC tube, placed alongside the thermojunction tube. Both tubes are potted into a PVC cap which screws onto the bottom of our instrument package (Caldwell and Dillon, 1981).

The recordings were made in fresh water, in Lake Tahoe, California-Nevada. The water of this lake is renowned for its purity, so no conclusions can be made from our results as to the usefulness of this transducer and technique in salty or more biologically-active waters. On the chart records of the differentiated signals, patches of thickness 1 m or so were found in which the thermocouple signal dominated its noise in the thermocline, several patches to a cast.

Five patches were selected for the analysis presented here. The resulting estimates of the response function H(f) (Fig. 2) fall quite near the estimates from the jet tests, although they seem to lie systematically above at the highest frequencies. The poor statistics from the field are manifested as scatter in the estimates, but the systematic difference is clearly not great. This agreement is somewhat remarkable when we consider that different thermistor units were used.

DISCUSSION

Seeing agreement between two such different methods of determining the response function, we conclude that they are both reasonably accurate. To discover how the uncertainty in the response function effects the estimation of spectra, we consider four hypothetical spectra with values of ε covering the oceanic range. A Batchelor spectrum is presumed in each, but its form is not essential. In each case the spectrum is attenuated as it would be attenuated by a thermistor with the response indicated by the laboratory tests. The attenuated spectrum is then corrected by the inverse of the response given by the field tests. The difference between assumed and corrected spectra is an indication of the uncertainty in corrected spectrum caused by our uncertainty in response function (Fig. 3).

For the lowest-frequency spectrum, the attenuation is slight and correction is near-perfect. As we consider spectra extending to higher and higher frequencies, correction becomes more necessary and the accuracy of the response determination becomes more vital, but the deviations between the assumed and undercorrected spectra are not great; the corrected spectra represent the original spectra fairly well.

REFERENCES

AAGAARD, E. E. (1969) Dynamic characteristics of sensors for marine temperature measurements. In: Marine Temperature Measurements Symposium, Miami, June 1969, Marine Technical Society Transactions, 117-125.

BATCHELOR, G. K. (1959) Small-scale variation of convected quantities like temperature in a turbulent fluid. Journal of Fluid Mechanics, 5,113-133.

CALDWELL, D. R., T. M. CHRISS, P. A. NEWBERGER and T. M. DILLON (1981) The thinness of oceanic temperature gradients. Journal of Geophysical Research, in press.

CALDWELL, D. R. and T. M. DILLON (1981) An oceanic microstructure-measuring system. Ref. 81-00, School of Oceanography, Oregon State University, Corvallis, OR 97331.

DILLON, T. M. and D. R. CALDWELL (1980) The Batchelor spectrum and dissipation in the upper ocean. Journal of Geophysical Research, 85,1910-1916.

FABULA, A. G. (1969) The dynamic response of towed thermistors, Journal of Fluid Mechanics, 34,449-464.

GREGG, M. C., C. S. COX and P. W. HACKER (1973) Vertical microstructure measurements in the central North Pacific, Journal of Physical Oceanography, 3,458-469.

GREGG, M. C. and T. B. MEAGHER (1980) The dynamic response of glass rod thermistors. Journal of Geophysical Research, 85,2779-2786.

LUECK, R. G., O. HERTZMAN and T. R. OSBORN (1977) The spectral response of thermistors. Deep-Sea Research, 24,951-970.

FIGURE CAPTIONS

1. Estimates of dynamics response obtained by passing a Thermometrics P-85 thermistor through a warm jet. Three fits to the data are shown, as described in the text, but two agree closely and cannot be differentiated on the figure. The best single-pole fit has 3-dB frequency of 5.83 Hz.

2. Photograph of thermojunction (upper left) and Thermometrics P-85 thermistor. The temperature sensitive material and its glass coating projects upward from the glass body. For scale, the thermojunction wires are 0.0025 cm in diameter.

3. Comparison of dynamic response determined in the laboratory (as in Figure 1) compared with in-situ determination by comparison with thermojunction (o laboratory, o in situ). Different thermistors were used, both Thermometrics model P-85.

4. Uncertainties in corrected spectra introduced by discrepancies in determination of dynamic response. A Batchelor spectrum of specific energy dissipation rate is assumed, with a q of 3. It is plotted as it would be seen by a probe descending at 10 cm s^{-1}. Then the spectrum is replotted as it would be seen by a P-85 thermistor, attenuated by the response function determined in the laboratory tests. Then the spectrum of the attenuated signal is corrected, assuming the response function determined in the in-situ test. Comparison of the "assumed" curve and the "undercorrected" curve indicates the uncertainty in the corrected spectra.

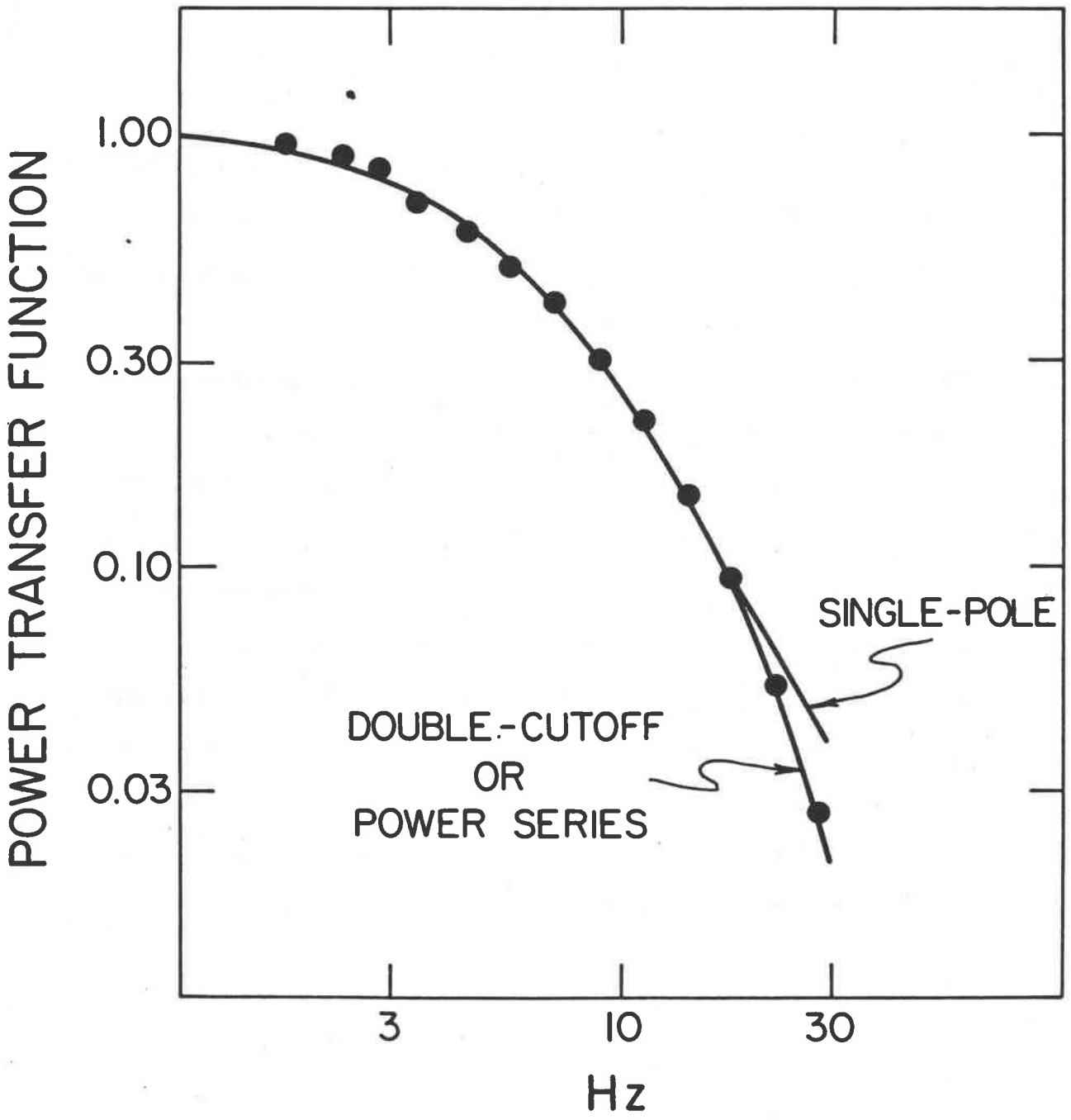
POWER TRANSFER FUNCTION
1.00
0.30
0.10
0.03
SINGLE-POLE
DOUBLE-CUTOFF
OR
POWER SERIES
3
10
30
Hz

FIGURE 1.

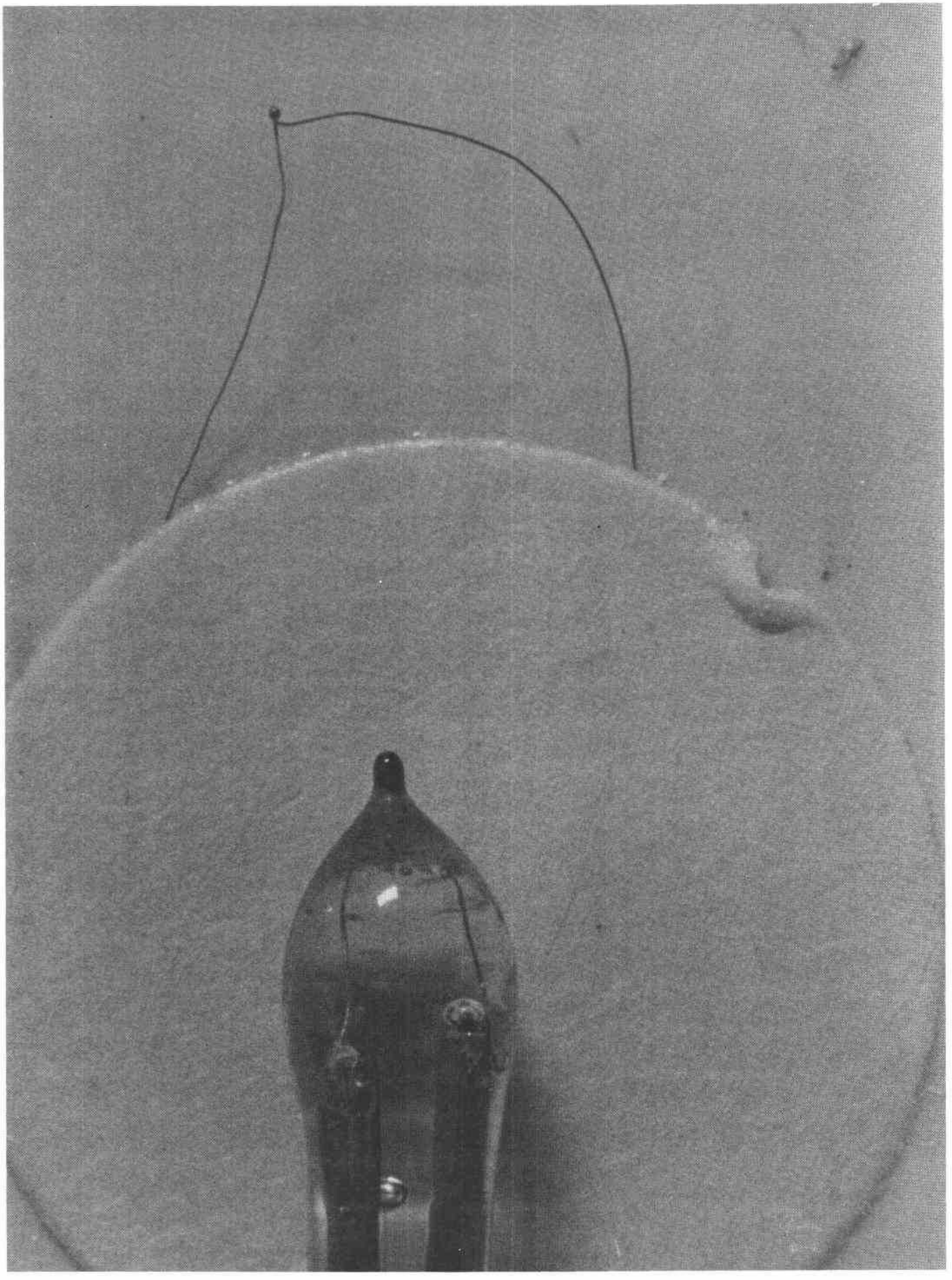

FIGURE 2.

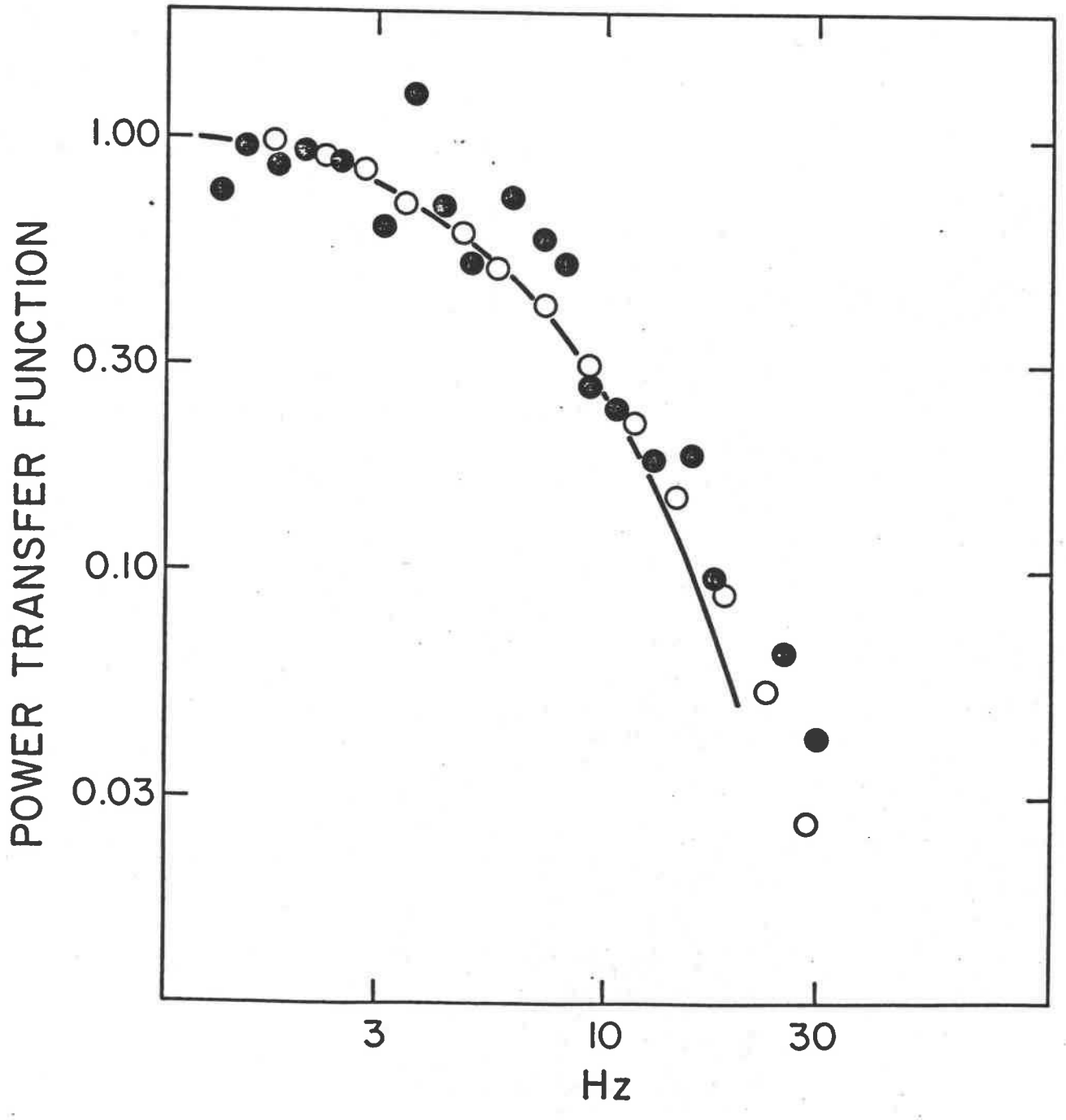

FIGURE 3.

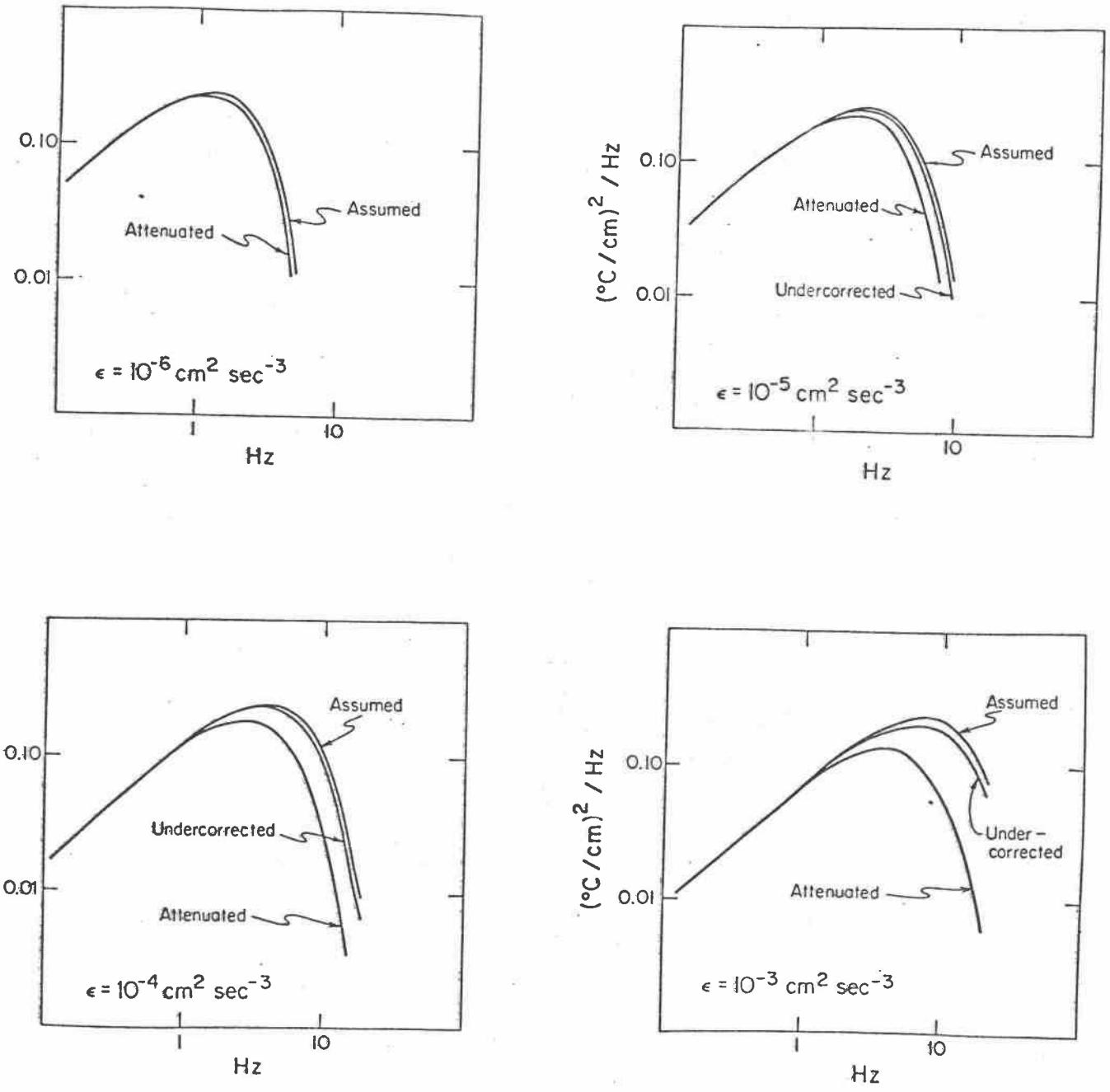
0.10
0.01
Assumed
Attenuated
$\epsilon = 10^{-6}\,cm^2\,sec^{-3}$
1
10
Hz
$(°C/cm)^2$ / Hz
Undercorrected
$\epsilon = 10^{-5}\,cm^2\,sec^{-3}$
$\epsilon = 10^{-4}\,cm^2\,sec^{-3}$
Under – corrected
$\epsilon = 10^{-3}\,cm^2\,sec^{-3}$

FIGURE 4.

A NEW METHOD FOR DETERMINING THE FREQUENCY RESPONSE OF MICROSTRUCTURE TEMPERATURE SENSORS

Douglas R. Caldwell

John M. Brubaker

Victor T. Neal

School of Oceanography
Oregon State University
Corvallis, Oregon 97331

ABSTRACT

Thermally-active patches in the thermocline are used to determine the temperature-signal attenuation of a freely-falling thermistor, by comparing the gradient spectrum of the patch as seen by the thermistor with the gradient spectrum from a simultaneous, nearby thermojunction. The thermojunction itself cannot be used as a temperature sensor except in very active patches because its signal is so low that amplifier noise swamps it. The spectral gain function as a function of frequency f, can be represented as $[1 + (f/f_o)^2]^{-1}$ where $f_o = 4.7U^{0.2}$ Hz, U being the descent rate. The data were not sufficient to determine whether a two pole filter would better represent them.

INTRODUCTION

The determination of the response of temperature sensors, usually thermistors, as a function of frequency has been a serious problem for investigators of small-scale structure in the ocean. These investigators usually record the output of a thermistor mounted on an instrument package which freely descends through the water column. The dissipation limit of the temperature-gradient spectrum lies at wavenumbers where the response of the sensor is seriously attenuated (Gregg, Cox and Hacker, 1973). Faster-responding transducers which have sufficiently low noise levels are not available, so we are forced to somehow measure the response as a function of frequency and correct our data for it, usually in a spectral presentation.

Previous attempts to measure response functions have been carried out in the laboratory (Fabula, 1968; Aagaard, 1969). Often the flow speeds have not been the same as the drop speed of the instrument package, the turbulence level may not be defined, and often a prototype transducer is used in the test rather than the unit used for data-taking. An on-the-spot determination under the conditions actually experienced by the data-taking sensor would be much better.

Our method is to determine the vertical wavenumber spectrum of temperature gradient in very active patches in the thermocline by means of a 0.005 cm-diameter thermojunction and comparing the result with a spectrum calculated in the same patch from the thermistor record. The ratio of the spectral estimates from each transducer (thermistor ÷ thermocouple) at a given frequency is just the squared modulus of the transfer function of the thermistor if: (1) the thermojunction's response is unattenuated at that frequency; (2) the noise in neither transducer is significant (as we shall see, the

thermojunction's noise must be corrected for); and (3) the two signals can be regarded as realizations of the same process. Note that we do not, in (3), require coherence of the signals, i.e. the transducers need not see identical signals. By working from the spectral estimates rather than cross-spectra, phase information is lost, and without additional information or assumptions the correction in the time domain cannot be determined by this method.

How can the above assumptions be tested? For (1), the thermocouple attenuation, we can first argue that for such a small sensor the fluid boundary layer is larger than the transducer and therefore controls the response. The Reynold's Number, R, is Ud/ν, U being the drop speed, d the diameter and ν the kinematic viscosity of water. R is approximately $10 \cdot 0.005/0.01 \sim 5$, so the flow is fairly laminar and we can use the Blasius formula, $\delta = 5(\nu d/U)^{1/2}$, to determine δ, the boundary layer thickness. For the thermojunction $\delta \sim 5(0.01 \cdot 0.005/10)^{1/2} = 0.011$ cm, somewhat larger than d = 0.005 cm. Especially for a sperical transducer, most of the material that must be cooled or heated to effect a temperature change of the transducer is water. The time-constant τ should then depend on δ as $\tau \sim \delta^2/\kappa$. Therefore τ is linearly dependent on d. (To the extent the thermal capacity of the sensor itself has influence, the d-dependence is stronger.) Aagaard (1969) compares τ for .05 and .25 cm thermistors, and finds the ratio of time constants to be 4.3, so in that case at least τ was roughly proportional to d. So we conclude that the thermojunction's rolloff in response occurs at a frequency higher than that of the thermistor by at least a factor of the ratio of their diameters (thermistor ÷ thermojunction). The effective diameter of our thermistors (Thermometrics P-85)

is not easily defined because the thermally-sensitive material lies in a bit of glass approximately 0.015 cm in diameter which protrudes from a piece of glass 0.25 cm in diameter. Previous measurements in the laboratory led us to estimate the effective diameter as 0.025 cm. Therefore, the rolloff in response for the thermojunction is expected to occur at least 5 x higher in frequency than it occurs for the thermistor. In the region between the thermistor's rolloff and the thermocouple's rolloff, assumption (1) will be satisfied and a useful response function can be calculated.

As we shall see the 3-dB frequency for the thermistor is approximately 8 Hz, so the 3-dB frequency for the thermocouple should be at least 40 Hz, and at 25 Hz, the highest frequency we use, the thermocouple response is attenuated by less than 28%. This estimate is probably conservative, so we shall ignore this source of error.

Noise in the thermocouple signal presents a problem (Assumption #2). Throughout most of the water column the signal from a single junction is so small that even the best amplifiers bury the signal in noise. Our amplifiers introduce noise equivalent to about 0.002°C, but we usually find a few patches, typically 1 to 2 m in thickness, in the thermocline where the signal does emerge from the noise. These patches can be identified on a chart record and isolated from the digital tape record for computations. Sections between active patches were used for computation of the noise spectrum, which was subtracted from the thermocouple spectral estimates. The noise in the thermistor signal is 30-dB lower, and not detectable in the active patches.

To examine assumption (3) we can only look at ensemble averages of response functions, assuming that if the averaging process leads to values that "make sense" in terms of our intuitive ideas of the form of the response, and seem to have standard deviations comparable with those of a chi-squared distribution with the same number of degrees of freedom, then this assumption is validated.

TRANSDUCERS

The thermocouple tranducer comprises two butt-welded junctions between 0.0025-cm copper and constantan wires. One junction is supported only by its wires and extends about 0.3 cm from a 0.31 cm diameter PVC tube into which it is expoxy-potted. The reference junction is approximately 1 cm up the tube. Because it is potted into the expoxy inside the PVC tube, its response time, relative to water temperature changes, is more than 1 minute. Therefore, the couple responds to changes in ambient water temperature which occur faster than the reference junctions' response, but slower than the "active" junction's response. We are interested only in frequencies at which the thermistor's response is frequency-dependent, so the characteristics of the reference junction are not significant, as long as signals above 1 Hz are not affected.

The thermistor protrudes from a similar 0.31 cm PVC tube, placed alongside the thermojunction tube. Thermojunction and thermistor are alongside each other, about 0.2 cm apart. Both tubes are potted into a PVC cap which screws onto the bottom of our instrument package (Caldwell, Wilcox, and Matsler, 1975).

THE DATA

The recordings were made in fresh water, in Lake Tahoe, California-Nevada. The water of this lake is reknown for its purity, so no conclusions can be made from our results as to the usefulness of this transducer and technique in salty or more biologically active waters. Thirty-five drops were made on 12-13 September, 1976. The surface mixed layer extended down to 20 m or so, and a strong thermocline with mean gradients as high as 0.5°C/m lay beneath it. On the chart records of the differentiated signals, patches of thickness 1 m or so were found in which the thermocouple signal dominated its noise in this thermocline, several patches to a drop (Fig. 1). It can be seen that the thermocouple signal becomes active when the thermistor signal does, but individual features cannot be matched. The drop speed was varied from 5 to 35 cm/sec by changing the angle of attack of the wings. Four speeds were chosen for this analysis, 5, 11, 15, and 35 cm/sec. These particular ones were selected because our usual descent speed is between 11 and 15 cm/sec, so we wanted to concentrate on these, and 5 and 35 were added to give a large enough range to evaluate the dependence of response on drop speed.

Spectra of the thermocouple signal (Fig. 2) often show a +1 dependence of spectral estimate on frequency, as expected from consideration of "universal" turbulence forms (Gibson, Vega and Williams, 1974). (The "universal" forms have been derived from laboratory measurements in homogeneous fluids. We expect to see such forms in the presense of a mean gradient only when shear overcomes buoyancy forces.) Spectra of the thermistor signal fall off at higher frequencies because, we assume of the attenuation caused by limited time response.

RESULTS

The response is presented in terms of a spectral gain function G, computed at a given frequency as the ratio of spectral values of thermistor and thermocouple. G is assumed to represent the spectral gain function of the thermistor alone, the thermocouple signal being regarded as suffering no attenuation at frequencies of interest, 25 Hz and less. Spectral values were computed and band-averaged for each patch, then their ratios were constructed and ensemble-averaged for all patches seen at each drop speed (Table 1).

In previous work, on somewhat larger (.05 cm) and simpler thermistors, G has been represented by a single-pole filter, $G = [1 + (f/f_0)^2]^{-1}$, by Aagaard (1969) and also as a two-pole filter, $G = [1 + (f/f_0)^2]^{-2}$, by Gregg, Cox and Hacker (1973). We fit both forms to the data at each drop speed (Fig. 3). A consideration of either the data points (Fig. 3) or the percentage errors (Table I) shows no advantage to either form. Either a larger frequency range or better statistics is needed to determine which form is better. Neither is necessarily correct. The single-pole form is arbitrarily chosen for use as a correction factor and in further discussion.

The variation of the 3-dB frequency, f_0, with drop-speed is not great (Fig. 4), a result found in the previous work. It clearly increases with drop-speed, U, but not nearly as fast as $U^{1/2}$. The values inversely weighted as their confidence limits can be fit by the formula $f_0 = 4.7\ U^{0.2}$ (Hz) with a r.m.s. deviation of 0.42 Hz.

The multiplicative correction factor to be applied to the thermistor temperature-gradient spectrum is thus $1 + (f/f_0)^2$, where f_0 is given above.

The principal problem in using this technique lies in the paucity of data. The errors in the measurement are caused by poor statistical definition

of the spectral estimates. If the thermocouple's noise level could be reduced, then larger sections of signal would emerge and the response of the thermistor could be much better defined. Ideally, of course, we would simply use the thermocouple as our main transducer, but a factor of 100 improvement in noise-amplitude would be required. There are some prospects for improvement, but probably not by that much.

Acknowledgments: This work was supported by the oceanography section, National Science Foundation, under Grant OCE75-10616.

REFERENCES

AAGAARD, E.E (1969) Dynamic characteristics of sensors for marine temperature measurements. In: Marine Temperature Measurements Symposium, Miami, June 1969, Marine Technical Society Transactions, 117-125.

CALDWELL, D.R., S.D. WILCOX, and M. MATSLER (1975). A relatively simple freely-falling probe for small-scale temperature gradients. Limnology and Oceanography, 20, 1035-1042.

FABULA, A.G. (1968) The dynamic response of towed thermometers. Journal of Fluid Mechanics, 34, 449-464.

GIBSON, C.H., L.A. VEGA and R.B. WILLIAMS (1974). Turbulent diffusion of heat and momentum in the ocean. Advances in Geophysics, 18A, 353-370.

GREGG, M.C., C.S. COX, and P.W. HACKER (1973). Vertical microstructure measurements in the Central North Pacific. Journal of Physical Oceanography, 3, 458-469.

TABLE CAPTION

Table 1. Quantities used in analysis. f_o is the 3-dB frequency for the single-pole filter and F_o the 3-dB frequency for the two-pole filter. $\Delta f_o/f_o$ represents the 95% confidence-bound in the determination of f_o, and similarly for $\Delta F_o/F_o$. These latter numbers can be used as a simple estimate of goodness-of-fit, no preference being seen for either form.

TABLE 1

Drop Speed	No. Patches	f_o	$\Delta f_o/f_o$	F_o	$\Delta F_o/F_o$
5 cm/sec	6	7.0 ± 0.8 Hz	0.11	7.4 ± 0.7 Hz	0.09
11 cm/sec	5	7.8 ± 1.0 Hz	0.13	9.0 ± 0.9 Hz	0.10
15 cm/sec	5	7.4 ± 0.7 Hz	0.09	8.1 ± 0.9	0.11
35 cm/sec	5	9.3 ± 0.7 Hz	0.08	9.8 ± 0.8	0.08

FIGURE CAPTIONS

FIG 1: An active patch 20m deep, in the transition region region between mixed layer and thermocline as seen by the differentiated signal from the thermistor (right) and the differentiated signal from the thermocouple (left). A stable temperature-gradient is represented by an excursion to the left.

FIG. 2: Estimates of temperature-gradient spectra derived from ● thermocouple and O thermistor signals in a single patch. The line represents a fit to the thermocouple noise spectrum, computed from a quiet section. The sharp fall-off at just above 30 Hz is caused by electronic filters.

FIG. 3: Ensemble-averaged estimates of the spectral gain function. Curves fitted to single and double pole filter forms are shown.

FIG. 4: Measurements of (●) 3 dB frequencies with 95% confidence intervals vs. drop speed. The results of ■ Gregg, Cox and Hacker (1973) and ○ Aagaard (1969) for larger (0.05 cm) thermistors are also shown. The solid line represents the empirical formula $4.7\ U^{0.2}$.

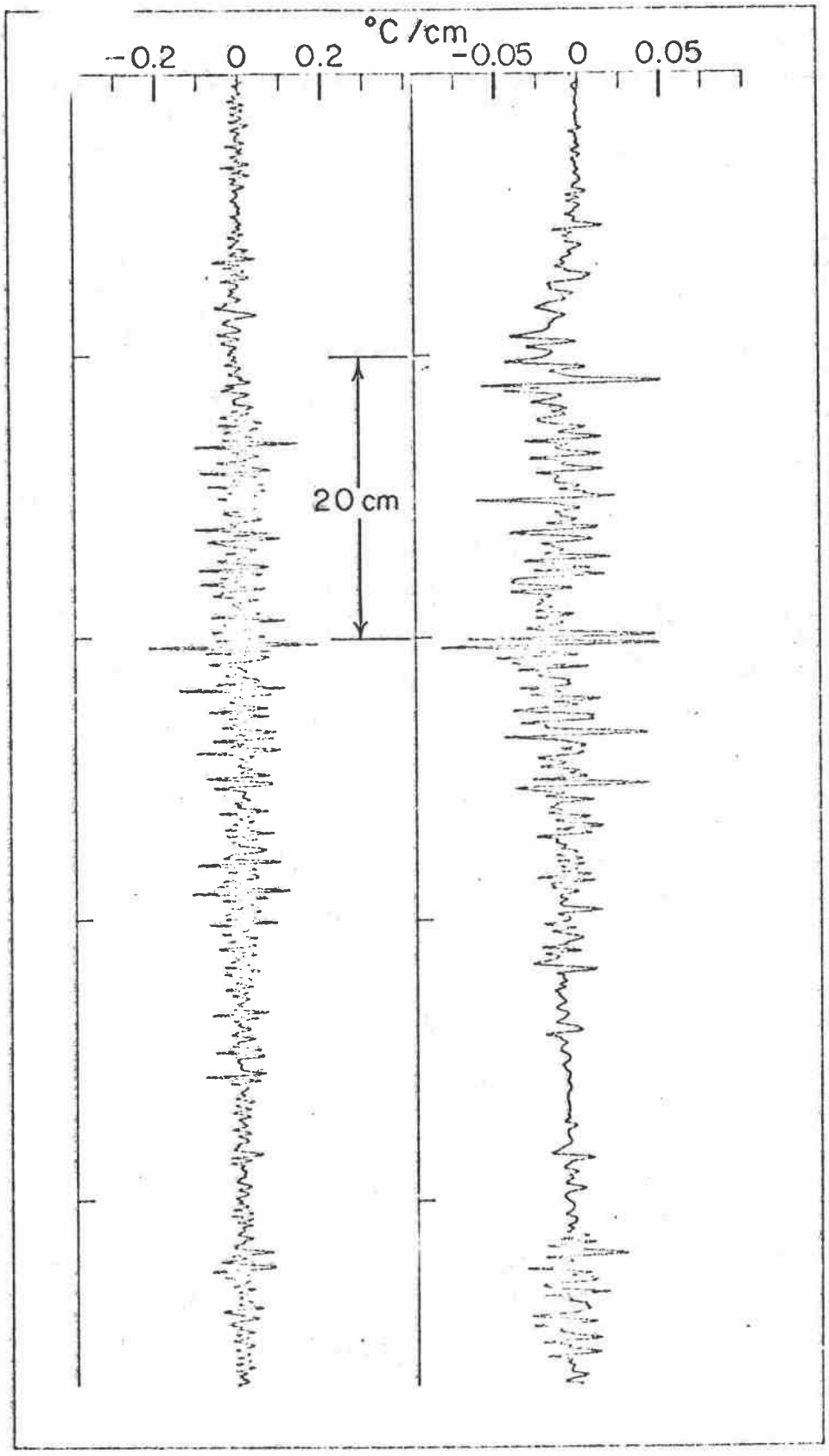

FIGURE 1.

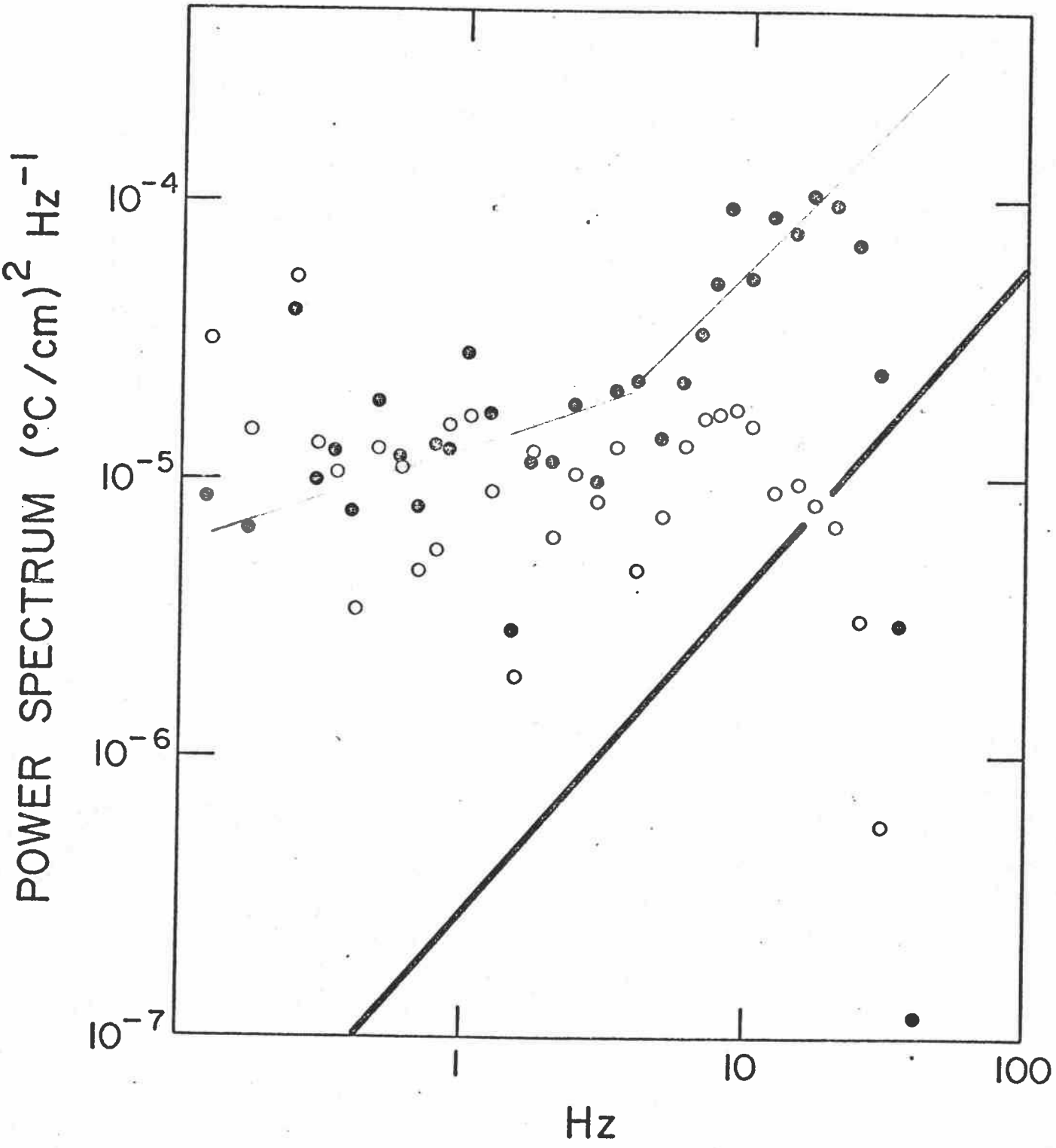

FIGURE 2.

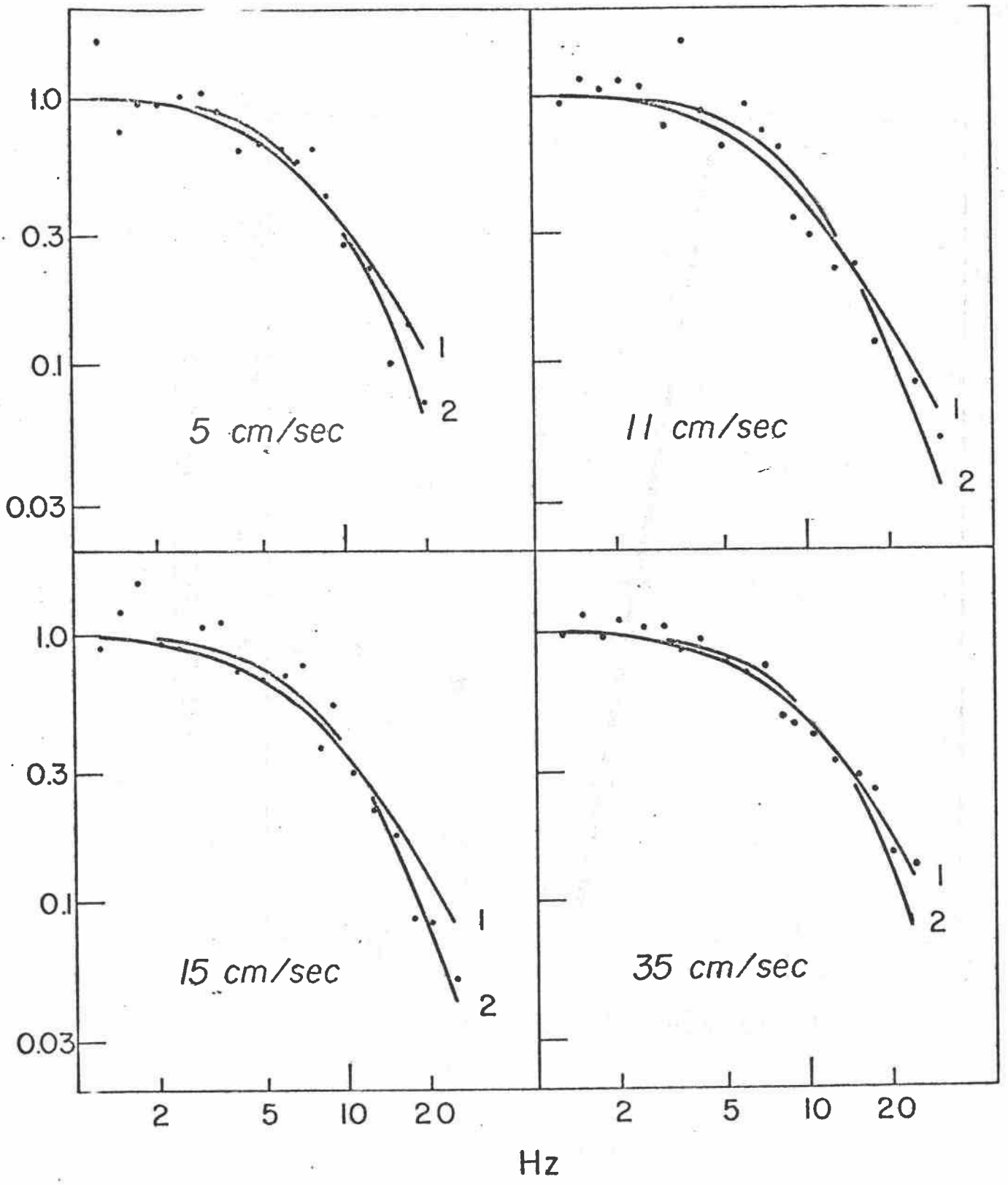

FIGURE 3.

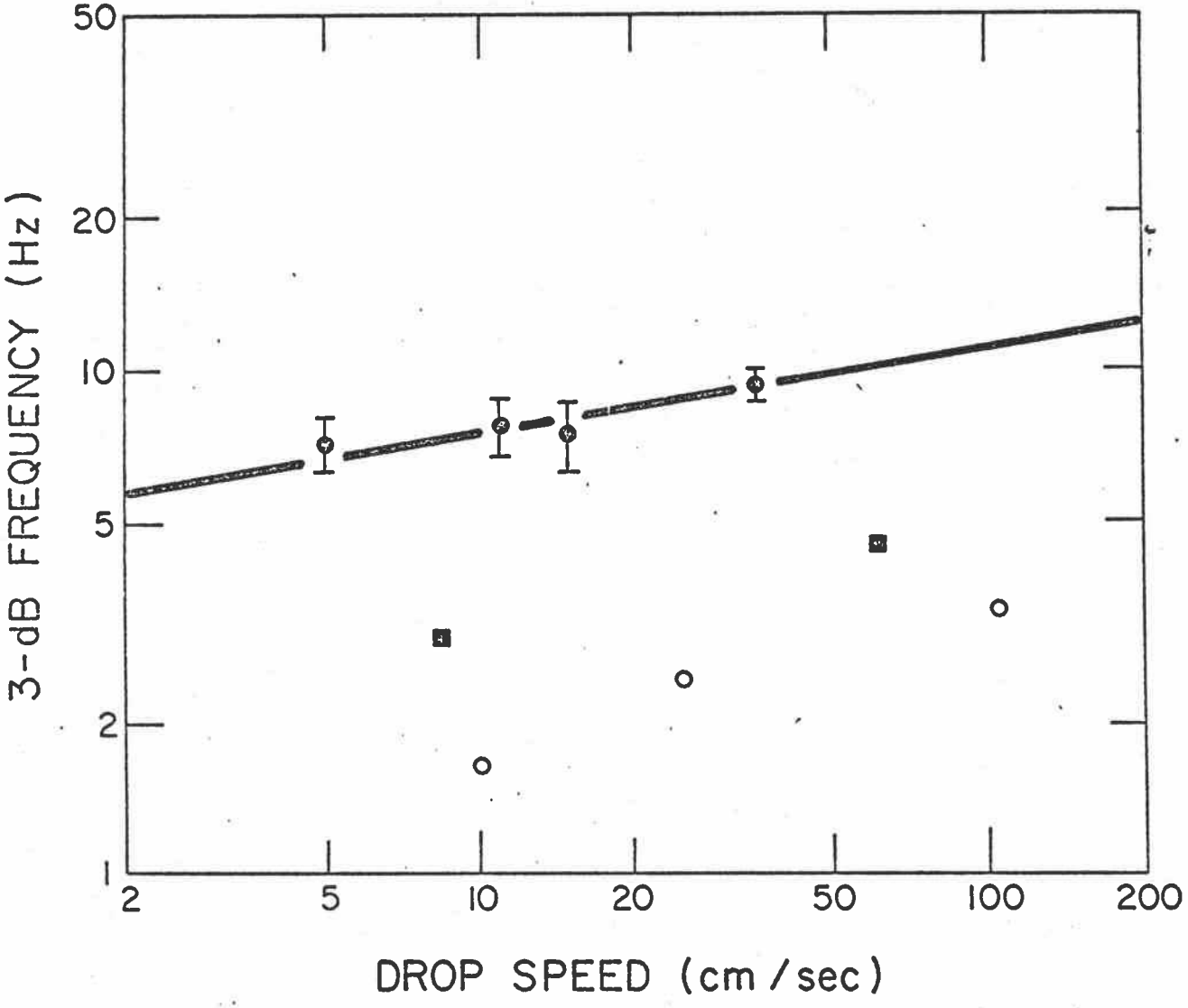
50
20
10
5
2
1
3-dB FREQUENCY (Hz)
2
5
10
20
50
100
200
DROP SPEED (cm / sec)

FIGURE 4.